Optimum Spanloads Incorporating Wing Structural Considerations And Formation Flying

Sergio Iglesias

Thesis submitted to the Faculty of
Virginia Polytechnic Institute and State University
in partial fulfillment of the requirements for the degree of

Master of Science
in
Aerospace Engineering

W.H. Mason, Chair
B. Grossman
J.A. Schetz

November 10, 2000
Blacksburg, Virginia

Keywords: Spanload Optimization, Structural Constraint,
Formation Flight

Optimum Spanloads Incorporating Wing Structural Considerations And Formation Flying

Sergio Iglesias

(ABSTRACT)

The classic minimum induced drag spanload is not necessarily the best choice for an aircraft. For a single aircraft configuration, variations from the elliptic, minimum drag optimum load distribution can produce wing weight savings that result in airplane performance benefits. For a group of aircraft flying in formation, non-elliptic lift distributions can give high induced drag reductions both for the formation and for each airplane.

For single aircraft, a discrete vortex method which performs the calculations in the Trefftz plane has been used to calculate optimum spanloads for non-coplanar multi-surface configurations. The method includes constraints for lift coefficient, pitching moment coefficient and wing root bending moment. This wing structural constraint has been introduced such that wing geometry is not changed but the modified load distributions can be related to wing weight. Changes in wing induced drag and weight were converted to aircraft total gross weight and fuel weight benefits, so that optimum spanloads that give maximum take-off gross weight reductions can be found. Results show that a reduction in root bending moment from a lift distribution that gives minimum induced drag leads to more triangular spanloads, where the loads are shifted towards the root, reducing wing weight and increasing induced drag. A slight reduction in root bending moment is always beneficial, since the initial increase in induced drag is very small compared to the wing weight decrease. Total weight benefits were studied for a Boeing 777-200IGW type configuration, obtaining take-off gross weight improvements of about 1% for maximum range missions. When performing economical, reduced-range missions, improvements can almost double. A long range, more aerodynamically driven aircraft like the Boeing 777-200IGW will experience lower benefits as a result of

increasing drag. Short to medium range aircraft will profit the most from more triangular lift distributions

Formation flight configurations can also result in large induced drag reductions for load distributions that deviate from the elliptical one. Optimum spanloads for a group of aircraft flying in an arrow formation were studied using the same discrete vortex method, now under constraints in lift, pitching moment and rolling moment coefficients. It has been shown that large general improvements in induced drag can be obtained when the spanwise and vertical distances between aircraft are small. In certain cases, using our potential flow vortex model, this results in negative (thrust) induced drag on some airplanes in the configuration. The optimum load distributions necessary to achieve these benefits may, however, correspond to a geometry that will produce impractical lift distributions if the aircraft are flying alone. Optimum separation among airplanes in this type of formation is determined by such diverse factors as the ability to generate the required optimum load distributions or the need for collision avoidance.

Acknowledgements

I would like to thank the people that helped me through this work in many ways. Without them, this research would have not been possible.

First of all, I would like to acknowledge my advisor, Dr. W.H. Mason, for his support, guidance, and knowledge. His vast experience in aircraft design methods and practice was helpful in generating analysis tools that could reflect reality. Also, his large knowledge of the literature not only made my work easier, but enjoyable. I should thank him for his willingness to share this knowledge with me, for his multiple advises and for always trying to provide me with a comfortable work environment for this project.

I wish to thank the people who worked before me and developed tools that made this research possible. Joel Grasmeyer did an incredible job as a graduate student at Virginia Tech, and his design and analysis aerodynamic codes were more than useful for the purposes of this study. Amir Naghshineh-Pour developed a wing bending material calculation subroutine that helped through this work. Regards are also due to some of the truss-braced wing team members at Virginia Tech, especially to Joel, Amir, and Andy Ko, who introduced me to the MDO methodology and to a wide variety of interesting projects.

I am also greatly indebted to Dr. Bernard Grossman and Dr. Joseph Schetz, for their thoughtfulness and desire to serve on my thesis committee.

My thanks to my other Virginia Tech professors for their inspiration and contribution to my future, with special regards to Wayne Durham, William Davenport and Joseph Schetz.

I am grateful to my friends at Virginia Tech especially Juan, Diego, Valerio, Paco, Alejandro and Sergio, who made my life easier and more enjoyable at Blacksburg. Thanks to my friends back in Saint Louis, Nacho, Yago, Isidro and Paco, for they made me build a good life in a foreign country. I also owe my thanks to friends in Spain, Juanjo, Julio and Juan, for being always there, for being my best friends.

I would like to express my warmest appreciation to my parents Marisol and Alejandro. Their long life support, inspiration and encouragement made all my accomplishments in life possible. They deserve my admiration for their willingness to make sacrifices in my life that I was not able to do for myself. My brothers, Senen, Alejandro and Nelly are always in my mind. They have showed me incredible support through my life in Blacksburg, and their different life perspectives made my mind open.

Finally, I should express the enormous appreciation that I feel for my greatest desire in life, my best friend and soul partner Gema. She gave me the strength during this year to overcome the bad moments. I will always be grateful to her for showing me what are the important things in life, and for making me fight for them. I will always admire her for her perseverance, well-founded ideas and mental strength, which gave me calm and joy through the largest of distances. For these reasons, and many others, I dedicate this work to her, as a small gift for her complete life dedication to me.

Table of Contents

List of Figures

List of Tables

Chapter 1 Introduction

1.1 Motivation

The problem of finding the optimum lift distribution for a given wing and aircraft configuration is difficult. Optimum spanloads that will give minimum induced drag for a given planform have been obtained since lifting line theory was developed by Prandtl. Planar wings were the main objective of this early method, although more advanced configurations (i.e. wing with winglets) were also treated. Recently, more advanced methods were developed that could deal with non-planar wings and multiple lifting surface configurations (i.e. a Vortex Lattice Method). These methods can find the lift distribution that gives minimum induced drag, generally performing the calculations in the Trefftz plane.

For a single aircraft configuration, the minimum induced drag spanload seems to be a reasonable design objective. For a planar wing, this will give an elliptic lift distribution. However, the problem is more involved than this, since minimum drag will not be the only requirement for finding an optimum lift distribution. Indeed, the spanload will affect the wing structural weight. A useful method for finding the optimum spanload should in fact involve aerodynamics and structures together. It is then an interdisciplinary problem, and it is this connection between disciplines that makes the problem difficult. Including wing structural considerations in the spanload optimization problem can lead to total aircraft gross weight reductions as a result of wing weight savings.

For a group of aircraft flying in formation, induced drag savings are experienced due to the upwash coming from nearby airplanes. Formation flight benefits can be observed in nature in the flying disposition of migrating birds, often adopting V-shaped formations. These formations help birds save energy by decreasing air resistance so that they can travel through longer distances.

The variability in the geometry of bird's wings, together with their highly controllable flight allows them to change their wing geometry and fly very close to each other. This makes them take full advantage of formation flying. For a rigid wing aircraft the capability of adapting wing geometry is very limited, close flying is not possible because of collision dangers and control problems can appear. However, large induced drag benefits can be obtained for the whole formation and for each airplane if the spanloads are altered from the elliptic, single flight minimum drag optimum. Advantages of formation flying will be dependent on the relative distance between aircraft and the adaptability and limitations of rigid aircraft, that impose restrictions on the benefits that can actually be achieved.

1.2 Previous work on spanload optimization with wing structural considerations

Several attempts have been made previously to treat both aerodynamics and structures. Prandtl[1] himself was the first one to notice that the spanload for minimum induced drag was not the "optimum" spanload, and he calculated analytically the lift distribution giving minimum induced drag with a constraint in integrated bending moment[§] for planar wings. Jones[2] also performed analytical calculations for planar wings, using a root bending moment constraint. Later on, Jones[3] studied minimum induced drag for wings with winglets using an integrated bending moment constraint, the same kind of constraint Prandtl used for his analysis. Klein and Viswanathan[4,5], combined both constraints of integrated and root bending moment and solved analytically for the optimum spanload for a given lift. More recently, numerical approaches have also been developed, such as those of Kroo[6], McGeer[7] and Craig and MacLean[8]. Kroo developed a computer program to optimize spanloads for arbitrary multiple lifting surface configurations. His program optimized induced drag for a given total lift, wing weight and trim. McGeer used an iterative scheme to find the optimum spanload for minimum drag with a fixed wing weight and parasite drag, including aeroelastic effects. Craig and McLean further introduced aeroelastic effects and body-surface interactions using the theory developed

[§] The classical structural models used as constraints for spanload calculations are a root bending moment constraint (the area under the load curve is kept constant) and an integrated bending constraint (the area under the bending moment curve is kept constant). Prandtl used this last constraint in his approach.

by Gray and Schenk[9], and studied wing weight and total drag (including profile drag) trade-offs. Kroo, McGeer, and Craig and McLean employed more advanced structural models than a bending moment constraint. All the authors mentioned above let the span vary while maintaining a fixed wing weight, no matter what structural model they used.

An optimum spanload for minimum induced drag under weight constraints is then the general approach that most authors have used for aerodynamic-structural load optimization. It should be noted that a different perspective, not so widely treated, could be equally valid, in which the wing weight is minimized with a constraint in induced drag coefficient. Haftka[10] optimized the weight of a wing of known geometry with a constraint in induced drag for a fighter aircraft in a pull-up maneuver. However, a general optimization in which wing twist and camber distributions are not known and induced drag is found at the cruise condition is needed.

The studies performed by the authors previously mentioned led to the conclusion that significant drag savings could be obtained if wing span was increased while keeping wing weight constant. This was achieved by shifting the minimum drag elliptic load distributions towards more triangular ones, reducing loads outboard.

1.3 Previous work on spanload optimization in formation flight

Formation flight has been studied frequently in the past. Schlichting[11][*] inspired the work in this field with his pioneering efforts on formation flight studies. Hoerner[12] apparently used Schlichting's work to show the influence of aircraft separation on airplane drag. Schollenberger and Lissaman[13] investigated the formation flight of birds. They realized that the bird flexibility was an important requirement to obtain maximum advantage in formation flying. Their analysis showed that a 40% induced drag reduction could be achieved for each bird flying in an arrow formation consisting of just three birds. When 25 birds were flying in an arrow formation, induced drag savings as large as 65% could be achieved for each bird according to the authors, and this drag reduction can result in a range increase of about 71%. Jenkinson[14] used the induced drag savings

[*] We have not yet been able to obtain this reference.

calculated by Schlichting to establish the possible advantages of transport aircraft flying in formation as a solution for the growing demand in future large aircraft. Feifel[15] used a vortex lattice method with calculations performed in the near field to obtain the advantages of formation flying in an array of five airplanes of known geometry flying in a V-formation. Feifel only shows results for one test case, so that the magnitude of the induced drag reduction and its variation with spacing between aircraft cannot be shown. Maskew[16], using again a vortex lattice method, but with a Trefftz plane analysis, studied the induced drag variation for each aircraft and for the whole formation as a function of the distance (in the three space coordinates) between airplanes for an arrow formation consisting of three equal aircraft. An experimental investigation of the possible benefits for three aircraft flying in an arrow formation has been recently performed by Gingras[17]. Beukenberg and Hummel[18] gave flight test data for three aircraft flying in an arrow formation, and compared it to the theoretical aerodynamic results obtained with various vortex models.

Promising results have been obtained by these authors, and large induced drag savings for each aircraft and the configuration could be achieved. However, high induced drag savings coincide with close spacing between aircraft. Collision and control problems may arise at these close distances.

1.4 Overview

This work studies the possible benefits of load distributions that deviate from the aerodynamic, single flight optimum, that is, from the classical elliptical load distribution. First, for a single aircraft configuration, optimum spanloads will be obtained with an applied root bending moment constraint. Aerodynamic and structural formulation and modeling for this problem will be given in Chapter 2. In Chapter 3, the different aircraft configurations that will be studied are introduced. Chapter 4 shows the results for these configurations, in which optimum spanloads for maximum weight reductions will be found. Then, spanloads giving minimum induced drag for an arrow formation flight configuration will be studied. Chapter 5 gives the formulation and theory used for the spanload optimization in formation flight. Chapter 6 shows the arrow formations that will

be used as test cases for the different studies, and Chapter 7 will give the results and potential aircraft performance benefits from a formation configuration. Finally, concluding remarks are presented in Chapter 8. Appendix A and Appendix B show sample input and output files for both the single aircraft study with a root bending moment constraint and the formation flight case.

Chapter 2 Methodology for spanload optimization with a root bending moment constraint

2.1 Objective

Several authors have addressed the problem of incorporating wing structural constraints for the optimization of load distributions in the past (refer to section 1.2), and general tendencies have been obtained. For example, for a cantilever wing, keeping the weight fixed and increasing its span will produce a shift from the elliptical loading towards a more triangular one that, maintaining the total lift constant, will reduce induced drag (due to the increased span). In spite of these trends, a general conclusion about which should be the optimum spanload cannot yet be achieved. In particular, the interest must be centered in the lift distribution for a fixed planform. This is the problem that would be naturally incorporated in an MDO process for the complete aircraft.

The difficulty in finding optimum spanloads comes from the analysis carried out by these authors. First of all, varying the span while keeping the wing weight fixed will not be very helpful when trying to compare lift distributions for a given planform, since comparisons will be made for essentially different wings. A new approach is needed, in which the spanload is varied but the wing planform is not, and the wing weight will then vary according to the spanload. Secondly, the analysis must consider the entire configuration. The interdisciplinary nature of the problem should not be reduced to wing structures and wing drag, since the optimum spanload will be that bringing maximum benefits to the whole aircraft, not to the wing alone. When the lift distribution is varied, it is not only important to know how it will affect induced drag and wing weight, but how it will change wing, fuel, and ultimately, gross weights. Taking gross weight as a real measure of effectiveness (certainly better than wing weight or induced drag) will be helpful in finding the optimum lift distribution that will produce the maximum weight reductions.

Here the problem is treated through a different perspective that will allow to differentiate between the spanloads that will be beneficial to the complete aircraft configurations and those that will not bring any improvement at all.

2.2 General Approach

The lift distributions were obtained using a computer program (a general description of this program is given below), which optimizes the spanload of multiple lifting surface configurations with a constraint on root bending moment (root bending moment will be defined in section 2.3.1). It is clear that this is the simplest structural constraint that can be imposed on the problem, and it may be argued that the approaches of Kroo[6] and Craig and McLean[8] will give better results, since they used more advanced structural models. This would be true if wing weight were assumed to be a simple function of root bending moment. Instead, a general functional relationship is assumed of the form:

$$W_{wing} = f(root\_bending\_moment,...) \qquad (2.1)$$

Then, root bending moment is taken only as a constraint for generating spanloads, but it is not really the structural model used for wing weight calculations. Another important consideration comes from the fact that it is needed to change wing weight keeping the planform shape a constant. This will be achieved through a special implementation of the root bending moment constraint in the aerodynamics code (see section 2.3).

The structural model will be described in section 2.4. For now it will be enough to say that given the load distribution (calculated using the root bending moment constraint) and the planform characteristics of the configuration, the model used calculates wing weight, but the aircraft gross weight is needed for this calculation also.

Finally, once a new spanload is obtained, which corresponds to a new induced drag coefficient and wing weight, it is necessary to study the effect they will have in fuel and total gross weight. For that reason, the Breguet range equation is used. The description of how the Breguet equation was implemented in the program will be discussed later.

If fuel weight and gross weight variations can be obtained for different lift distributions, the task of finding the optimum spanload will then be a matter of choosing which one is the best measure of effectiveness for this optimization problem: that is, wing weight, fuel weight, gross weight, or a prescribed combination of them.

2.3 Description of the aerodynamics code

The method used for calculating the lift distributions is a discrete vortex method with a Trefftz plane analysis. It was developed by Blackwell[19], Lamar[20], Kuhlman[21] and Kroo[6] for pure aerodynamic optimization, that is, to determine the lift distribution corresponding to the minimum induced drag of the configuration. The implementation by Grasmeyer[22] in a FORTRAN code (*idrag* version 1.1) was used here. The code also includes an optional trim constraint, in which the pitching moment coefficient can be fixed if several surfaces are analyzed. Given the geometry for a number of surfaces, the program finds the spanload that gives minimum induced drag for a specific value of lift coefficient and moment coefficient using the method of Lagrange multipliers[22]. The number of vortices in which the lifting surfaces for a certain configuration are discretized determine the accuracy of the induced drag and optimum spanload calculations. As the number of vortices increases, the calculations converge to a certain value. The number of vortices for a given configuration must be the minimum number (because the computational cost increases with number of vortices) that still provides an accurate induced drag and optimum spanload calculation. Grasmeyer[22] studied the convergence of these results as a function of the number of vortices.

The code was modified to implement an extra constraint: a root bending moment constraint. Then, a new strategy was implemented in the code in order to obtain lift distributions with this constraint. The spanload for minimum induced drag is found first without taking into consideration any bending moment constraints (i.e. for a planar wing, this will give an elliptic lift distribution). Once this spanload is obtained, the root bending moment it produces is calculated. This bending moment will correspond to a particular wing weight. Now, the root bending moment is reduced by an arbitrary amount (say, for example, 10%) corresponding to a lower wing weight, and a new spanload will be

calculated with the same lift it had before and the reduced root bending moment constraint. In that way, for a given planform, and knowing the relationship between weight and root bending moment[†], the reduction in weight can be compared to the increase in induced drag.

2.3.1 Root bending moment constraint formulation

The bending moment constraint has been implemented in the *idrag* code using the method of Lagrange multipliers, and this constraint can also be turned on or off in combination with the trim constraint. The root bending moment coefficient is given by the equation:

$$C_{RBM} = \int_{s_{ref}}^{s_{final}} \frac{c_l}{b_{ref}} \left[\left(y - y_{ref} \right) \cos\theta + \left(z - z_{ref} \right) \sin\theta \right] ds \tag{2.2}$$

In this equation, s_{ref} is the point about which the root bending moment calculations are performed, and s_{final} is the final location for root bending moment calculations, that is, the wing tip. In the discrete vortex model equation 2.2 takes the form:

$$C_{RBM} = \sum_{j=1}^{m} \frac{\{c_n c\}_j}{c_{avg}} s_j \left[\frac{1}{b_{ref}} \left\{ \left(y_j - y_{ref} \right) \cos\theta_j + \left(z_j - z_{ref} \right) \sin\theta_j \right\} \right] \tag{2.3}$$

Where the geometry definition is taken from the discrete vortex method formulation by Blackwell [19](see Figure 2-1).

This constraint is only applied for wing surfaces. In equation 2.3, c is the local chord of each lifting element, c_{avg} is the average chord of the reference surface, c_n is the normal force coefficient at each station (at each control point) and s is a non-dimensional vortex semi-width. The result is that the first term in equation 2.3 is simply the lift coefficient at each station. The term in brackets accounts for the moment arm caused by this lift coefficient with respect to a reference point. In this term, y_{ref} and z_{ref} are the y and z

[†] The spanload generated with the root bending moment constraint is used to calculate wing weight using weight equations from FLOPS[23]. A detailed description of this weight calculation is given in section 2.4.

locations of the reference point, usually equal to the center of gravity of the aircraft. Note that the streamwise moment arm is neglected, that is, no root bending moment is calculated in the *x* direction. The moment caused by the load at each station due to streamwise distance is really a pitching moment that must be counterbalanced with the help of tail surfaces (pitching moment constraint), and no structural moment is produced.

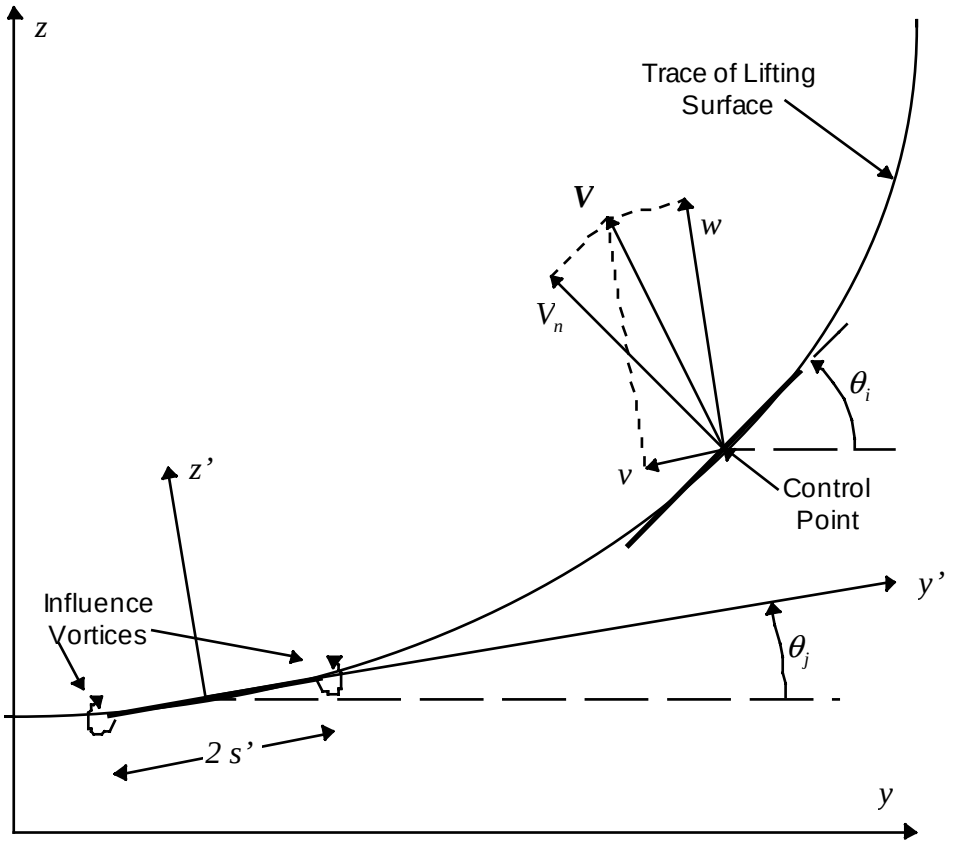

Figure 2-1. Discrete vortex method coordinate systems (Ref. 19)

The root bending moment coefficients calculated in the code were validated by introducing elliptical and triangular load distributions. The code calculated root bending moment coefficients for these spanloads with equation 2.3. Results were compared to those obtained by numerical integration of equation 2.2 using a standard mathematical package. These results showed excellent agreement between both equations.

2.3.2 Aerodynamics code connectivity for spanload optimization with a root bending moment constraint

Since the strategy in the aerodynamics code has changed as a result of the addition of the root bending moment constraint, the flowchart of the code has also changed. Figure 2-2 shows this flowchart when only lift and pitching moment constraints were included. Figure 2-3 shows the new code connectivity after the changes were made.

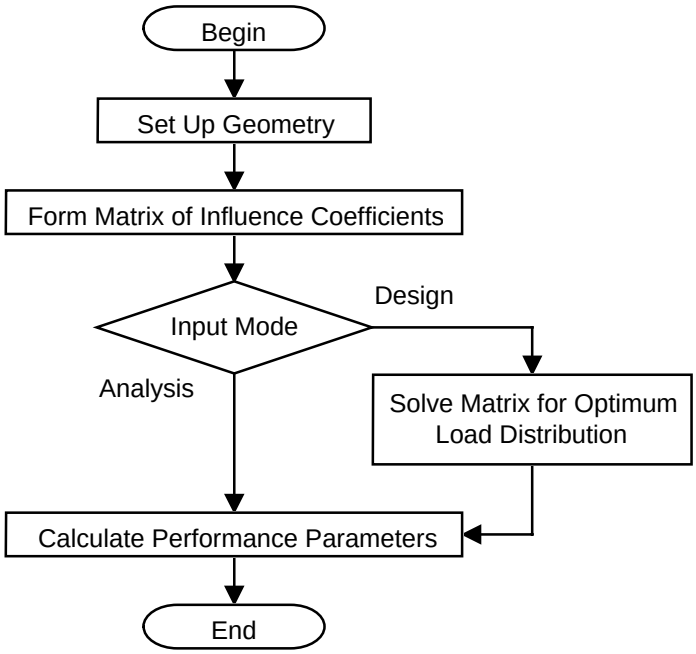

Figure 2-2. Flowchart of *idrag* code before a root bending moment constraint was implemented (Ref. 22)

Note that the *idrag* code has also an analysis capability, in which performance parameters can be calculated if the loads at each station are supplied. These performance parameters now include the root bending moment coefficient. In this study, only the design capability is used, in which loads are found to give minimum induced drag for the aircraft configuration.

The modifications made to the code have introduced a significant penalty in terms of computational time. Now, the system of equations whose solution is the optimum load distribution must be solved twice: with no root bending moment constraint and with an active bending moment constraint. Since the system of equations solution is by far the most computationally expensive task performed in the code, the result is that computational time has doubled. This approach is however necessary since a previous knowledge of the root bending moment caused by a minimum drag spanload is essential. It is in fact the only way of knowing if the bending moment at the wing root is increased or reduced, and therefore, if wing weight is higher or lower.

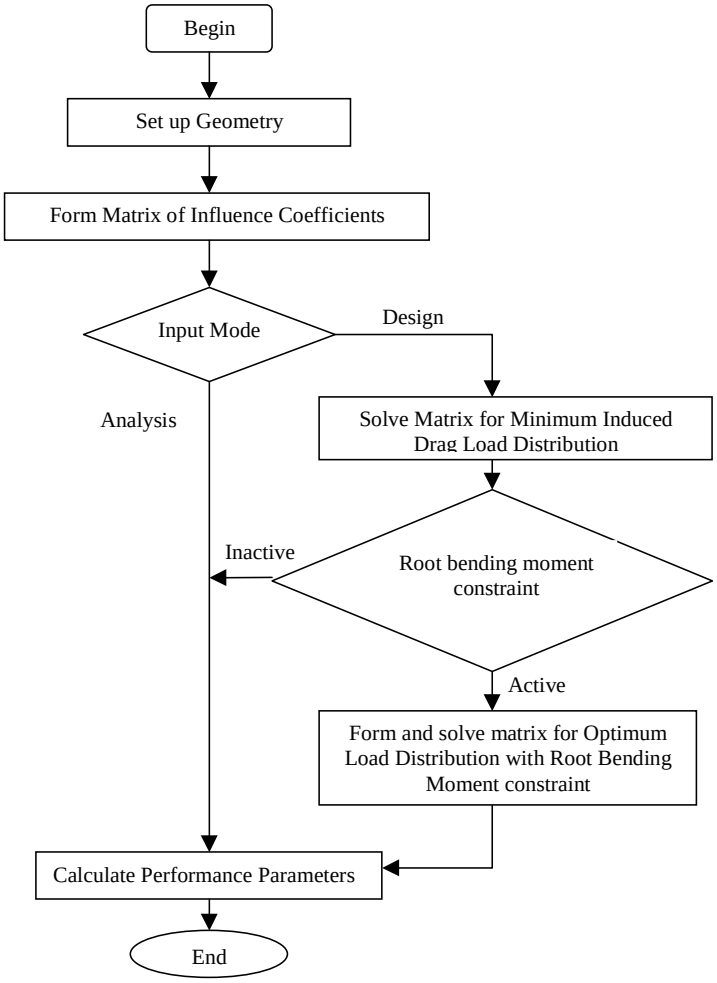

Figure 2-3. Flowchart of *idrag* code after a root bending moment constraint was implemented.

2.3.3 Preliminary results

Several configurations have been studied with this method. One of them is shown in Figure 2-4. It shows the load distribution in cruise flight for minimum induced drag, that is, with no bending moment constraint, and with an arbitrary root bending moment reduction (in the figure 11%). Trimmed flight has been assumed, so that both bending moment and trim constraints are active. Note that the spanwise distances over which loads are plotted are perpendicular to the plane of symmetry of the aircraft, as shown in Figure 2-5.

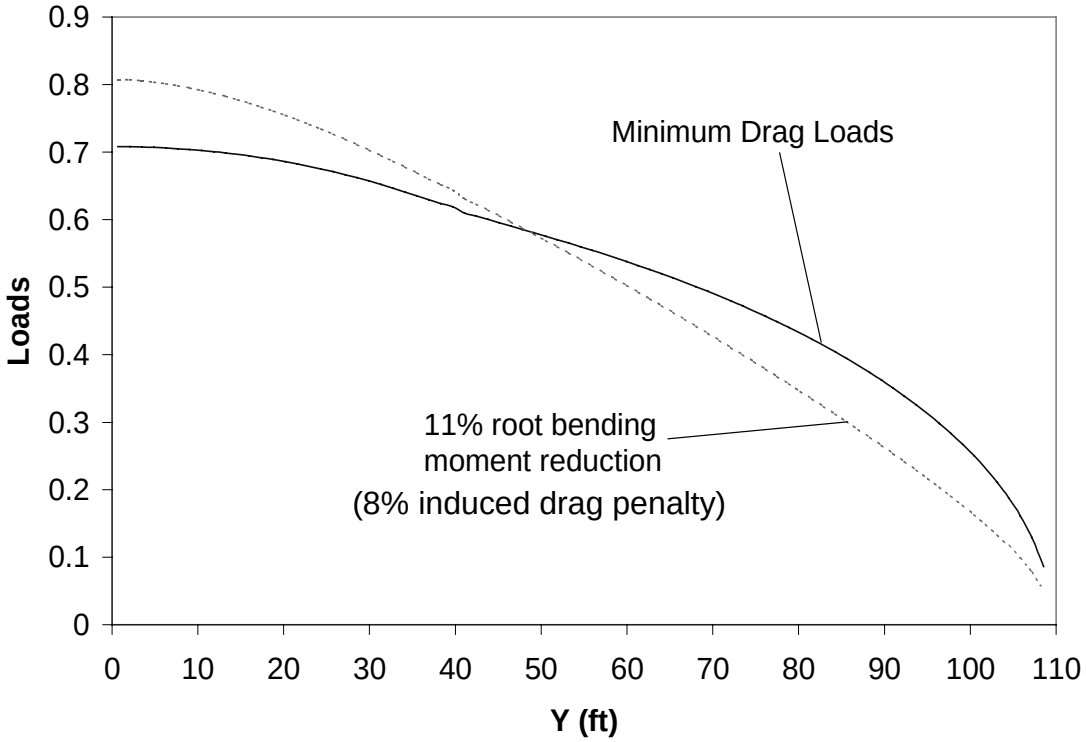

Figure 2-4. Span load distribution for minimum induced drag and with an arbitrary root bending moment reduction for a Boeing 777-200IGW type configuration.

General trends expected can be observed in Figure 2-4. A reduction in root bending moment shifts the load curve towards a more triangularly loaded wing that will still have the same area under the curve (same lift). Since the load is shifted inwards, wing weight should be reduced with this new loading, and the induced drag will necessarily be increased since the spanload deviates from the minimum induced drag distribution. The actual induced drag increase obtained with the aerodynamic code for the 11% root

bending moment reduction is about 8%. Another important consideration that should not be disregarded is that, as the load curve becomes more triangular, the load at the wing root also becomes larger for the same lift coefficient. For a very high load near the wing root, stall at this location will occur necessarily at a low lift coefficient value compared to that for a more elliptically loaded wing. Then, although it will be shown that shifting the lift distribution towards a more triangularly loaded wing will in some cases reduce gross weight, there will be a limit on "how triangular" the spanload really can become based on stall considerations. For the purposes of this study, it will be assumed that no limits based on stall are imposed on the optimization, and this will be true as long as the spanload does not become "too triangular", with a high load value at the wing root.

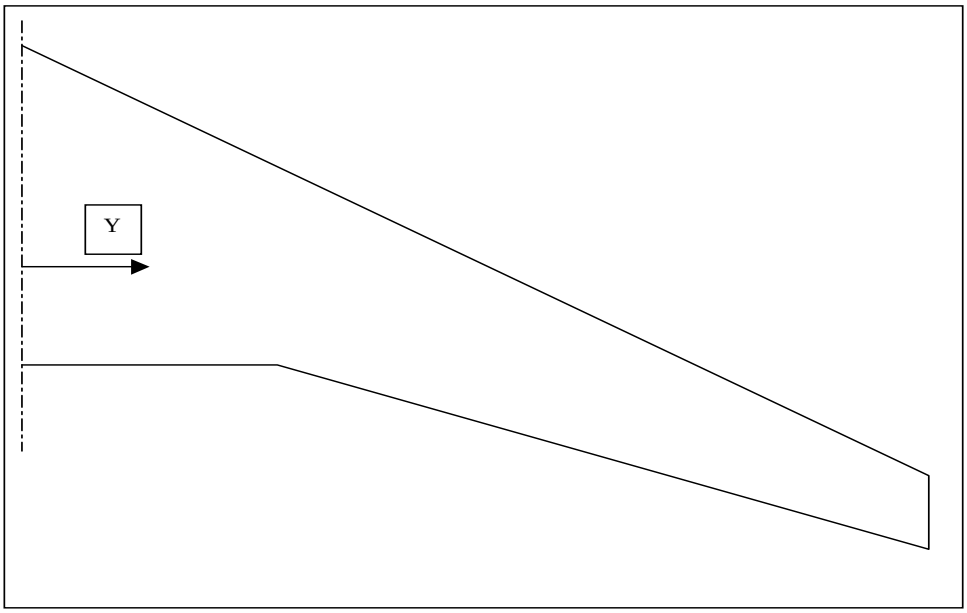

Figure 2-5. Definition of spanwise distance Y

The test case studied here corresponds to a Boeing 777-200IGW type configuration in cruise flight. For this type of aircraft, normal cruise is performed in the transonic region (in this case the cruise mach number for the 777-200IGW class aircraft was assumed to be 0.85). The total drag of the configuration will, of course, depend on Mach number, since wave drag becomes an important part of the total drag coefficient in the transonic region. However, the induced drag for a certain configuration and the spanload giving

minimum induced drag for that configuration are independent of Mach number. Only induced drag and optimum spanload variations will be studied in this thesis. For this reason, Mach number considerations are not taken into account.

2.4 Structural Model

The structural model used for calculating the wing bending material weight was developed by Naghshineh-Pour[24] at Virginia Polytechnic Institute and State University. Cantilever wings as well as strut-braced wings can be treated with this model. It was implemented in a code by the same author and has been shown to be a realistic structural model, valid at least for preliminary design purposes. The code requires the wing planform shape, together with airfoil thickness distributions and the load curve as inputs, and it gives wing bending material weight as an output. The required bending material weight along a variable box beam is calculated by integrating over the area under the bending moment curve, and engine inertia relief factors are also included. Several structural analyses can be performed in the code, including taxi bump load analysis, but they are not carried out in this study for simplicity purposes, since detailed aircraft data (such as fuel distribution over the wing) are needed for these calculations. The only structural analysis used to calculate bending material weight was a maximum load factor condition. A value of *2.5* with a safety margin of *1.5* was the maximum allowable load factor used, since it is typical of transport aircraft. Loads were calculated for this load factor using the modified *idrag* code and they were introduced in the structural program for bending material weight calculations.

The loads calculated for the maximum load factor condition with the aerodynamic code have the same shape as the loads for cruise design lift coefficient. This means that a rigid wing is assumed, in which no aeroelastic effects are included. A truly optimal wing would be aeroelastically tailored to have minimum root bending moment in worst-case load conditions while having minimum induced drag at the design lift coefficient. In this study the rigid wing assumption will neglect the aeroelastic effects for maximum load

factor conditions. However, this simplified model provides insight into the potential performance benefits that can be obtained with reduced root bending moment spanloads.

The bending material weight is then used to calculate wing weight using equations taken from the general optimization code FLOPS[23] (Flight Optimization System) developed at NASA. The wing weight calculations involve corrections for wing sweep, wing area, flap area, aeroelastic tailoring factors and another factor accounting for the amount of composite materials used in the wing. The final weight equation used in the FLOPS subroutine is given here because it will become important when the Breguet range equation is introduced:

$$W_{wing} = \frac{GW \cdot w_1 + w_2 + w_3}{1 + w_1} \tag{2.4}$$

Where, in this equation:

GW is the aircraft gross weight.

w_1 is a factor that accounts for bending material weight, planform shape, engine inertia relief and aeroelastic and composite factors. It is the value supplied by the Naghshineh-Pour code.

w_2 is an extra correction due to flap area

w_3 further corrects wing weight for the amount of composites used.

Equation 2.4 was introduced here for one key reason: to show that the wing weight calculation requires a knowledge of the aircraft total gross weight. The purpose of this study is to change the lift distribution and observe how induced drag and wing weight will change. This in turn will affect total fuel and gross weights. However, if the wing weight is dependent on aircraft gross weight, something must be done to close the loop. It will be shown that the implementation of the Breguet equation will not only serve as a method for calculating fuel and gross weights from a knowledge of induced drag and wing weight, but to close the loop connecting gross weight and wing weight.

2.5 Implementation of the Breguet Range Equation

The Breguet range equation has been introduced as a means of relating wing weight and induced drag for a certain aircraft configuration to fuel and gross weights. Given the gross weight of a transport aircraft for a certain mission and the fuel weight and range for that same mission, the lift coefficient, drag coefficient and specific fuel consumption at the mission altitude and velocity can be calculated. The lift coefficient for the mission altitude and velocity is found as an average lift coefficient:

$$C_L\_design = \frac{TOGW + (TOGW - W_{FUEL})}{2q_{cruise}S_{ref}} \tag{2.5}$$

The specific fuel consumption at the cruise velocity is calculated with the equation[25]:

$$sfc_{cruise} = \left(\frac{T_{cruise}}{T_{sea\_level}}\right)^{0.4704} (sfc_{static} + 0.4021Mach) \tag{2.6}$$

And an average total drag coefficient is calculated with the help of the Breguet range equation:

$$Range = \frac{Speed \cdot C_L\_design}{sfc_{cruise} \cdot C_D\_total} \ln\left(\frac{TOGW}{TOGW - W_{FUEL}}\right) \tag{2.7}$$

$$C_D\_total = \frac{Speed \cdot C_L\_design}{sfc_{cruise} \cdot Range} \ln\left(\frac{TOGW}{TOGW - W_{FUEL}}\right) \tag{2.8}$$

The induced drag and lift distribution for minimum drag at the design lift coefficient can be obtained using the aerodynamics code (section 2.3), and the corresponding wing weight is calculated with the structural model (section 2.4). At this design lift coefficient, once the induced drag is calculated, the following relationship is established:

$$C_D\_total = C_{D\_rest} + C_{D\_induced(C_L\_design)} \tag{2.9}$$

That is, the drag will be divided in two parts: the induced drag and the drag not covered by it.

The loads supplied for wing weight calculations are obtained by calling the aerodynamics code with a different lift coefficient than the design minimum drag value. The lift coefficient for maximum load calculation is found using:

$$C_L\_weight\_calculation = \frac{Ultimate\_factor \cdot C_L\_cruise\_initial}{1.5} \tag{2.10}$$

$$C_L\_cruise\_initial = \frac{TOGW}{q_{cruise} S_{ref}} \tag{2.11}$$

Once minimum induced drag and wing weight are calculated, the following assumptions are made: the weight of the aircraft that does not include wing and fuel weight will remain constant, and the drag of the aircraft that does not include induced drag will also remain fixed. The validity of the results obtained in this study will depend on the validity of these assumptions. As for the first one, the structural weight of the whole aircraft will depend on wing weight and fuel weight, so that if these weights change, the structural weight should also change. However, for small variations in wing and fuel weight, that is, small changes in aircraft gross weight, it is not a bad assumption to presume that the rest of the structural weight (and of course, the payload weight) remains constant. In any event, if gross weight is reduced the structural weight should decrease. Hence, the gross weight reductions obtained here will be in fact minimum expected reductions. In the second assumption, it is presumed that changing the twist or camber distribution of the wing (recall that the planform remains the same) does not change profile or pressure drag. It seems clear that drag will change, but as long as the aircraft is still at the same speed, altitude, and lift coefficient conditions, the effects of the changing profile and pressure drag on the wing should be minor.

Once the assumption is made that the only changing weights are wing and fuel weights and that the only changing drag is induced drag, the spanload can be modified to see the variation it will produce on aircraft weights. The root bending moment is then decreased

from the initial minimum drag configuration, producing a more triangularly loaded lift distribution with an increased value of induced drag. The new loads (with the root bending moment reduction but now with maximum load conditions) are then used in the structural model so that wing weight can be calculated. It was noted earlier that gross weight is needed to calculate wing weight from the FLOPS weight equation 2.4. Assuming that the mission range is constant (that is, the aircraft still has to meet the same mission requirements), all that is needed to calculate take-off weight from the Breguet range equation is the wing weight. Solving for the take-off weight from the Breguet equation will give:

$$TOGW = (TOGW - W_{FUEL}) \exp\left(\frac{Range \cdot sfc_{cruise} \cdot C_{D\_total}}{Speed \cdot C_{L\_design}} \right) \tag{2.12}$$

or, put in another way:

$$TOGW = (W_{Wing} + W_{rest}) \exp\left(\frac{Range \cdot sfc_{cruise} \cdot (C_{D\_rest} + C_{D\_induced})}{Speed \cdot C_{L\_design}} \right) \tag{2.13}$$

In this equation, W_{rest} is simply the weight assumed to remain constant, that is, the weight not covered by fuel or wing weight, and C_{D_rest} is the drag that also remains constant (the drag excluding induced drag). For the maximum range configuration, where the aircraft has a full fuel load, it will be assumed that take-off weight equals aircraft gross weight. Combining equation 2.4 to calculate wing weight with equation 2.13 to calculate gross weight it is clear that an iteration will yield simultaneously both the aircraft gross weight and wing weight. This is the approach that will be followed. Now, a change in wing lift distribution towards a more triangular curve can be related to changes in wing weight, fuel weight and gross weight, so that an optimum lift distribution can be found.

With the new take-off and wing weights calculated using the iteration mentioned above, fuel weights are simply found with the equation:

$$W_{FUEL\_new} = TOGW_{new} - W_{wing\_new} - W_{rest} \tag{2.14}$$

When new gross weights are calculated corresponding to new lift distributions, the lift coefficient will change if the aircraft still flies at the same altitude, so that the loads used do not actually reflect the calculated gross weights. Cruise altitude is then changed with gross weight variation to keep the cruise lift coefficient constant. In that way, the load distributions will correspond to weight variations. The actual altitude change needed to keep the lift coefficient constant is in fact small (less than 500 ft. for a Boeing 777-200IGW class test case)

This is not the only approach that could have been used. Instead of varying gross weight and keeping mission range constant, the opposite could have been done, that is, the gross weight could be kept a constant, so that any wing weight reduction would be compensated by a fuel weight increase in the same amount, and the different ranges that different spanloads would produce could be compared. In the approach used here, fuel weight is just calculated so that the required range is met, and different gross weights are compared for the same mission. This perspective was believed to have more significance, since the approach corresponds to standard aircraft design practice.

2.6 Code connectivity for maximum fuel configurations

Figure 2-6 shows the general flowchart of the code, where the connection between the aerodynamics and structures codes can be seen. This flowchart is only valid for the study of maximum fuel, maximum range configurations. Section 2.7 deals with the modifications introduced in this code to include the capability of studying aircraft configurations with reduced fuel-loads.

Starting with minimum induced drag loads (first iteration), the root bending moment will be reduced from this minimum induced drag value in steps to find new wing, fuel and gross weights. In the first iteration, the wing weight calculation can be performed directly using equation 2.4 because the initial gross weight is known. The weight that will be assumed to remain constant throughout, that is, W_{rest} will be calculated by subtracting wing weight and total fuel weight from the given gross weight in the first iteration. C_{D_rest} will be found subtracting the minimum induced drag from C_{D_total}.

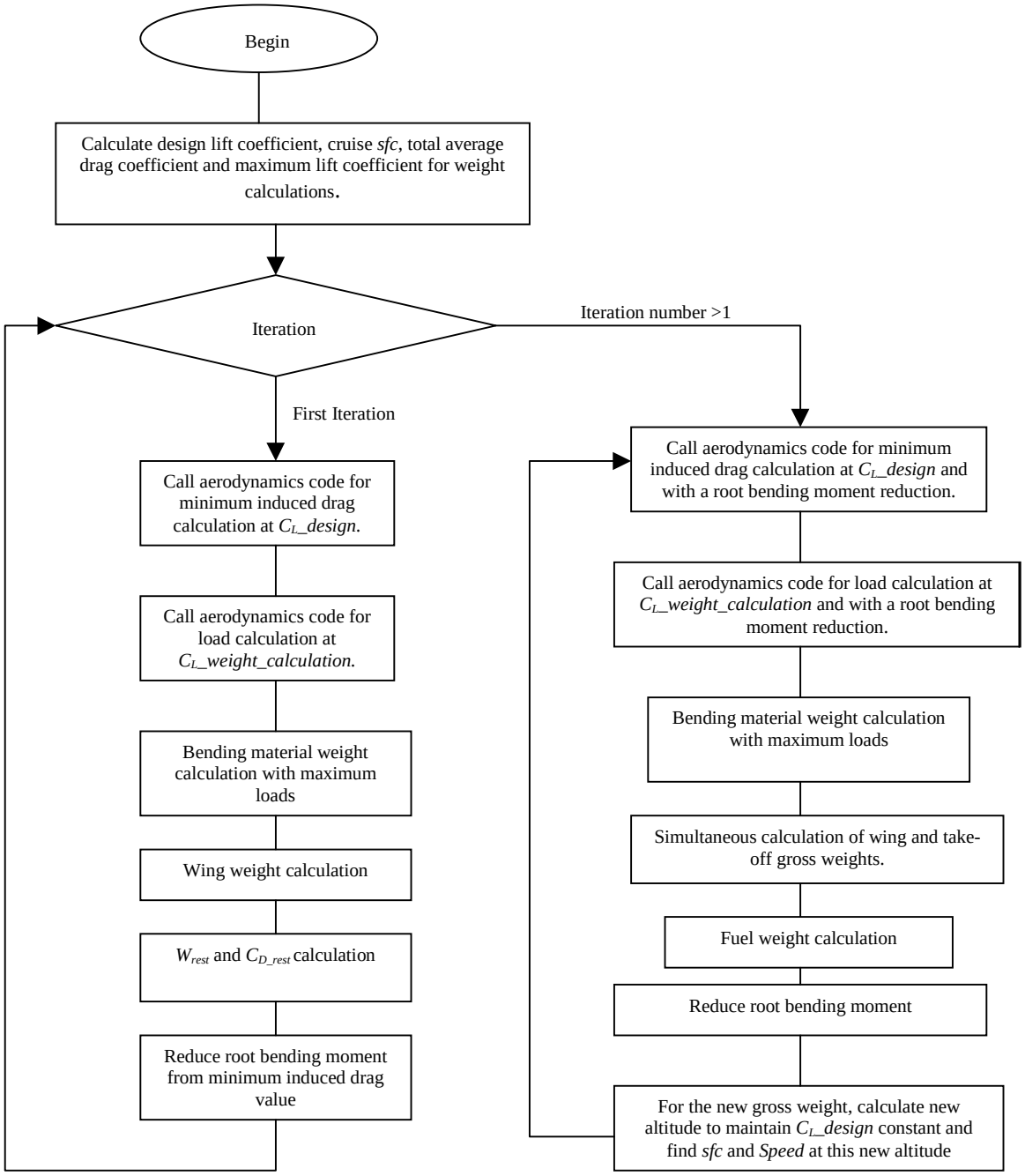

Figure 2-6. Flowchart of the spanload optimization code with a root bending moment constraint, maximum range configuration.

When the root bending moment is reduced from the minimum drag value the wing weight will change and consequently gross weight will also. The iteration between equations 2.4 and 2.13 is needed in this case to calculate simultaneously wing and gross weights. The new gross weights certainly will not match the lift coefficient and altitude conditions prescribed before. For that reason, cruise altitude is changed so that the lift coefficient is unchanged. The variation in altitude affects cruise specific fuel consumption and speed (cruise mach number is assumed constant), which in turn will affect equation 2.13. For a cruise altitude greater than 36000 ft., temperature does not change, so that specific fuel consumption and speed are constant for altitude changes above this limit. The ideal thing to do is enclose the iteration between equation 2.4 and 2.13 inside another loop that changes altitude conditions. That is, a take-off weight will be calculated, which will change altitude (*sfc* and *Speed*), then a new take-off weight will be found with equations 2.4 and 2.13 which will again change altitude conditions, until convergence is achieved.

To decrease computational time, another approach was used here. No iteration is made to match altitude for the new weight conditions. Instead, a lagging altitude is used. The altitude for specific fuel consumption and speed calculations will be assumed to be the one corresponding to the previous case, that is, to the previous root bending moment reduction and gross weight. For root bending moment reduction steps of 1%, where gross weight changes are small from case to case, so are altitude changes. For a Boeing 777 class aircraft test case, with a design cruise altitude of 40000 ft., altitude changes from step to step are lower than 40 ft. Above 36000 ft. altitude changes will not have any effect on the calculations. Even if cruise altitude were below this limit, a 40 ft error will mean a deviation in ambient temperature of 0.26 Kelvin, resulting in negligible changes in speed and specific fuel consumption.

2.7 Methodology for reduced mission ranges

So far, the code developed can give the optimum spanload for a given aircraft, that is, the spanload that will produce a maximum reduction in gross weight. However, the only test cases that can be studied with the method so far are those corresponding to a maximum take-off weight configuration. Aircraft generally fly through shorter distances than their

design maximum range, often in economic missions. It is then important to study how the spanloads generated by the root bending moment reduction will affect fuel weights and in turn take-off weights for these different missions. A modified FORTRAN code was then developed to carry out this study, the description of which follows here:

2.7.1 Code modifications to study different mission ranges

The code developed to study weight variations for different mission ranges includes only a few modifications.

Maximum take-off weight (equal to aircraft gross weight), maximum fuel weight and maximum range are still needed together with the new fuel weights for which weight variations will be studied. The code assumes that the initial take-off weight (take-off weight for minimum drag with no structural constraint added) is reduced by the same amount from the maximum take-off weight than the fuel weight is reduced from the maximum fuel weight, that is, all the missions will have the same payload:

$$TOW_{initial} = TOGW - (W_{FUEL\_MAX} - W_{FUEL\_NEW\_MISSION}) \tag{2.15}$$

A new value of cruise lift coefficient for the new weights is calculated. This lift coefficient is found using equation 2.5, substituting *TOGW* by *TOW* and W_{FUEL} by $W_{FUEL\_NEW\_MISSION}$. It is then assumed that the drag coefficient not due to induced drag is still constant, with the same value it had for the maximum range configuration. Note that this assumption is really more restrictive than the one made before for the drag coefficient, since the cruise lift coefficient is changing now, and consequently the angle of attack, which will change the drag coefficient. However, the mission is still performed at the same altitude and speed, and the lift coefficient varies little from the initial maximum weight configuration, so that drag coefficient will remain almost unchanged by the new conditions:

$$C_{D\_rest}(reduced\_mission\_range) = C_{D\_rest}(\max\_mission\_range) \tag{2.16}$$

The weight not covered by fuel weight spent during cruise or wing weight is also the same as in the maximum mission range configuration, since the payload weight remains the same:

$$W_{rest}(reduced\_mission\_range) = W_{rest}(\max\_mission\_range) \tag{2.17}$$

The range for the new fuel weight can be calculated using the Breguet equation (equation 2.7). In this equation fuel and take-off weights and the design lift coefficient must be changed to the new values. The total drag coefficient is set as the sum of C_{D_rest} and the induced drag coefficient calculated using the aerodynamics code for minimum induced drag with the new value of lift coefficient. The induced drag increase (non-dimensional) for a given configuration due to a specific root bending moment reduction from the minimum drag value is exactly the same no matter what the design lift coefficient is. That is, the induced drag increase

$$ind\_drag\_increase = \frac{C_{D\_induced(bending\_moment\_reduction)} - C_{D\_induced(\min imum\_drag)}}{C_{D\_induced(\min imum\_drag)}} \tag{2.18}$$

is not dependent on mission range. This happens because for a given planform, the optimum loads are directly proportional to the lift coefficient, so that variations in induced drag coefficients are the same. To calculate the new induced drags for the reduced mission range calling the aerodynamics code for each root bending moment reduction is not needed. If the induced drag increase is calculated using equation 2.18 for the maximum range configuration, only the induced drag for minimum drag in the new reduced range configuration must be found. The induced drag coefficient for any root bending moment reduction can then be calculated using:

$$C_{D\_induced(bending\_moment\_reduction)} = C_{D\_induced(\min imum\_drag)}(1 + ind\_drag\_increase) \tag{2.19}$$

In this way, the aerodynamics subroutine is only used once for each new mission range.

The approach that was used for the maximum range configuration to calculate wing weight can no longer be applied. Using an iteration between the Breguet equation solved for the take-off weight (equation 2.13) and the wing weight equation from FLOPS

(equation 2.4) will lead to inconsistent results. The take-off weight calculated in this iteration will serve as the gross weight used in the wing weight calculations, and for a reduced range mission take-off weight and gross weight will certainly be different. Since for a specified root bending moment reduction the aircraft still has to meet the maximum range, the gross weights calculated for the maximum range configuration at the specific root bending moment reduction are still valid, and so are the wing weights calculated for this configuration. These wing weights are then the weights used for the reduced range configurations, the iteration is removed and the wing weights for different mission ranges are the same. The actual take-off weight is then calculated once the wing weight is known using equation 2.13, and fuel weights are found in the same way they were before (equation 2.14).

One final consideration must be pointed out: to compare take-off weight variations and fuel weight variations for different mission ranges, the fuel weight subtracted from the maximum fuel weight and maximum take-off weight is added back once the calculations are finished, so that again total take-off weights and total fuel weights variations are compared. Otherwise, comparisons would be made for variations that are non-dimensionalized by different take-off weights.

2.7.2 Code connectivity for the spanload optimization for different mission ranges

If calculations have been performed for the maximum range configuration, the computational cost required for the study of reduced mission ranges will be minimal. The aerodynamics code is only called once for induced drag calculations at the minimum drag condition (no root bending moment constraint) for each new fuel weight (new range). The rest of the induced drag coefficients and wing weights corresponding to different root bending moment reductions are already known from the maximum range analysis. Induced drag coefficients and wing weights can be quickly related to gross and fuel weights with analytical equations of negligible computational cost. For that reason, if the maximum range analysis is performed, calculations can be made for several fuel weights with no important decrease in performance. Figure 2-7 shows a flowchart of the code.

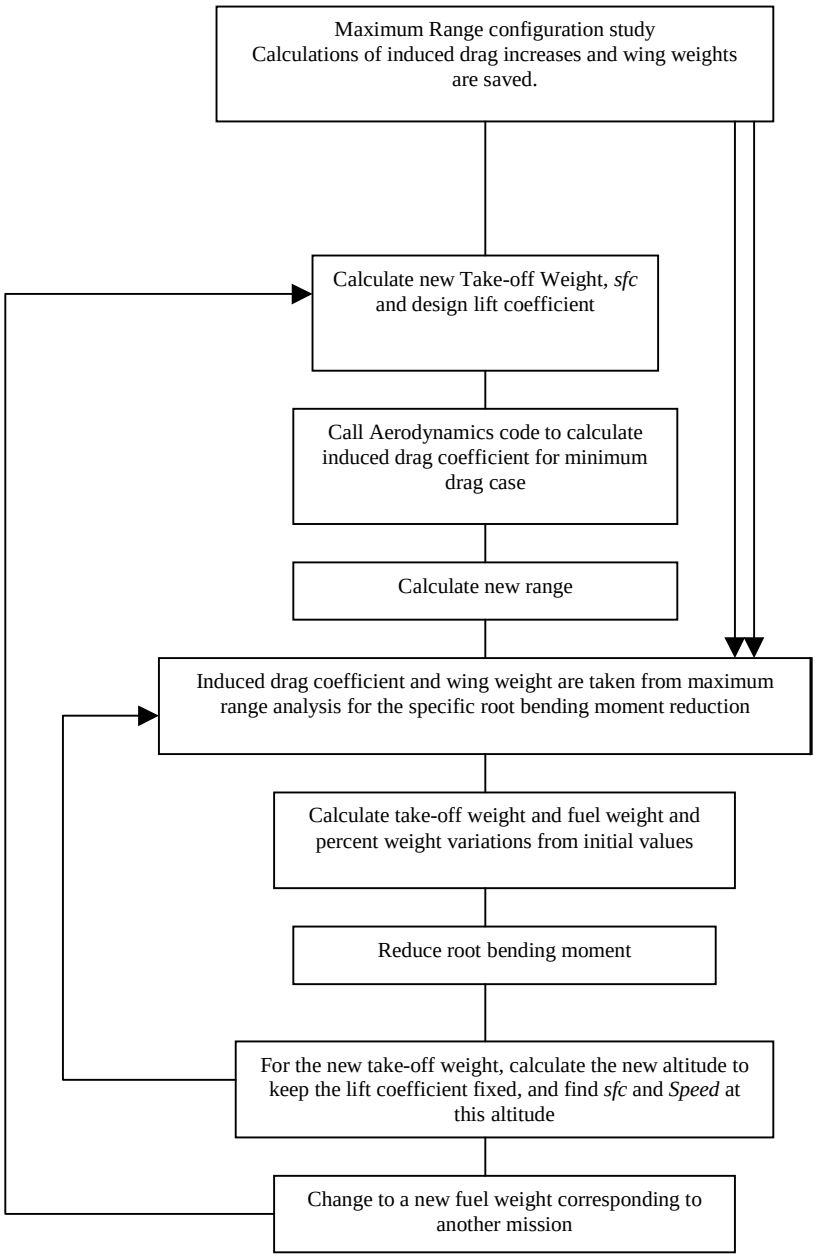

Figure 2-7. Code connectivity for the spanload optimization with a root bending moment constraint, reduced mission range configurations.

The code starts performing the calculations for a maximum range configuration (see Figure 2-6). Wing weights and induced drag increases for the different root bending moment reductions are saved in this step. A loop is then started for different fuel weights that correspond to different mission ranges. For each mission, a separate study is performed in which root bending moment is reduced in steps (in the same way as it was done for the maximum range configuration). The induced drag coefficient and wing weight for each root bending moment reduction are found using the saved results from the maximum range analysis, and they are related to fuel and take-off weights. To keep the lift coefficient constant for each mission range, the same approach used for maximum range studies is also used here. Altitude is changed with a lagging technique, that is, the altitude corresponding to the aircraft take-off weight of the previous root bending moment reduction is used for specific fuel consumption and speed calculations for the new root bending moment reduction. Again, for small steps in root bending moment reductions, altitude changes are also small (not larger than 40 ft), so that speed and altitude changes from the real values are negligible using this technique.

Chapter 3 Spanload optimization problem with a root bending moment constraint

The spanloads over the wings of existing aircraft configurations are to be optimized. Load distributions will be found that give minimum induced drag for the aircraft under study with the constraints in lift, pitching moment and root bending moment coefficient. The root bending moment will be applied at the aircraft wing to include wing structural considerations. Starting from a load distribution for minimum induced drag, the root bending moment produced by this minimum drag spanload will be reduced. New spanloads with the applied root bending moment constraint will be related to changes in wing, fuel, and take-off weights, and a conclusion about which spanload will be optimum for a certain aircraft configuration will be made.

A certain spanload that produces weight changes for an aircraft configuration when performing its maximum range mission, will produce different changes in aircraft weights when reduced range missions are performed. For that reason, both maximum range configurations and reduced fuel loads studies will be performed.

3.1 Maximum range configurations

Test studies have been performed for Boeing 777-200IGW and Boeing 747-100 class airplanes. Note that the configuration under study here is a maximum take-off weight, maximum range, maximum fuel arrangement. Other missions for the same aircraft will generate different results. These other missions will be treated later.

3.1.1 Boeing 777-200IGW class aircraft, maximum range configuration

The basic data introduced in the code is given in Table 3-1

Table 3-1. Boeing 777-200IGW class aircraft test data for maximum range configurations

	WING GEOMETRY	
1	Location of Wing Chord Break Point (non-dimensional)	0.37
2	Wing Half Span (ft)	109.21
3	Inboard Wing Sweep (deg)	28.29
4	Outboard Wing Sweep (deg)	28.29
5	Wing Dihedral Angle (deg)	6
6	Wing Chord at Fuselage Center Line (ft)	52
7	Wing Chord at Break Point (ft)	25.83
8	Wing Chord at Wing Tip (ft)	7.35
9	Thickness to Chord at Fuselage Center Line (ft)	0.111
10	Thickness to Chord at Wing Break Point (ft)	0.1
11	Thickness to Chord at Wing Tip (ft)	0.08
	HORIZONTAL TAIL GEOMETRY	
12	Horizontal Distance from wing to tail leading edges at center line	120
13	Vertical Distance from Wing to Tail Leading Edges at Center Line	12
14	Tail Half-Span (ft)	36.913
15	Tail Sweep Angle (deg)	37
16	Tail Dihedral Angle (deg)	0
17	Tail Root Chord (ft)	22.618
18	Tail Tip Chord (ft)	7.35
	PERFORMANCE SPECIFICATIONS	
19	Maximum Gross-Weight (lbs)	588893
20	Fuel Weight (lbs)	215000
21	Maximum Range (nm)	7600 + 500 reserve range
22	Cruise Mach Number	0.85
23	Cruise Altitude (ft)	40000
24	Static Specific Fuel Consumption (lb/hr/lb)	0.29
	ENGINE SPECIFICATIONS	
25	Number of Engines on Wing	2
26	Engine Weight (lbs)	16278
27	Spanwise location of Engine on Wing	0.33
	MISCELLANEOUS	
28	Ultimate Factor	2.5
29	Ratio of Wing Area Covered by Flaps	0.333
30	Location of Aircraft Center of Gravity from wing centerline leading edge(ft)	35
31	Fuselage Diameter (ft)	20.33

3.1.1.1 Geometry definition

Variables 1 to 18 define wing and tail geometry. They are not design variables and will remain fixed throughout the calculations. Variables 1 to 8 specify the wing planform geometry that will be used by the aerodynamics code for loads and induced drag calculations. Note that it is assumed that the wing is composed of two panels, the point where the first panel (inboard panel) ends and the second (outboard panel) begins is the breakpoint. Horizontal tail geometry is also given in variables 12 to18, specifying both planform and streamwise distance to the wing. This will also be used by the

aerodynamics code for loads and pitching moment coefficient calculations. Variables 9 to 11 establish the thickness to chord distributions. It is assumed that this distribution is linear for each wing panel. The thickness to chord distribution is used by the structural code for bending material weight calculations.

3.1.1.2 Performance specification

The use of variables 19 to 24 can be seen from section 2.5. They allow the calculation of an average cruise-design lift coefficient, a cruise specific fuel consumption and an averaged cruise total drag coefficient. It is important to realize that the performance specification is treated as that corresponding to a minimum induced drag spanload with no root bending moment constraint. That is, it is supposed that the aircraft is designed with an aerodynamically optimum spanload. This may not be the case, but the key purpose here is to study percent weight variations as a result of more triangularly loaded wings (reductions in root bending moment from the minimum induced drag value). The fact that this type of aircraft may not be designed for the minimum drag spanload will not affect this study.

3.1.1.3 Engine specification

The weight and location of the engines are specified in variables 25 to 27. Engine inertia relief factors can be calculated in the structural code using these variables.

3.1.1.4 Miscellaneous

The maximum load factor (variable 28) is used to calculate the lift coefficient that will be used for weight calculations (equation 2.10). The aerodynamics code will generate the load distribution for this lift coefficient, and the loads will be transferred for weight calculations. Variable 29, the wing flap area, simply introduced a correction in the wing weight calculations through the FLOPS weight equation 2.4. The location of the aircraft center of gravity is important for pitching moment calculations (variable 30). Finally, the fuselage diameter (variable 31), is introduced here to include the pitching moment coefficient caused by the fuselage about the center of gravity. This calculation requires a

knowledge of the fuselage pitching moment derivative with respect to aircraft lift coefficient. This may not always be known. Fortunately, this term is negligible for the calculations. If the pitching moment caused by the fuselage is not taken into account, optimum spanloads and weight variations remain the same.

3.1.1.5 Constraints

The load distributions are found from the aerodynamics code under the constraints of a design lift coefficient, a pitching moment coefficient about the center of gravity and a wing root bending moment coefficient. Note that this last constraint is applied only to one side of the wing. If the whole wing root bending moment is calculated, it would be zero for a symmetrical load distribution since loads will be the same but moment arms will change signs (equation 2.3). No other constraints are imposed on the calculations.

3.1.1.6 Changing variables

The performance specifications are assumed to correspond to a minimum induced drag (aerodynamically optimum) load distribution. The root bending moment for this spanload is calculated. Weight variations will be studied for different root bending moment reductions from this minimum drag value. The only forced changing variable is then the root bending moment reduction. In this study, root bending moment coefficient will be reduced from the aerodynamic optimum from 0% to 30% in 0.5% increments.

3.1.1.7 Optimized variables

The only parameter that is really optimized is the induced drag of the aircraft configuration. An optimum minimum induced drag spanload is obtained for each root bending moment reduction. These spanloads are in turn related to aircraft weights. Weight variation curves as a function of root bending moment reduction can be obtained. The choice of an optimum spanload that corresponds to a minimum aircraft weight will be made by looking at these curves. In no case will the aircraft weight actually be minimized.

3.1.1.8 Measures of effectiveness

Induced drag, wing weight, fuel weight, wing plus fuel weight and take-off weight are studied for each root bending moment reduction. Each one, or even a combination of them, could be taken as the measure of effectiveness for determining the optimum spanload. General aircraft design practice tells, however, that take-off weight will be the best measure of effectiveness.

3.1.2 Boeing 747-100 class aircraft, maximum range configuration

The basic data introduced in the code for a Boeing 747-100 class aircraft configuration for a maximum range mission is given in Table 3-2.

Geometry definitions, performance, engine specifications and other variables apply in the same way they did for the previous Boeing 777-200IGW class case (section 3.1.1). Root bending moment reductions from the minimum drag configuration will also be changed from 0% to 30% in 0.5% increments, and weight variations will be studied. Take-off weight will again be the most important measure of effectiveness to determine optimum load distributions.

The study of a different test case than the Boeing 777 class configuration will be important for several reasons. First of all, the trends that are observed in the Boeing 777-200IGW case study are expected for the Boeing 747-100 class aircraft (and for other airplanes). A greater generality on the results can be obtained with the study of two different airplane configurations. Secondly, it is expected that lower range airplanes will benefit the most from greater root bending moment reductions (more triangular spanloads), since they are more driven by structural considerations than by aerodynamic ones (any increase in induced drag is more important for a long range aircraft). The Boeing 747-100 class aircraft is a lower range aircraft, but it is also a heavier one. The effects of aircraft characteristics on the weight variations due to more triangular spanloads can therefore be studied.

Table 3-2. Boeing 747-100 class aircraft test data for maximum range configuration.

	WING GEOMETRY	
1	Location of Wing Chord Break Point (non-dimensional)	0.47
2	Wing Half Span (ft)	97.80
3	Inboard Wing Sweep (deg)	37.50
4	Outboard Wing Sweep (deg)	37.50
5	Wing Dihedral Angle (deg)	7.00
6	Wing Chord at Fuselage Center Line (ft)	54.30
7	Wing Chord at Break Point (ft)	29.00
8	Wing Chord at Wing Tip (ft)	13.30
9	Thickness to Chord at Fuselage Center Line (ft)	0.1344
10	Thickness to Chord at Wing Break Point (ft)	0.08
11	Thickness to Chord at Wing Tip (ft)	0.08
	HORIZONTAL TAIL GEOMETRY	
12	Horizontal Distance from wing to tail leading edges at center line	120
13	Vertical Distance from Wing to Tail Leading Edges at Center Line	17
14	Tail Half-Span (ft)	36.40
15	Tail Sweep Angle (deg)	37.50
16	Tail Dihedral Angle (deg)	7
17	Tail Root Chord (ft)	32.00
18	Tail Tip Chord (ft)	8.30
	PERFORMANCE SPECIFICATIONS	
19	Maximum Gross-Weight (lbs)	718825
20	Fuel Weight (lbs)	274955
21	Maximum Range (nm)	5500+ 500 reserve range
22	Cruise Mach Number	0.8
23	Cruise Altitude (ft)	35401
24	Static Specific Fuel Consumption (lb/hr/lb)	0.36
	ENGINE SPECIFICATIONS	
25	Number of Engines on Wing	4
26	Engine Weight (lbs)	12727
27	Spanwise location of Engine on Wing	0.40, 0.71
	MISCELLANEOUS	
28	Ultimate Factor	2.5
29	Ratio of Wing Area Covered by Flaps	0.33
30	Location of Aircraft Center of Gravity (ft)	49
31	Fuselage Diameter (ft)	23.00

3.2 Reduced range configurations

The effect of the different spanloads on the aircraft weights for reduced fuel, reduced range missions configurations will be studied only for the Boeing 777-200IGW class aircraft. The comparisons between Boeing 747-100 and Boeing 777-200IGW class airplanes can be made by looking at the maximum range configurations. The weight variations for reduced fuel weights will be relatively the same for both aircraft, so that the Boeing 747-100 class aircraft was not studied for reduced ranges.

3.2.1 Boeing 777-200IGW class aircraft, reduced range configurations

The input data that is needed for the Boeing 777-200IGW class configuration study was given in Table 3-1 for the maximum range configuration. The same table is valid for reduced fuel, reduced range configurations. The geometry definition will of course remain the same, together with the engine specifications and miscellaneous variable definitions. Maximum range performance specifications are also needed and will remain the same, since the calculations for reduced range configurations start with a maximum range study (see section 2.7 and Figure 2-7).

Calculations will start, then, performing a maximum range configuration analysis in which root bending moment reduction will be varied from 0% to 30% in 0.5% step increments as before. Once wing weights and induced drag increases are found for the maximum range configuration, calculations can begin for reduced range configurations (refer to section 2.7 for a description of how reduced fuel configuration calculations are carried out).

Calculations will be performed for the Boeing 777-200IGW class aircraft test study for a variety of fuel weights, starting from the maximum one. Table 3-3 shows the fuel weights that will be considered:

Table 3-3. Fuel weights used for reduced range configuration calculations, Boeing 777-200IGW class aircraft.

Fuel Weight 1 (maximum)	215000 lbs
Fuel Weight 2	185000 lbs
Fuel Weight 3	155000 lbs
Fuel Weight 4	125000 lbs
Fuel Weight 5	95000 lbs
Number of Fuel Weights Studied	5

A new, reduced aircraft range corresponds to each fuel weight. For each configuration the root bending moment will be reduced from 0% to 30% in 0.5% step increments, and take-off weight and fuel weight variations will be studied.

Appendix A.1 gives a sample input for the code. It corresponds to the Boeing 777-200IGW class aircraft test case for a reduced range configuration. The first part of the

input file is common for all studies, both maximum range and reduced fuel loads. The second part is simply the definition of the fuel loads that will be analyzed. In this sample input file only one reduced fuel load is studied (185000 lbs.).

Chapter 4 Results for the spanload optimization problem with a root bending moment constraint

Results are presented here using the FORTRAN code that has been developed which generates spanloads for a given aircraft configuration corresponding to different root bending moments, calculates wing weights using the structural model described before, and studies the effect the different lift distributions have on fuel weights and aircraft gross weight.

Studies have been performed on both Boeing 777-200IGW and Boeing 747-100 class aircraft.

4.1 Results for maximum range configurations

Boeing 777-200IGW and Boeing 747-100 type aircraft data are given in Tables 3-1 and 3-2, respectively. Note that the configuration under study is a maximum take-off weight, maximum range, maximum fuel arrangement. Other missions for the same aircraft will generate different results. As the root bending moment is decreased and new spanloads are calculated, the induced drag increases and the wing weight decreases. To compare induced drag increase to wing weight reduction as the root bending moment decreases, nondimensional parameters for both variables are developed as follows:

$$ind\_drag\_increase = 100 \times \frac{C_{Dinduced} - C_{Dinduced_0}}{C_{Dinduced_0}} \tag{4.1}$$

$$W_{wing}\_reduction = 100 \times \frac{W_{wing_0} - W_{wing}}{W_{wing_0}} \tag{4.2}$$

In these equations, $C_{Dinduced0}$ and W_{wing0} are the induced drag and wing weight corresponding to the aerodynamically optimum spanload, with no root bending moment constraint applied. Note that variations are expressed as a percentage change.

4.1.1 Results for the Boeing 777-200IGW type aircraft, maximum range configuration

Wing weight reduction and induced drag increase as a function of root bending moment reduction from the aerodynamic optimum value are shown in Figure 4-1 for the Boeing 777-200IGW type test case (input data shown in Table 3-1).

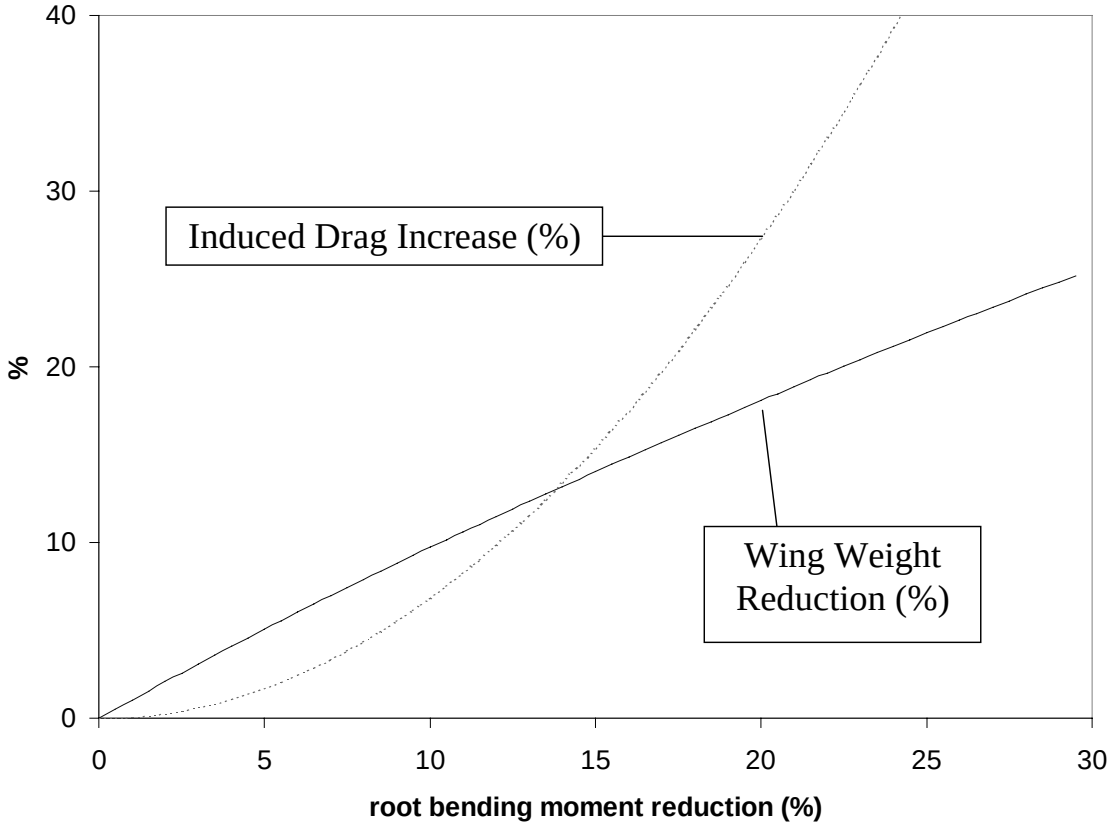

Figure 4-1. Wing weight reduction and induced drag increase versus root bending moment reduction. Boeing 777-200IGW type aircraft, maximum range configuration.

Wing weight reductions and induced drag increases correspond to equations 4.1 and 4.2 respectively.

The induced drag curve shows that the drag increase from the minimum induced drag point (that is, zero root bending moment reduction) is parabolic, with zero slope at the starting point, as expected, since that should mean that the zero root bending moment reduction point is in fact a minimum for induced drag. The induced drag increase curve turns out to be exactly parabolic for every aircraft and planform configuration.

The wing weight reduction curve is much more interesting. Note the nearly linear behavior of this line. Even when a structural model was used that calculates wing bending material weight and takes into account such diverse factors in wing weight calculations as engine inertia relief or the use of composite materials, the variation of wing weight with root bending moment seems to be almost linear.

It was presumed that the root bending moment constraint was a crude structural model from a first point of view. However, it has been shown that, at least for this test case, it turns out to be a quite good one, and no further structural models would in fact be needed.

It should be realized that the linearity of the wing weight reduction curve is in fact dependent on the test case, so that a different aircraft would yield a different curve. A wide variety of airplanes of different sizes, weights and mission ranges should be tested to prove that the linearity of the wing weight reduction versus root bending moment curve is in fact general, and that a straight line can be fit through this curve in all cases with a low loss in accuracy. If this presumption is true, the whole spanload optimization will only require the study of two values for the wing weight and induced drag, one for minimum induced drag (zero root bending moment reduction) and another for an arbitrary root bending moment reduction. Curves would then be fit through these two points and the whole optimization process could be greatly improved, since the need of making calculations covering a wide range of root bending moment reductions would no longer be necessary.

Induced drag and wing weight variations have been related to fuel and take-off weight changes. Fuel weight variations versus root bending moment reductions for the same test case are shown in Figure 4-2. Fuel weight is actually decreased when the root bending moment reduction is low (from zero to six percent), even when the induced drag is increasing. This is due to the rapid decrease in wing weight compared to the increase in induced drag for these low values of root bending moment reduction, leading to an essentially lighter aircraft with the same drag characteristics, so that less fuel is required to complete the mission. Nevertheless, when the root bending moment reduction becomes

high, the fuel weight increases sharply, and this will in fact limit the value beyond which a more triangular spanload will be beneficial.

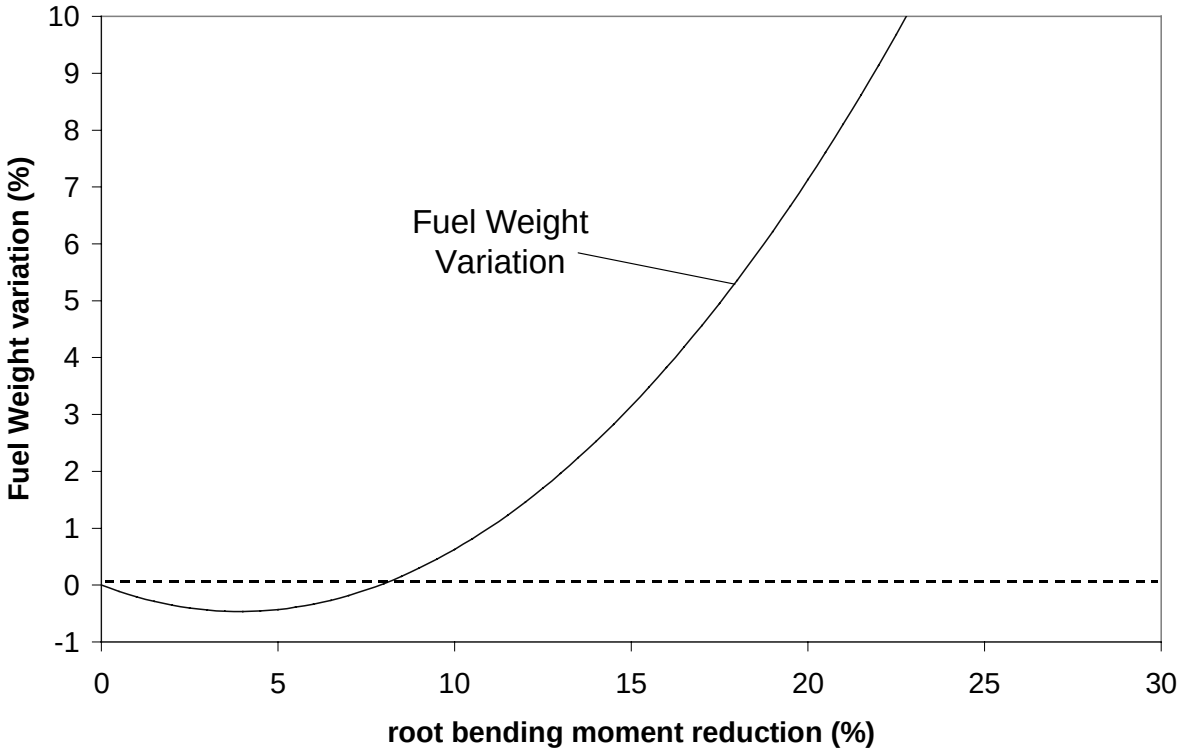

Figure 4-2. Fuel weight variation versus root bending moment reduction. Boeing 777-200IGW type aircraft, maximum range configuration.

Figure 4-3 is a plot of the variation of the sum of wing and fuel weights, also showing the variation of gross weight. These two curves are essentially the same plot, since the weight of the aircraft not covered by the wing and fuel weights was assumed to be constant. The minimum gross weight for the test case is found for a root bending moment reduction of about 10%. The spanload corresponding to this minimum gross weight is given in Figure 4-4, together with the lift distribution for minimum induced drag. Note that the maximum gross weight reduction obtained for this test case is small, yet non-negligible (close to 1%). For a long-range aircraft, like the Boeing 777-200IGW, any increase in drag would bring a large penalty in fuel weight, so that only a low root bending moment reduction would be beneficial. Low gross weight reductions are then expected for this type of airplane. For low range transport aircraft, where structures become more important than

aerodynamics, a larger root bending moment reduction will still produce benefits, and the total gross weight savings will be higher.

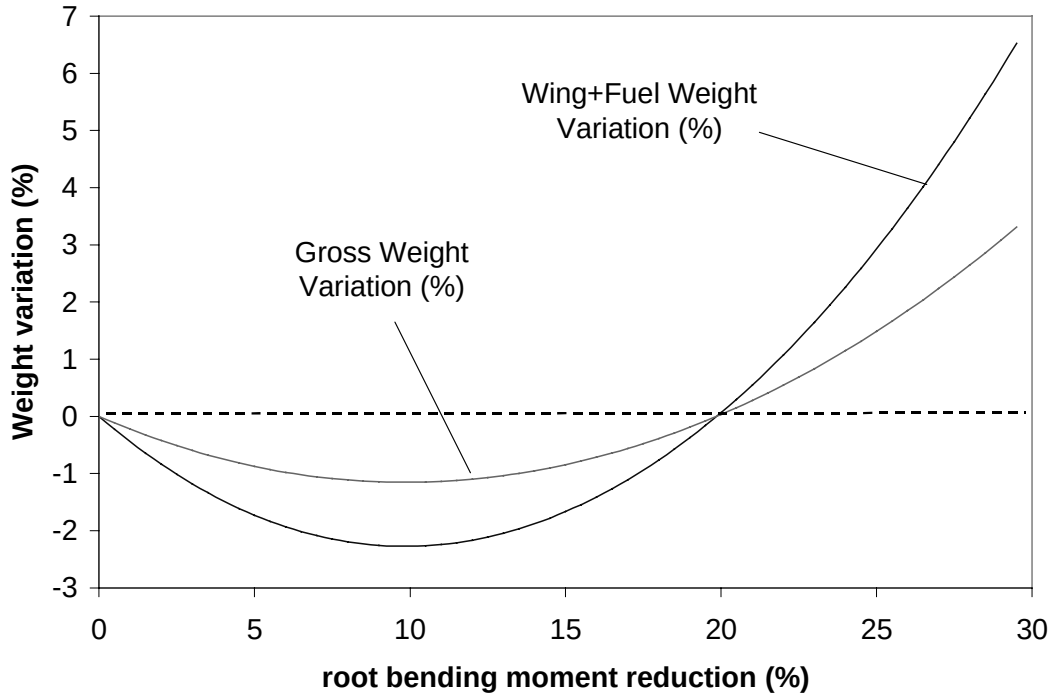

Figure 4-3. Wing plus fuel and gross weight variations versus root bending moment reductions. Boeing 777-200IGW type aircraft, maximum range configuration.

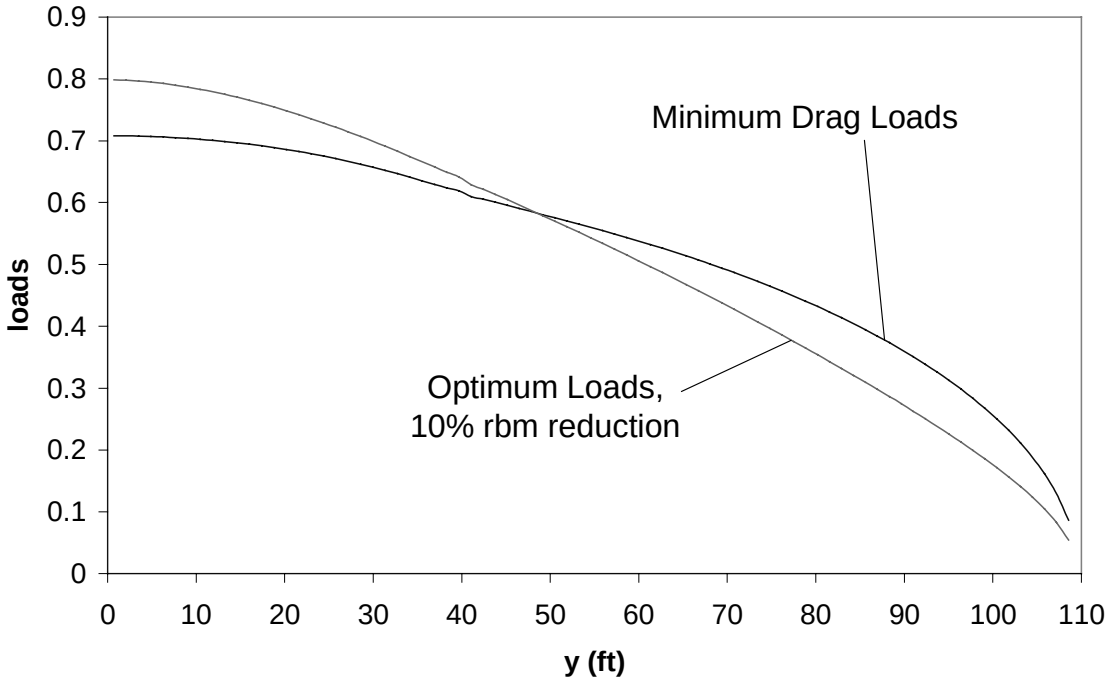

Figure 4-4. Span load distribution for minimum induced drag compared to optimum load distribution. Boeing 777-200IGW type aircraft, maximum range configuration

4.1.2 Results for the Boeing 747-100 type aircraft, maximum range configuration

The Boeing 747-100 class aircraft input data for maximum range configuration is given in Table 3-2. Figure 4-5 shows wing weight reduction and induced drag increase (equations 4.1 and 4.2) as a function of root bending moment reduction for this test case.

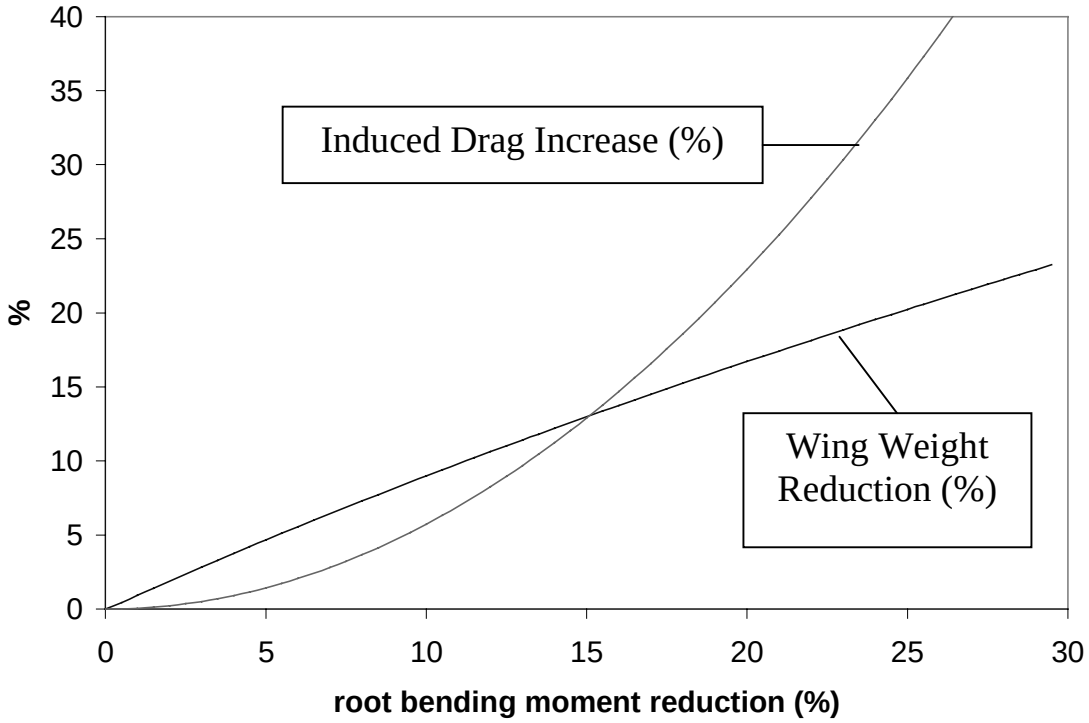

Figure 4-5. Wing weight reduction and induced drag increase versus root bending moment reduction. Boeing 747-100 type aircraft, maximum range configuration.

The induced drag increase curve is exactly parabolic with a zero slope for no root bending moment reduction (minimum drag). In this case, the wing weight reduction curve is also nearly linear, so that a straight line can be fit through this curve with a low loss in accuracy. However, a general conclusion about the linearity of this curve cannot yet be achieved, since only two test cases have been studied.

Comparing figures 4-1 and 4-5, it can be seen that the wing weight reduction with root bending moment reduction is lower for the 747 class aircraft than for the 777 configuration. This will make total weight reductions smaller. This lower wing weight reduction can be explained by looking at the FLOPS wing weight equation:

$$W_{wing} = \frac{GW \cdot w_1 + w_2 + w_3}{1 + w_1} \tag{2.4}$$

Here, w_1 (essentially the bending material weight) changes the same for both airplanes due to root bending moment changes. The next term, w_2, is a correction for flap area, and it should not make any difference between aircraft. The difference must lie then in the aircraft *GW* and w_3. This last term, w_3, implements a weight correction for wing area and the amount of composites used in the wing construction. In the studies performed here, it was assumed that no composite materials were used in the wing construction of any airplane. w_3, however, has a larger value for the Boeing 747-100 class configuration due to its larger reference area. On the other hand the gross weight of the Boeing 747-100 type aircraft is also larger (see tables 3-1 and 3-2). As a result, with a certain reduction in bending material weight (reduction in w_1), the wing weight of the bigger, heavier aircraft will be reduced by a lower amount. Note that with a similar bending material weight reduction the numerator of equation 2.3 diminishes less in comparison to the denominator for a higher *GW* and w_3.

Figure 4-6 shows fuel weight variation as a function of root bending moment reduction for the Boeing 747-100 test case. Comparing Figures 4-2 and 4-6, the percent fuel weight increase for a given root bending moment reduction is very similar for both test cases. Also note that the initial maximum fuel weight for both airplanes is similar (215000 lbs. for the 777-200IGW class aircraft and 275000 lbs. for the 747-100 type). This makes the non-dimensionalization to calculate percent variations similar. But it was noted that the wing weight reduction is lower for the heavier, 747-100 type aircraft. It seems that this aircraft should have a greater increase in fuel drag because the benefits of wing weight reduction are not so large. This is where aircraft range comes into play. For a lower range aircraft, like the Boeing 747-100, any increase in induced drag caused by a root bending moment reduction will need a lower fuel increment to complete the required range, since the incremental drag is applied through a shorter distance. The result is that the lower benefit that the Boeing 747-100 class aircraft receives from lower wing weight reductions is compensated by larger fuel savings due to its lower range.

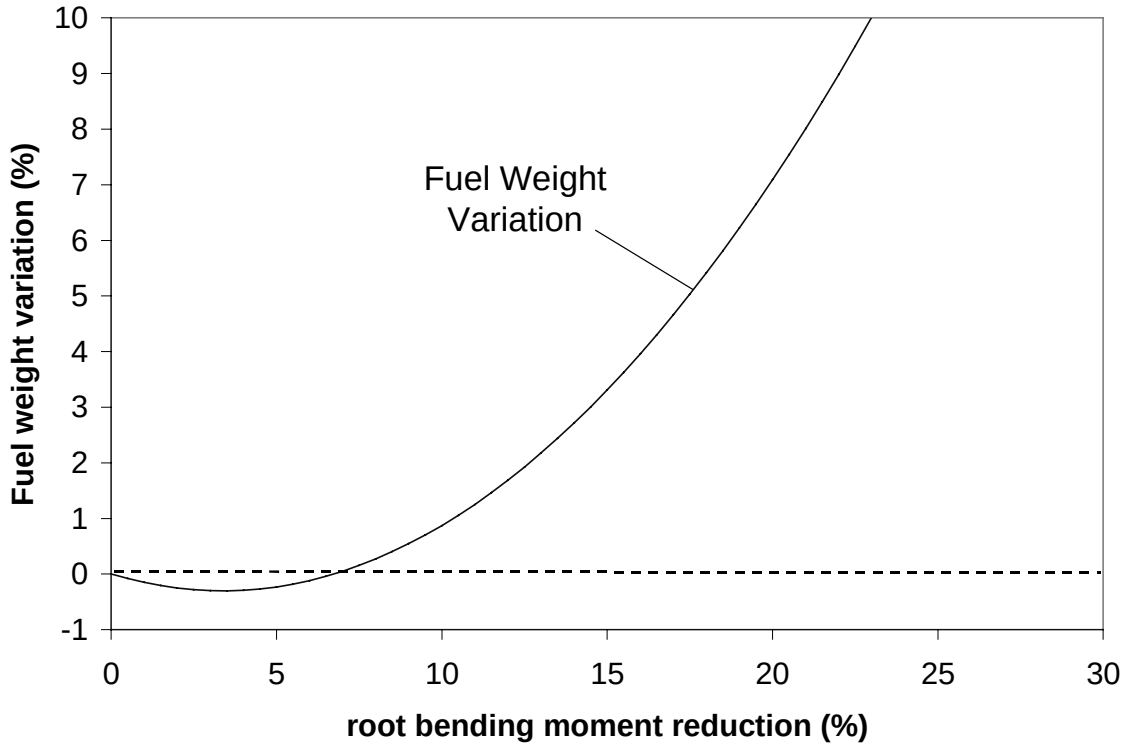

Figure 4-6. Fuel weight variation versus root bending moment reduction. Boeing 747-100 type aircraft, maximum range configuration.

Wing plus fuel weight variations and gross weight variations for the Boeing 747-100 class aircraft are shown in figure 4-7. As in the previous case, both curves reflect the same changes since the weight not covered by wing or fuel weight is assumed to be constant. Figure 4-7 shows that the Boeing 747-100 class configuration has lower maximum gross weight reductions than those obtained for the Boeing 777-200IGW class aircraft. For a 20% root bending moment reduction, for example, the wing weight reduction for the Boeing 747-100 class aircraft is 17%, compared to the 18.5% wing weight reduction that is achieved for the Boeing 777-200IGW. It has been shown that fuel weight variations are almost the same for both aircraft. The difference is then in the wing weight variation. The lower wing weight reduction experienced by the Boeing 747-100 class airplane results in lower gross weight reductions. Besides, for the Boeing 777-200IGW, the ratio of wing weight to aircraft gross weight is about 0.14, that is, wing weight accounts for 14% of the maximum take-off weight. For the 747-100 class aircraft, however, wing weight accounts only for 11% of aircraft gross weight. As a result, any weight saving obtained due to wing weight reductions will reflect less in the 747-100

aircraft gross weight. Optimum load distributions for this case (corresponding to a root bending moment reduction of about 8%) are shown in figure 4-8, together with minimum drag loads.

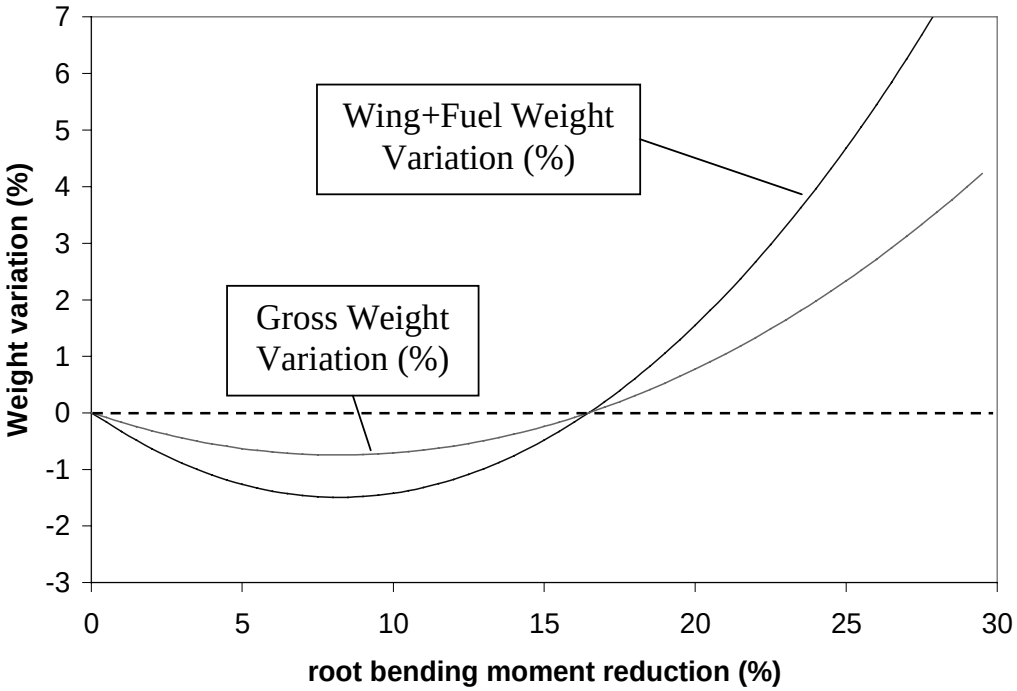

Figure 4-7. Wing plus fuel and gross weight variations versus root bending moment reductions. Boeing 747-100 type aircraft, maximum range configuration.

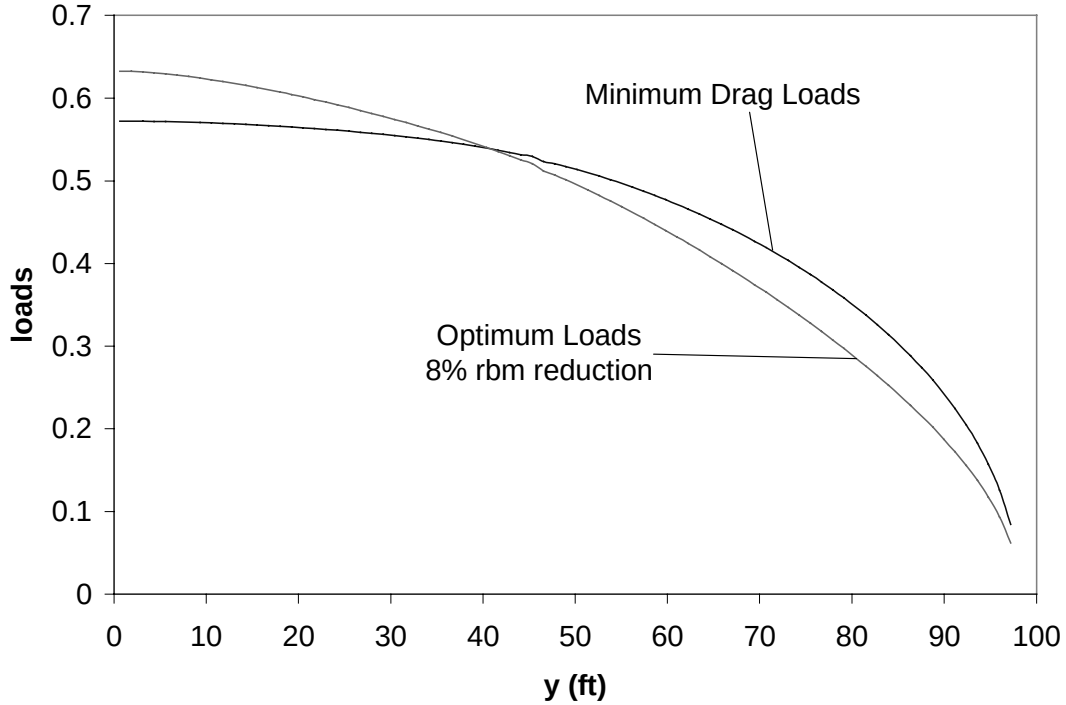

Figure 4-8. Span load distribution for minimum induced drag compared to optimum load distribution, Boeing 747-100 class aircraft.

It has been shown that the optimum spanload of a certain aircraft configuration can be found, that is, the spanload that will produce a maximum reduction in gross weight. The maximum gross weight reductions are dependent on such different things as aircraft range, gross weight, wing reference area and percent of the gross weight covered by the wing weight. These test cases studied are maximum take-off weight, maximum range configurations. It is now necessary to study the effect of the different spanloads generated using the root bending moment constraint on reduced fuel, reduced range configurations.

4.2 Results for reduced range configurations

A Boeing 777-200IGW class aircraft test study will be performed for reduced fuel loads. In this case the spanload is optimized for a reduced range, while the aircraft still meets the full, long range mission requirement as a constraint. In minimizing the take-off weight at a shorter range, a penalty will be incurred for the full range mission compared to the basic aero-alone optimum weight. The relative magnitude of the benefit for shorter range flight compared to the penalty at the full mission range is found as part of the results, and can be used in determining the best design target choice. The input data for this study is given in Table 3-1, and the different mission fuel weights are given in Table 3-3. Table 4-1 shows these fuel weights again, together with the mission range to which they correspond.

Table 4-1. Fuel weights and ranges for reduced fuel configurations. Boeing 777-200IGW class aircraft.

Case study	Mission Fuel	Mission
1	215000 lbs.	8508 nm
2	185000 lbs.	7446 nm
3	155000 lbs.	6346 nm
4	125000 lbs.	5205 nm
5	95000 lbs.	4025 nm

Note that the mission range calculated for the new mission fuel weights is found under the assumption of a minimum drag load distribution, with no root bending moment constraint (see Figure 2-7)

The study is then performed reducing fuel weights so that ranges vary approximately from 4000 to 8000 nautical miles, which are typical mission ranges for the 777-200IGW. Wing weights for different root bending moment reductions will have the same value as those obtained for the maximum range configuration since the aircraft still has to meet this maximum range requirement and has to comply with the maximum range weights, so that its variation will not be shown here.

Appendix A.2 shows the output files that are generated by the code. These output files correspond to the input data given in Appendix A.1, that is, to the Boeing 777-200IGW type test case with a reduced fuel load of 185000 lbs., corresponding to test case 2 in Table 4-1. Five different output files are generated. *loads.out* give the minimum drag load distribution and the optimum load distribution for the reduced range configuration. *ww-id.out* gives the wing weight and induced drag coefficient for the reduced fuel load for different values of root bending moment reduction (recall that wing weight is the same for all missions). *wred-dinc.out* is the same file but results for wing weight and induced drag are given as percent variations from the initial, minimum drag value. Finally, *weights.out* gives wing, fuel, wing plus fuel, and take-off weights for the reduced fuel load configuration. Note that the fuel weight subtracted from the maximum range configuration is added back in this file, for comparison purposes with other fuel load configurations. *weight-variation.out* gives the percent variations for these weights.

Figure 4-9 shows the fuel weight variation as a function of root bending moment reduction for different mission ranges. Since the aircraft has now a different initial fuel load for each configuration, the non-dimensionalization performed to obtain percent fuel weight variation can be confusing. The fuel weight variation will be given by:

$$Fuel\_Weight\_Variation = \frac{W_{FUEL}(new) - W_{FUEL}(initial)}{W_{FUEL}(\max\_range)} \tag{4.3}$$

Let us assume that the Boeing 777-200IGW class configuration is being studied, with a reduced fuel load equal to 155000 lbs. (case study 3 in Table 4-1). For this case, $W_{FUEL}(initial)=155000$ *lbs.*, $W_{FUEL}(max\_range)=215000$ *lbs.*, equal for all cases, and finally, $W_{FUEL}(new)$ is the new fuel weight calculated for the specific mission for a given

root bending moment reduction. Starting from the initial fuel weight for the reduced range mission, the root bending moment is reduced from the minimum drag configuration, which changes fuel weight to a new value $W_{FUEL}(new)$. The fuel weight variations are non-dimesionalized in all cases by the same fuel weight (maximum range configuration fuel weight).

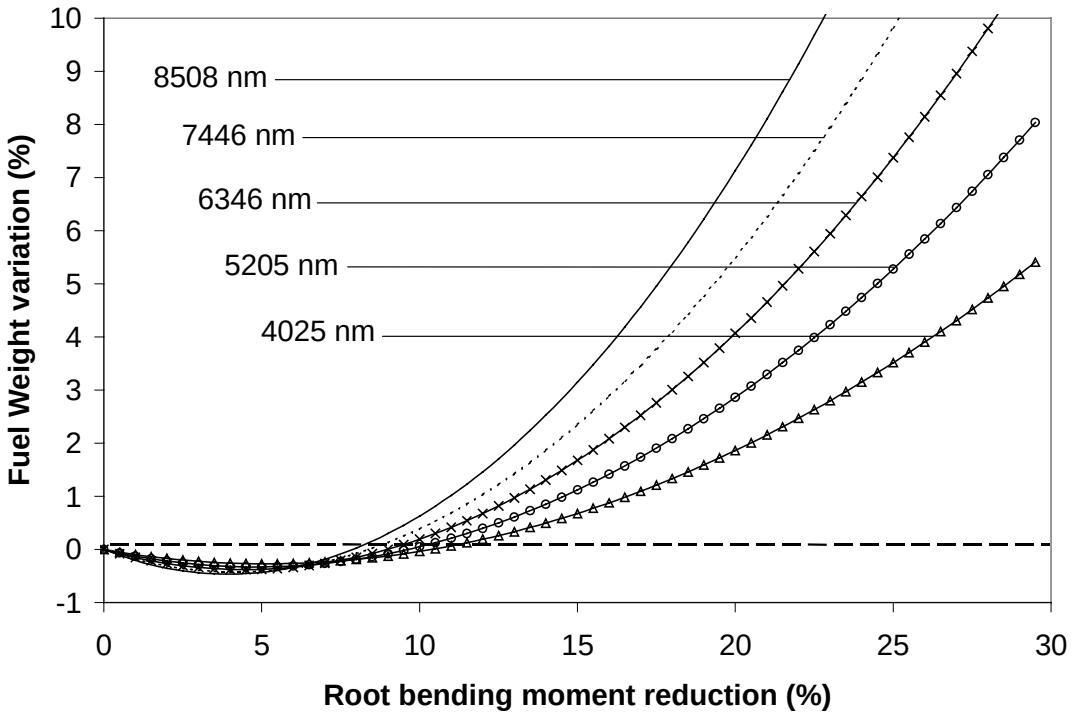

Figure 4-9. Fuel weight variation with root bending moment reduction for different mission ranges. Boeing 777-200IGW type aircraft.

In Figure 4-9, all the curves appear close to each other when the root bending moment reduction is low, but for high values of root bending moment reduction (more triangular spanloads), the needed fuel weight to complete the mission range increases much more sharply for high mission ranges, and this will be reflected in aircraft take-off weight.

Figure 4-10 represents the variation of the sum of wing and fuel weights as a function of root bending moment reduction. Figure 4-11 depicts take-off weight variation. Both of these percent variations are non-dimensionalized by dividing the weight difference by the wing plus fuel weight or take-off weight corresponding to the maximum range configuration. Again figures 4-10 and 4-11 are essentially the same graph, since wing and

fuel weights are the only weights that change in our model. The general result is that a larger take-off weight reduction can be achieved for lower ranges, also corresponding to a higher root bending moment reduction and a more triangular lift distribution. This means that the take-off weight savings due to reduced wing weights become more important than the fuel weight increments due to increased drag for lower mission ranges, as expected. Take-off weight reductions for a reduced fuel weight corresponding to a range of 4025 nm. are almost 2%, doubling the reductions that can be obtained for the maximum range configuration. However, this take-off weight reduction is obtained at a root bending moment reduction of about 22%. This will make the optimum load distribution very triangular, with a high load near the wing root. Stall at the inboard part of the wing will be likely to occur when the aircraft is at the 2.5g load condition. It was noted earlier that wing root stall will be an important factor for determining the optimum lift distribution that can be achieved. In this study, no constraints on section lift coefficient are imposed to account for this effect, but it must be realized that in some cases an optimum spanload corresponding to a high root bending moment reduction will not be actually possible.

It should also be realized that the optimum load distributions for short range configurations can result in weight penalties for the maximum range mission. Figure 4-11 shows the maximum take-off weight reduction for the 4025 nm. mission range case, corresponding to a 22% root bending moment reduction. Weight savings when performing this reduced mission range are given by Δ_{saving} in Figure 4-11 (around 2%). However, for the same spanload, if the maximum mission range is performed, a take-off weight penalty of $\Delta_{penalty}$ (around 0.5%) will be experienced. It is then important to choose an optimum spanload that represents a compromise between weight savings for the different mission ranges that the aircraft will perform.

Care must also be taken with respect to fuel weight when choosing the desired lift distribution. In this test case, for example, choosing a spanload that will give optimum gross weight savings for reduced mission ranges (for example a 22% root bending moment reduction spanload) will increase the required fuel weight by about 10% when the maximum mission range is performed (see Figure 4-9).

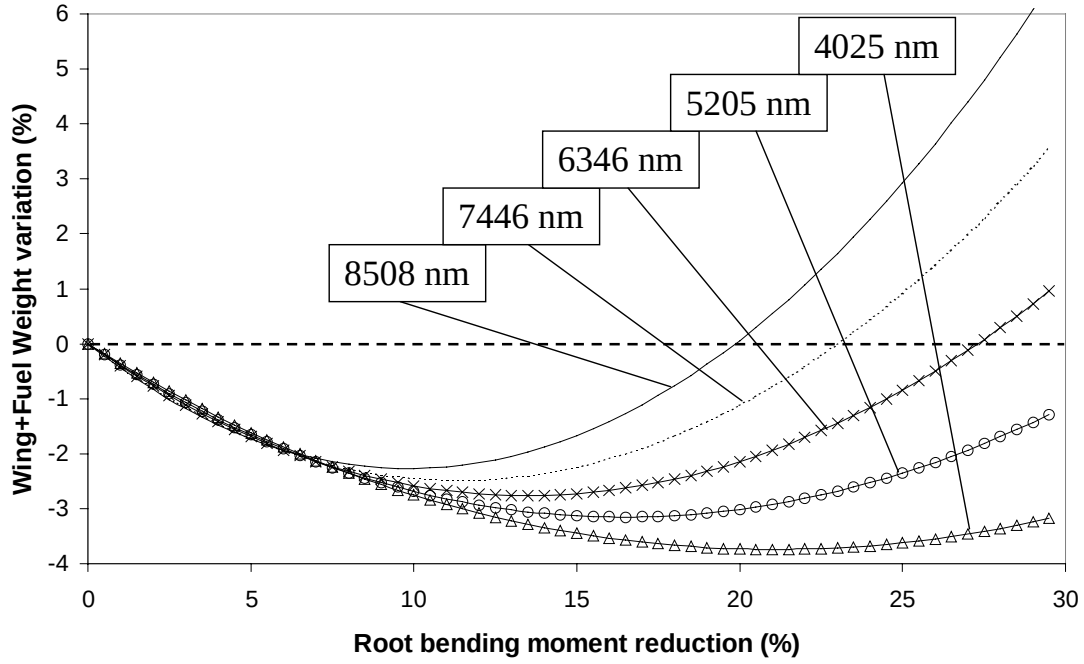

Figure 4-10. Wing plus fuel weight variation versus root bending moment reduction for different mission ranges. Boeing 777-200IGW type aircraft.

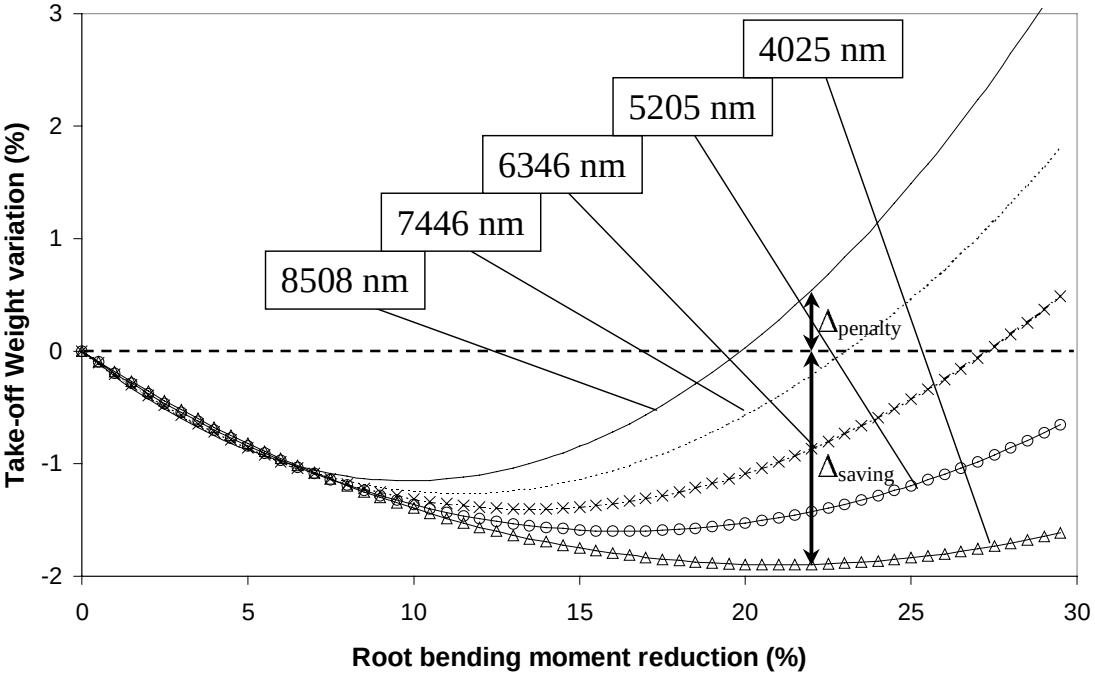

Figure 4-11. Take-off weight variation versus root bending moment reduction for different mission ranges. Boeing 777-200IGW type aircraft.

Chapter 5 Methodology For Spanload Optimization In Formation Flight

5.1 Objective

Airplanes flying in close formation will obtain important performance benefits as a result of the induced drag reduction they can experience in these configurations. The downwash distribution that each aircraft causes on itself (due to lift) can be compensated by the upwash emanating from the tips of the accompanying airplanes, causing an induced drag reduction. Several formation configurations are possible, in which the arrangement of the aircraft in the formation can be varied to obtain the desired drag reductions on specific airplanes. The most common formation flight configuration is an arrow formation. It is a symmetric configuration consisting of one central airplane (generally leading the formation), with several aircraft on its sides forming a V-shape. Migrating birds usually fly in such V-formations. Figure 5-1 shows an example of this type of configuration.

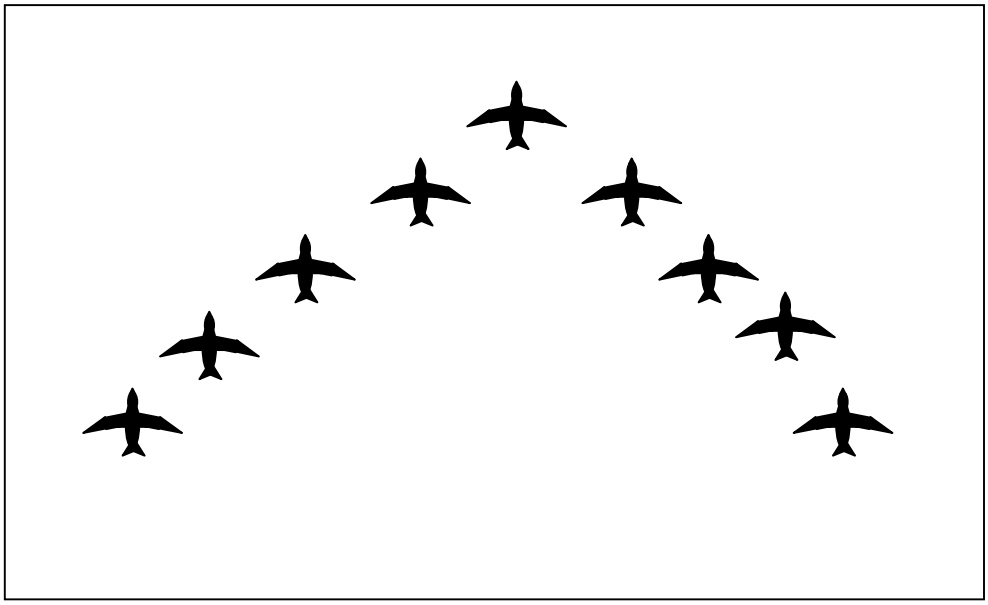

Figure 5-1. Birds flying in a V-shaped formation

When dealing with arrow formations, all the aircraft that are off-center will have an asymmetrical load distribution due to the upwash distribution coming from the central

airplane. Of course, the rolling moment coefficient should equal zero for each and every aircraft flying in the formation. Feifel and Maskew have made quantitative studies for determining induced drag savings in aircraft formations (see section 1.3). They used in their studies aircraft of completely known geometry, that is, the twist distribution was specified for the wings (no twist for both authors) and the rolling coefficient was insured to be zero by the differential lift caused by ailerons, again, of known geometry.

A different approach was followed here, where no twist or camber distribution is known before-hand, and the loads are calculated to obtain minimum induced drag for the whole formation under individual aircraft constraints of lift coefficient, pitching moment coefficient and rolling moment coefficient. Then, Feifel[15] and Maskew[16] treated basically an analysis problem with known geometry, while this paper will address a design problem for which the twist or camber distribution is not prescribed. Instead, the actual geometry must be found after the calculations are made to produce the required load distributions. Attacking the problem in a design mode will give maximum achievable benefits for the whole formation.

5.2 General Approach

Airplanes in formation flight can achieve large advantages in induced drag reduction as a result of the influence that the upwash from other aircraft exert on them. A code has been developed to obtain the optimum load distributions for a group of airplanes flying in V-formation. Only aerodynamic considerations are taken into account, with no structural constraints. The analysis carried out in chapters 2 to 4 showed that a structural constraint could produce spanloads that, although increasing induced drag, can achieve performance benefits (take-off weight savings). In this case, an applied structural constraint will not be so useful. First of all, the calculations now depend on a larger number of variables (like the relative spacing between aircraft), and an additional constraint can hide general trends. Secondly, the optimum load distribution for each aircraft is dependent on airplane

separation. For this reason, wing weight calculations will become confusing (a new wing weight would be obtained for each aircraft position).

The main purpose of the code developed is to find the optimum spanload that gives minimum induced drag for the whole system of airplanes. The induced drag for each aircraft alone will also be of primary importance to study the effects of relative position on individual aircraft performance. Induced drag will be the measure of effectiveness, both for the formation and for the single aircraft.

An important aspect of the code developed and the studies performed must be pointed out. The flow is being modeled as potential, inviscid flow. A potential flow vortex model representation is being used. These models give usually quite good results for regions that are not near the vortex cores, which are small, where viscous effects become important.

A description of the aerodynamics code used for optimum load distribution design and induced drag calculations follows here.

5.3. Description of the aerodynamics code for spanload optimization in formation flight

The same aerodynamics code (see section 2.3) written by Grasmeyer[22] (*idrag* version 1.1) was modified here. This code applies the theory developed by Blackwell[19], Lamar[20], Kuhlman[21] and Kroo[6]. This theory is a discrete vortex method with a Trefftz plane analysis to calculate spanloads corresponding to the minimum induced drag of the configuration. Recall that the code includes an optional trim constraint, in which the pitching moment coefficient can be fixed for several lifting surface configurations. The minimum induced drag spanload for a specific value of lift coefficient and moment coefficient is calculated with the method of Lagrange multipliers.

Several modifications have been made to this code to include the capability of analyzing several aircraft configurations.

First of all, a lift coefficient constraint is now necessary for each aircraft, and a trim constraint on the rolling moment and the pitching moment of individual aircraft in the formation will also be required.

The code now assumes that the configuration is always symmetric, so that the geometry of V-formations can be specified only with the central aircraft and one side of the formation. The central aircraft, due to symmetry, will have an equal load distribution on both sides. Off-centered airplanes, on the contrary, will have asymmetrical spanloads because the formation does not meet the symmetry condition from their point of view. This asymmetry causes these airplanes to have non-zero rolling moment coefficients about their centers of gravity, so that an extra constraint to maintain rolling moment coefficient for off-centered aircraft equal to zero has also been imposed.

Optimum load distributions for a group of airplanes flying in V-formation is found using the method of Lagrange Multipliers under the constraints of a specified lift coefficient for each aircraft, a pitch trim constraint for each one of them, and a rolling moment coefficient constraint for all except the central one.

Another major modification has been introduced in the code to allow the analysis and induced drag calculations of separate airplanes.

The code used (*idrag* version 1.1) is merely an implementation of the equations used by Blackwell[19]. This theory makes use of Munk's Stagger Theorem[26]. According to the theorem, the induced drag of the whole configuration is independent of the streamwise location of the point of application of the loads. Once the optimum load distribution for the whole configuration has been found, that will always be the optimum no matter what changes in the streamwise location of different aircraft in the formation are made, and the formation induced drag will always remain the same. For this reason, Blackwell's theory assumes that all lifting surfaces are located at the same streamwise position, because optimum loads and total induced drag remain the same.

For a formation configuration, where the interest is not only centered on the induced drag as a whole, but rather on the induced drag of each airplane, Blackwell's theory alone

is not applicable, since the induced drag of each lifting surface is dependent on its streamwise position (the downwash distribution is dependent on streamwise position too) although total induced drag of all the aircraft is not.

The code was modified by assigning a streamwise coordinate position to each discrete vortex and control point. Control points are points on the lifting surfaces where downwash angles are calculated, in the approach used in this thesis they are located at the midpoint of each discrete bound vortex line. The influence of each trailing vortex on each control point was modified applying the Biot-Savart law in the streamwise direction and the influences of the bound vortex lines on the control points were also added. In that way, optimum spanloads are still independent of streamwise vortex locations, but individual downwash angles and induced drags have a strong dependence on movements along this axis (total induced drag of the complete system remains unchanged).

A description of the implementation of the rolling moment constraint, together with the methodology for the modifications introduced to Blackwell's theory follows in the next sections.

In section 2.3, it was shown that the accuracy that can be obtained in induced drag and spanload calculations using a discrete vortex model is dependent on the number of vortices used in the discretization. The larger the number of vortices, the greater the accuracy and the computational cost. The analysis performed by Grasmeyer[22] on the convergence of the optimization when the number of vortices is increased represents a good guideline for typical spanloads. These typical spanloads are, for example, the type of spanload that was dealt with in the first part of this thesis (Chapters 2, 3 and 4). For this kind of load distributions, the relative variation in load magnitude from vortex to vortex is small. That is, they are not rapidly changing spanloads as a function of spanwise distance.

When optimizing spanloads for a formation flight configuration, it will be shown that in some cases the optimum load distributions are quite different from the elliptical ones. In these configurations, load distributions with rapidly changing spanloads as a function of spanwise distance can be encountered, especially near the wing tips where peaks in the

load distributions can be obtained. The magnitude and shape of the optimum spanloads in formation configurations will be shown to be dependent on the actual configuration and the relative spacing between aircraft. Because of this, a general convergence study cannot be performed. Instead, for each configuration, the number of vortices must be increased until convergence in the results is achieved.

5.3.1 Rolling moment coefficient constraint formulation

The rolling moment coefficient constraint has been implemented in the *idrag* code using the method of Lagrange multipliers. The equation used for rolling moment coefficient calculations is:

$$C_l = \int_{s_{ref}}^{s_{final}} \frac{c_l}{b_{ref}} \left[\left(y - y_{ref} \right) \cos\theta + \left(z - z_{ref} \right) \sin\theta \right] ds \tag{5.1}$$

The nomenclature here can be confusing. The rolling moment coefficient is represented as C_l, and it is the term on the left side of the equal sign for equation 5.1. On the other hand, the lower case term c_l that appears on the right hand side of this equation represents the sectional, two-dimensional lift coefficient. In the discrete vortex model equation 5.1 takes the form:

$$C_l = \sum_{j=1}^{m} \frac{\{c_n c\}_j}{c_{avb}} s_j \left[\frac{1}{b_{ref}} \left\{ \left(y_j - y_{ref} \right) \cos\theta_j + \left(z_j - z_{ref} \right) \sin\theta_j \right\} \right] \tag{5.2}$$

The geometry and definitions for the different terms in this equation is the same as for the root bending moment constraint in Chapter 2 (see equation 2.3 and Figure 2-1). In fact, equation 5.2 is exactly the same as equation 2.3. Both equations represent the lift coefficient at each station multiplied by the moment arm about the aircraft centerline. This is the moment caused by the lift distribution about this line, representing both the root bending moment coefficient and the rolling moment coefficient. Of course, there must be something that helps differentiate between both constraints, since they are not the

same. For the root bending moment constraint calculations, only one side of the wing is included. This is the same as taking the absolute value of all the moment arms in equation 2.3, calculating the root bending moment coefficient over the whole wing, and dividing by 2 (note that symmetric load distributions were studied in Chapters 2 to 4). For the rolling moment coefficient, the whole wing must be included when calculations are performed with equation 5.2. That way, the left side rolling moment must balance the moment caused by the wing right side.

The rolling moment coefficient constraint is applied to the off-centered airplanes, since they are the ones that will have asymmetrical load distributions. Only one side of the central aircraft is specified in the code, so that this constraint cannot be applied here. However, there is no need to apply the rolling moment constraint to this aircraft since symmetry insures a zero rolling coefficient.

5.3.2 Methodology for changes made to Blackwell's theory

5.3.2.1 Brief description of Blackwell's theory

The coordinate system used by Blackwell was already shown in figure 2-1. This Figure will be repeated here for convenience in Figure 5-2.

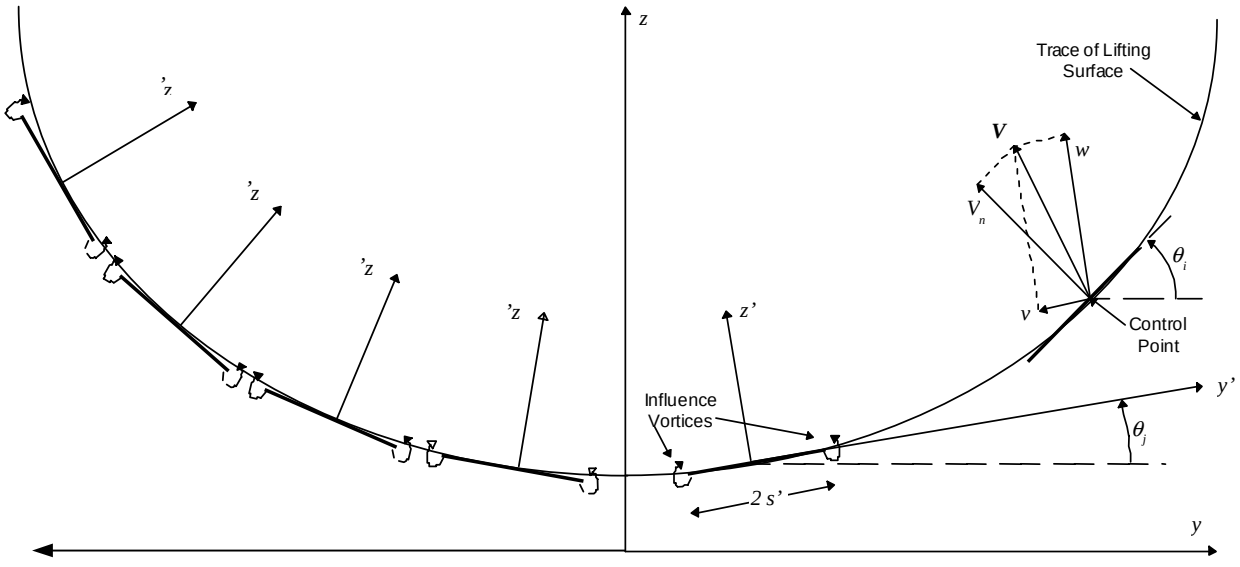

Figure 5-2. Discrete vortex method coordinate systems.(Ref 19)

Two coordinate systems are used in this method. The first is the traditional aerodynamic reference frame, with the *x*-axis pointing to the rear of the aircraft along the centerline, the *y*-axis pointing starboard, and the *z*-axis pointing up. The second is a set of local reference frames for each vortex element. Figure 5-2 corresponds to the lifting surface projection on the Trefftz plane. The Trefftz plane is a plane located at an infinite distance downstream of the lifting surface.

Each aerodynamic surface is represented by a set of discrete horseshoe vortices. The induced drag is then calculated in the Trefftz plane as a function of the velocity induced by the trailing segments of the horseshoe vortices.

Munk's stagger theorem[26] establishes that the minimum induced drag and the corresponding load distribution for the entire system are independent of the streamwise location of the point of application of the loads. For this reason, Blackwell assumes that all the discrete horseshoe vortices are at the same streamwise location as shown in Figure 5-3, because loads and total induced drag will remain the same. In Figure 5-3, the direction of the circulation for each discrete vortex is given by the right hand rule in the direction pointed by the arrows.

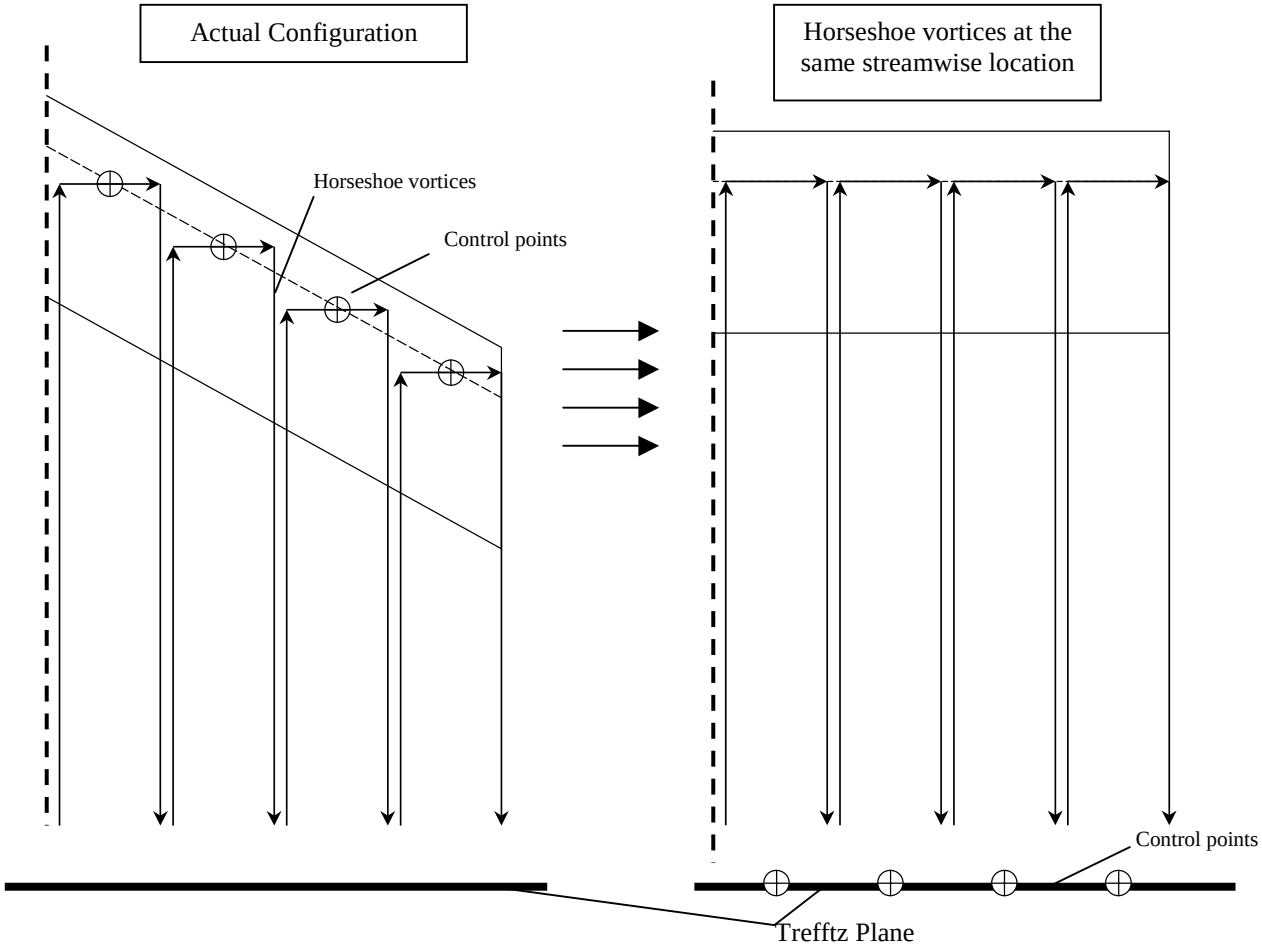

Figure 5-3. Horseshoe vortex discretization and streamwise vortex assumption in Blackwell's theory

The induced drag caused at each control point (control points are located at the Trefftz plane) by a trailing vortex is given by the Biot-Savart law. Since control points are located at a far downstream distance the Biot-Savart law reduces to:

$$V_{induced} = \frac{\Gamma}{2\pi h} \tag{5.3}$$

In equation 5.3, the induced velocity caused at the control point is perpendicular to the plane formed by the trailing vortex filament and the control point, and h is the perpendicular distance between them, as shown in Figure 5-4.

.

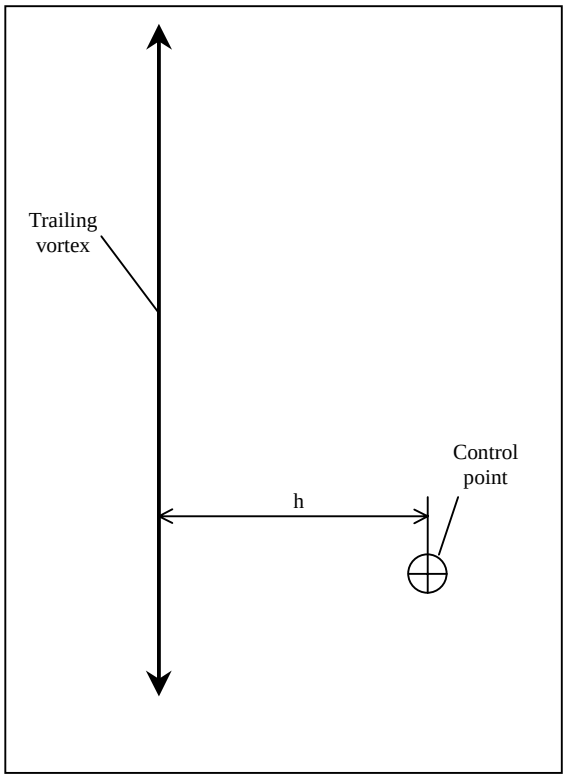

Figure 5-4. Geometry for induced velocity caused by a trailing semi-infinite vortex on a control point located at an infinite downstream distance.

Since all the control points are now located at a far downstream location (in the Trefftz plane), the bound vortices will not produce any downwash or upwash velocity on the control points and they do not need to be taken into account.

The equations describing the induced velocities in the Trefftz plane at a control point P(∞, y_i, z_i) by a horseshoe vortex located in the real plane at a point at P(x_j, y_j, z_j) are given below[19] (from the Biot-Savart law). Note that the geometry corresponds to Figure 5-2.

$$\frac{u_i}{V_\infty} = 0 \tag{5.4}$$

$$\frac{v_i}{V_\infty} = -\frac{1}{2\pi}\frac{\Gamma_j}{V_\infty}\left(\frac{z'}{R_1} - \frac{z'}{R_2}\right) \tag{5.5}$$

$$\frac{w_i}{V_\infty} = \frac{1}{2\pi}\frac{\Gamma_j}{V_\infty}\left(\frac{(y' - s')}{R_1} - \frac{(y' + s')}{R_2}\right) \tag{5.6}$$

where:

$$R_1 = (z')^2 + (y' - s')^2 \tag{5.7}$$

$$R_2 = (z')^2 + (y' + s')^2 \tag{5.8}$$

$$y' = (y_i - y_j)\cos\theta_j + (z_i - z_j)\sin\theta_j \tag{5.9}$$

$$z' = -(y_i - y_j)\sin\theta_j + (z_i - z_j)\cos\theta_j \tag{5.10}$$

Normal induced velocities are found with the equation:

$$\frac{V_{n_i}}{V_\infty} = \frac{w_i}{V_\infty}\cos(\theta_i - \theta_j) - \frac{v_i}{v_\infty}\sin(\theta_i - \theta_j) \tag{5.11}$$

and the induced drag coefficient is found by

$$C_{D_i} = \sum_{i=1}^{m}\frac{V_{n_i}}{V_\infty}\frac{(c_n c)_i}{c_{avg}}s_i \tag{5.12}$$

Although this theory is good for total induced drag and optimum spanload calculations, it does not give the distribution in induced drag.

5.3.2.2 Changes necessary to Blackwell's theory

It is true that the theory described above can give the induced drag coefficient and the optimum load distributions for any configuration, independently of the given number of lifting surfaces under study. That is, even if several aircraft flying in formation are analyzed, this method will be able to give the total induced drag and the optimum spanloads for all airplanes. However, it will not be able to find the induced drag of each separate lifting surface or airplane.

Moving discrete vortices to the same streamwise position simplifies the calculations because bound vortex effects are not needed and the Biot-Savart law has a quite simple form for this case (equation 5.3). This discrete vortex movement has no effect on total drag or optimum spanload by virtue of Munk's Stagger Theorem[26]. However, this does have an effect on the individual induced velocities at each control point, and, in turn, on the individual induced drags. A discrete vortex located far aft of the control point will obviously exert a very low influence on this control point. In contrast, if the control point is located aft of the discrete vortex it should feel a higher influence (the trailing vortices extend to infinity).

Since individual induced drags are dependent on vortex streamwise positions, and in a formation flight study the interest lies in the induced drag calculations for individual airplanes, the streamwise locations of individual vortices must be incorporated in the method. That is, the actual configuration must be studied. Vortex positions must not be moved to the same streamwise location.

Figure 5-5 shows an actual wing configuration in which the discrete vortices are located at their corresponding positions. If several aircraft are analyzed, they can now be separated in the streamwise coordinate, and induced drag variations can be obtained as this streamwise distance is changed.

Note from Figure 5-5 that the control points are now located at the midpoint of the bound vortex lines, and not in the Trefftz plane. It should also be noted that the bound vortex lines are aligned in a direction perpendicular to the incoming flow. They are not aligned with the wing quarter chord line. When the bound vortex lines were located in the same direction as the quarter chord line, results became inconsistent. It was then determined experimentally that the right way of orienting bound vortices is as shown in Figure 5-5, confirming the theoretical results by Tulinius[27].

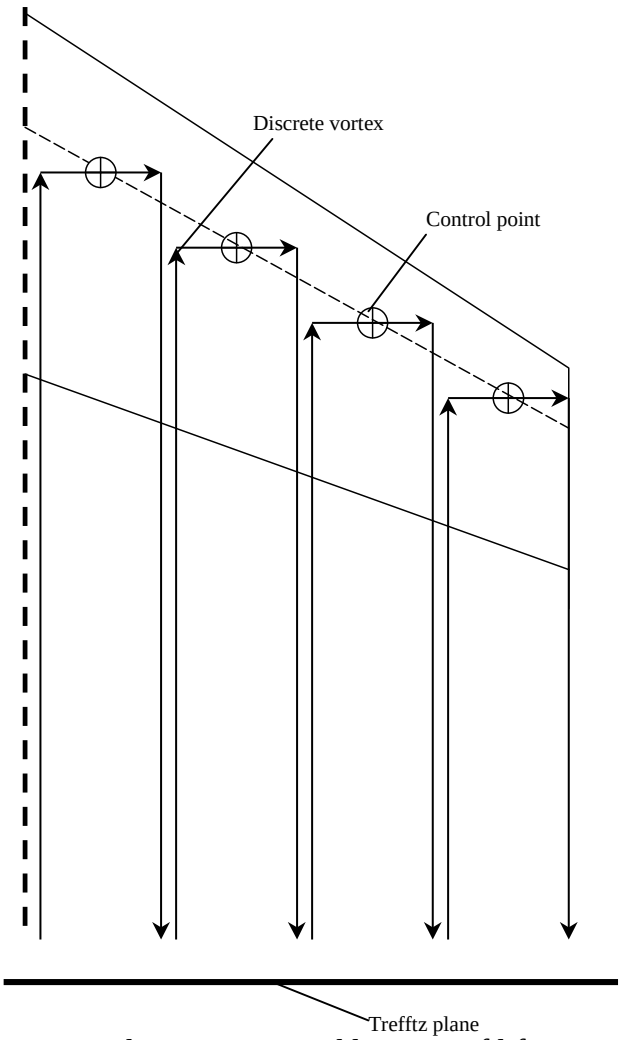

Figure 5-5. Vortex discretization and location of lifting surface with modified aerodynamic theory.

The vortex strengths to obtain minimum drag using this nearfield formulation have been found to give the same values obtained with the farfield calculation. However, the nearfield formulation allows us to find the distribution of induced drag using the local induced flowfield angle. In making this calculation, the induced angle of each control point on itself is taken to be identically zero. This assumption is required to make the nearfield and farfield calculations identical. The theoretical foundation remains to be established. The load at each wing station is assumed to be applied at the bound vortex. Once the induced angle is known for each control point, the induced drag at each station

is simply this induced angle times the corresponding load. The induced drag calculations are then straightforward. However, there is a drawback: a relation between the loads at each station and the wing geometry (twist or camber) at that station cannot be established. That is, it is not possible to determine the twist or camber distribution that is required to obtain a certain spanload.

To relate the minimum drag spanloads to the required twist or camber shape it will be necessary to include further considerations. Twist shape calculations could be performed following the development of Gray and Schenk[9]. This theory includes an additional control point for each wing station located at the ¾ chord line. The induced velocities due to the lifting vortices are calculated at these control points, and a relation between the resultant of the induced velocity and the flight velocity, and the section zero-lift line can be established. Namely, at these ¾ chord points, no flow exists normal to the zero-lift line. This way the induced velocity distribution can be related to twist distribution.

The calculation of the optimum camber shape required to achieve the minimum drag spanloads would be more involved, and a general vortex lattice method would be needed. Lamar[20] developed such a method for optimum mean camber shape calculations. In this thesis, neither twist nor camber shape are calculated. This study concentrates on the calculations of the optimum spanloads giving minimum induced drag for the configuration. The required twist and camber shape to achieve these spanloads will be left as a necessary extension to the studies presented here.

As a result of the location change of vortices and control points, the induced velocity calculations at each control point are not so simple, since the Biot-Savart law will not assume the mathematical form presented in equation 5.3.

The induced velocity caused by the trailing vortices on the control points will now be given by:

$$V_{induced} = \frac{\Gamma}{4\pi h}(1+\cos\alpha) \tag{5.13}$$

Again, the induced velocity is perpendicular to the plane formed by the trailing vortex filament and the control point, and *h* is the perpendicular distance as shown in Figure 5-6. Note that the term cosα brings the desired tendency, since a lower influence will be felt by control points that are upstream of the trailing vortices and vice versa.

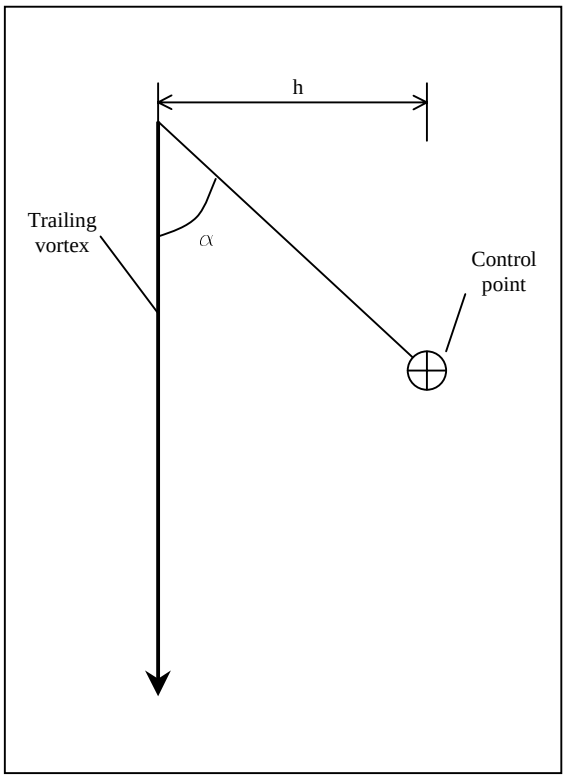

Figure 5-6. Geometry for induced velocity caused by a trailing semi-infinite vortex on a control point having a different streamwise location.

When the control points were located at an infinite downstream distance, the induced velocity at the control points caused by the bound vortex lines was zero. For that reason, bound vortex filaments were not included.

For the case treated here, it is clear that the bound vortex lines will produce normal induced velocities at the control points. These induced velocities will be given by:

$$V_{induced} = \frac{\Gamma}{4\pi h}(\cos\alpha_1 - \cos\alpha_2) \tag{5.14}$$

The induced velocity will be perpendicular to the plane formed by the bound vortex line and the control point, as shown in Figure 5-7.

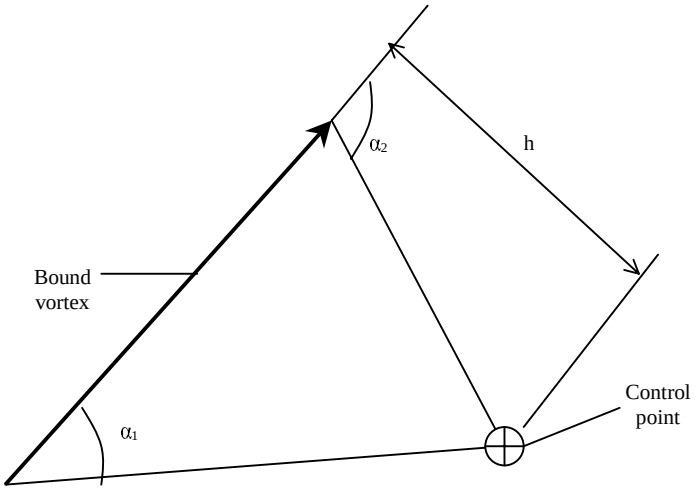

Figure 5-7. Geometry for induced velocity caused by a bound vortex filament on a control point having a different streamwise location.

Only normal velocities to the streamwise direction are necessary for induced drag calculation (see equation 5.12). If the control point is located at a different vertical position than the bound vortex line, a component of the induced velocity will be directed in the streamwise direction, as shown in Figure 5-8. The induced velocity obtained with the Biot-Savart law (equation 5.14) must be multiplied by the cosine of the corresponding angle to obtain the desired normal induced velocity.

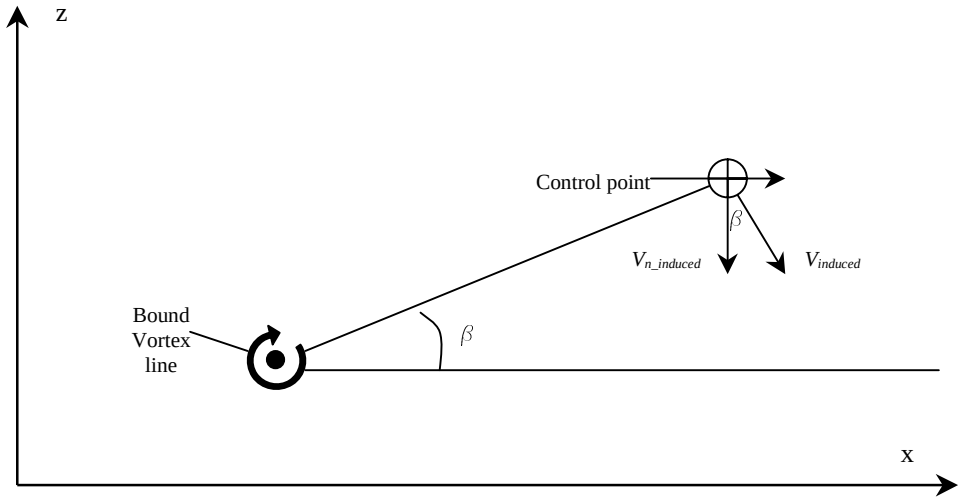

Figure 5-8. Normal induced velocity caused by a bound vortex line on a control point located at a different vertical distance.

The equations that gave the induced drag velocities at a control point according to the geometry of Figure 5-2 (equations 5.5 and 5.6) must now be changed to include the additional effects.

The induced velocity at a specific control point due to the trailing vortices of a discrete horseshoe vortex must be modified by the term (1+cosα), as shown in equation 5.13, and the bound vortex induced velocity at the control point must be added. When equations 5.5 and 5.6 are modified the result is:

$$\frac{v_i}{V_\infty} = -\frac{1}{2\pi}\frac{\Gamma_j}{V_\infty}\left\{\frac{z'}{R_1}\left(1+\frac{x_i-x_j}{\sqrt{R_1+(x_i-x_j)^2}}\right)-\frac{z'}{R_2}\left(1+\frac{x_i-x_j}{\sqrt{R_2+(x_i-x_j)^2}}\right)\right\} \tag{5.15}$$

$$\frac{w_i}{V_\infty} = \frac{1}{2\pi}\frac{\Gamma_j}{V_\infty}\left\{\frac{\{y'-s'\}}{R_1}\left(1+\frac{x_i-x_j}{\sqrt{R_1+(x_i-x_j)^2}}\right)-\frac{\{y'+s'\}}{R_2}\left(1+\frac{x_i-x_j}{\sqrt{R_2+(x_i-x_j)^2}}\right)+Effect_{bound\_vortex}\right\} \tag{5.16}$$

where the bound vortex effect is given by:

$$Effect_{bound\_vortex} = \frac{\cos\alpha_1-\cos\alpha_2}{h^2}(x_i-x_j) \tag{5.17}$$

$$\cos\alpha_1 = \frac{y' + s'}{\sqrt{(y' + s')^2 + h^2}} \tag{5.18}$$

$$\cos\alpha_2 = \frac{y' - s'}{\sqrt{(y' - s')^2 + h^2}} \tag{5.19}$$

$$h = \sqrt{(x_i - x_j)^2 + z'^2} \tag{5.20}$$

Note that the induced velocity due to the bound vortex line only acts in the w_i direction, that is, in the direction perpendicular to this vortex line. Once the induced velocities with equations 5.15 to 5.20 have been calculated, the normal induced velocities can be found with equation 5.11 and induced drag calculations can still be performed with equation 5.12.

The streamwise effects of the discrete vortices on the control points have then been added, and the calculations are no longer performed in the Trefftz plane.

The induced drag variations for separate airplanes flying in formation as a function of the relative distance (in the three space directions) can now be studied. With the modifications made to the code, it has been found that the total induced drag and optimum load distributions remain independent of the streamwise aircraft separation.

Chapter 6 Spanload Optimization Problem In Formation Flight

Optimum load distributions for a group of aircraft flying in an arrow formation will be found. A program has been developed that can give these optimum spanloads with applied constraints in lift and pitching moment coefficients for each aircraft and a rolling moment coefficient constraint applied to off-centered airplanes. This last constraint insures straight flight since the rolling moment is imposed to be zero for all aircraft. Total and individual drag savings as a function of aircraft relative distances to each other (in the three space directions) will be obtained.

The number of airplanes flying in arrow formation influences the drag benefits that they can obtain from the configuration (see Maskew[16]). The key purpose here, however, is the study of drag and load distribution variations as a function of aircraft relative distance. A high number of airplanes in the formation would mean a high number of variables (distances) to be studied. The arrow formations that will be treated here consist only of three airplanes, a central one and two off-centered aircraft.

Two different aircraft configurations will be studied. In the first one, the three airplanes in the formation will be of equal sizes, and no tail surfaces will be included. In the second study, a mother, large airplane will be leading and helping (in performance) to two smaller aircraft, located by its sides.

6.1. Equal aircraft problem

Optimum load distributions for a group of three equal aircraft flying in arrow formation will be found, and their induced drag compared as a function of relative distance in the three space directions. Planform geometry and the relative spacing between aircraft are the same as in Maskew's[16], with three airplanes, each one of them consisting only of planar wing panels so that pitching moment constraints do not need to be applied. Each

planform is trimmed with respect to rolling moment. The characteristics of the planform geometry are shown in Table 6-1 (from Maskew[16]).

Table 6-1. Basic wing geometry for equal aircraft configuration formation flight study.

Span	**2.0**
Geometric mean chord	**0.25**
Area	**0.5**
Aspect ratio	**8.0**
Taper ratio	**0.33**
Sweepback (quarter-chord line)	**5 deg**
Dihedral	**0**

The aircraft will be moved relative to the other in the *x* (streamwise), *y* (spanwise) and *z* (vertical) directions, studying the effects of these distances on load distributions and drag savings. Figure 6-1 shows how the off-centered airplane will be moved relative to the central one. Recall that it is assumed that the configuration will always be symmetric.

The off-centered aircraft (*Aircraft 2*) will be moved along the strong dotted line in Figure 6-1. First, from x/b=-3.0 to x/b=3.0, the variation in induced drag savings will be studied as a function of streamwise distance, maintaining a y/b=0.89 and a z/b=0.01. This small, but still significant value of vertical offset between airplanes is set due to numerical problems in the code when the projections of different lifting surfaces in the Trefftz plane come on top of each other.

Then, with a fixed x/b=3.0, the spanwise effect will be considered by letting z/b=0.01 and changing y/b, and finally, the vertical effect is obtained by letting z/b vary while setting x/b=3.0 and y/b=0.89. This is similar to the approach used by Maskew.

Although the planform geometry and movements of the airplanes are taken from Maskew's paper, the main purpose here is not to compare results. The geometric similarities will certainly make them resemble his results. However, Maskew solves an analysis problem in which the wing twist distribution is specified and the aileron deflection is found so that rolling moment equals zero. With the whole wing geometry fixed, downwash angles completely determine the loads at each station.

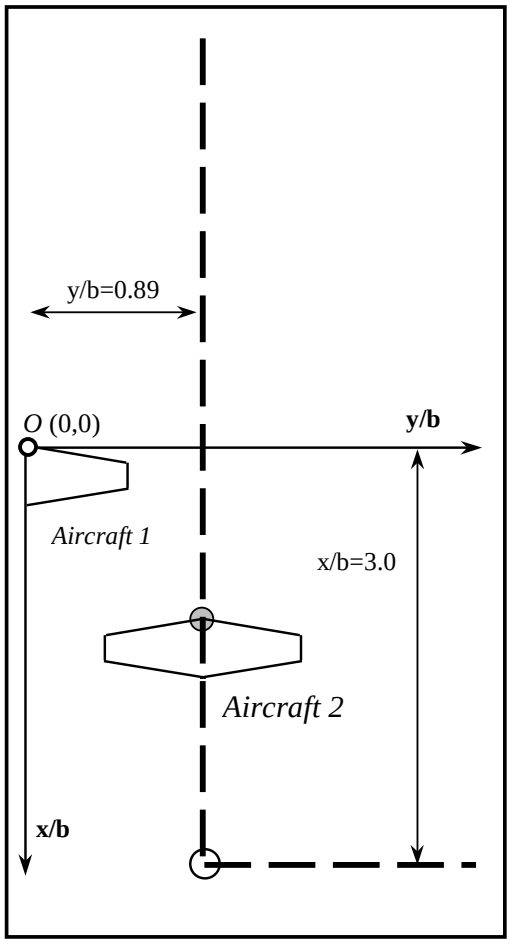

Figure 6-1. Movement of the off-centered aircraft relative to the central one for equal aircraft configuration formation flight study (from Maskew[16])

In this thesis a design problem is treated, in which only planform geometry is known and optimum loads are found. This time the loads are not determined by the downwash angles because twist or camber distribution at each station are not known. The only thing that determines loads and downwash angles is the requirement of minimum induced drag for the formation, together with the imposed constraints on lift and rolling moment.

To set the rolling moment coefficient to zero in the design problem, the aileron used by Maskew will not be useful, because calculations are not dependent on twist or camber, and therefore, angle of attack. The whole wing is then considered as a control surface and the rolling moment constraint is applied to each wing.

A sample design input file for obtaining optimum load distributions for this equal aircraft configuration is given in Appendix B.1. It corresponds to an *Aircraft 2* location of

x/b=3.0, *y/b*=0.89 and *z/b*=0.01. For a detailed description of the input file the reader should refer to the *idrag* formation code manual[22]. Here, a brief documentation of the most important parameters introduced is given.

6.1.1 Geometry definition

For each aircraft in the configuration (recall that only half of the formation must be specified), the *x* position for the center of gravity and the *y* and *z* locations about which rolling moment coefficient is to be calculated must be given. These parameters will be used when the pitching moment and rolling moment coefficient constraints are applied. The reference area (normally wing area) and reference chord (generally mean aerodynamic chord) must also be specified for each aircraft. These values will be used for the non-dimensionalization of loads and performance parameters (like the induced drag coefficient).

The actual geometry for the lifting surfaces is given by specifying the *x*, *y* and *z* positions of the four corners of each panel. The aircraft to which the panel corresponds must also be specified. Relative movement between airplanes will be given by three parameters, required for each aircraft, which determine the *x*, *y* and *z* movements of all the panels for the corresponding aircraft from the specified position. Center of gravity position and the point for rolling moment calculations will also be moved by these variables.

6.1.2 Constraints

A lift coefficient constraint is applied at each airplane. Then, a value of lift coefficient must be specified for each one of them. For this equal aircraft configuration formation flight study a lift coefficient of 0.6 will be assumed. A pitching moment coefficient constraint can also be used at each aircraft. However, in this configuration, only wing lifting surfaces are analyzed, so that the trim constraint is disengaged. As stated above, a

rolling moment coefficient constraint must be applied to off-centered aircraft so that their rolling moment equals zero. No input is needed for this constraint since the code applies it automatically.

6.1.3 Changing variables

The only variables that will be changed (manually, changing the input file) are the relative movements of the different airplanes in the configuration. *Aircraft 1* will be fixed, and the *x*, *y* and *z* movements for *Aircraft 2* will be varied.

6.1.4 Optimized variables and measures of effectiveness

The induced drag for the whole formation will be the variable optimized. Optimum spanloads that give minimum drag for the formation will be calculated, not for individual aircraft. However, the primary measure of effectiveness will be the induced drag of each separate airplane, since it is important to study the effects of formation flight on individual aircraft performance.

6.2 Different aircraft size problem

Recently, interest has been concentrated on systems of airplanes consisting of a leading, large size mother aircraft and two smaller aircraft flying to its sides. The greater loads that the mother aircraft experiences in flight produce large upwash velocities that can be used by the trailing airplanes. In this way smaller, less efficient airplanes can get large drag benefits from big, efficient aircraft with long ranges.

The configuration studied is shown in Figure 6-2. The planform characteristics of the mother aircraft are given in Table 6-2. *Aircraft 2* geometry is exactly equal to that of the

leading aircraft, with a scale factor of 0.5. That is, *Aircraft 1* is exactly twice as large as *Aircraft 2*. The lift coefficients of both airplanes are set to a value of 0.6.

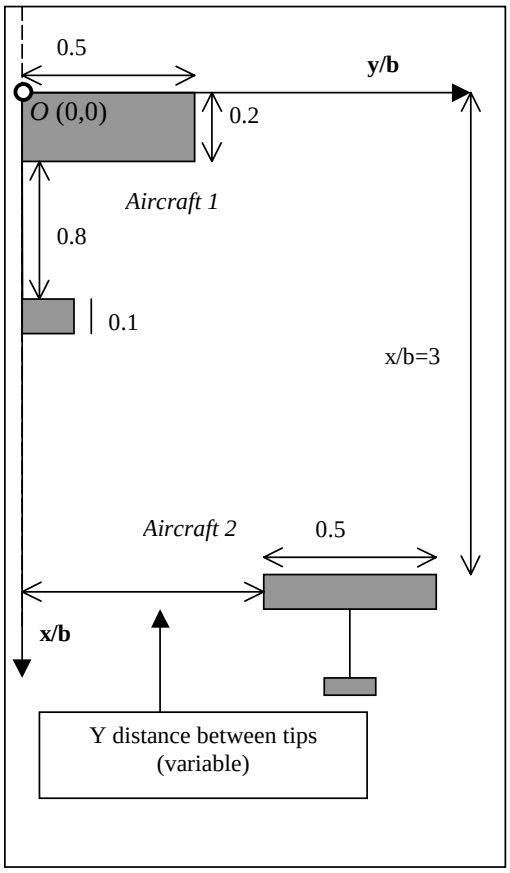

Figure 6-2. Geometry and relative movements between airplanes for different aircraft size configuration formation flight study.

Table 6-2. Basic wing geometry for mother aircraft, different aircraft size configuration formation flight study

Span	**1.0**
Geometric mean chord	**0.2**
Area	**0.2**
Aspect ratio	**5.0**
Taper ratio	**1.0**
Sweepback (quarter-chord line)	**0 deg**
Dihedral	**0**

Note that airplanes now have tail panels, so that the pitching moment coefficient can be included in the calculations. Optimum spanloads for minimum induced drag are found with constraints in lift, pitching moment and rolling moment coefficients.

Since the smaller, off-centered aircraft are the ones that must receive drag benefits from the central one, they are located trailing the formation. The streamwise distance between aircraft is set to be large enough so that aircraft collision can be avoided and induced drag coefficients are independent on x direction. Results will show that *Aircraft 2* obtains the largest benefit at this position and that vertical spacing between aircraft must approach zero for maximum drag reductions. In this study x/b will be set to a value of 3.0 and z/b=0.01. These values are non-dimensionalized by the span of the mother aircraft (b=1.0). The small vertical spacing again avoids numerical problems.

Appendix B.2 shows an input file for a different aircraft size configuration study corresponding to Figure 6-2. In this input file, x/b=3.0, y/b=1.05 and z/b=0.01. The description of the input parameters follows the same considerations stated for the equal aircraft configuration with two exemptions. First of all, the pitching moment constraint is applied since the configuration has horizontal tail lifting surfaces. A value for the pitching moment coefficient about the center of gravity must be fixed for each airplane. It is of course usual to set this moment coefficient to zero. Secondly, only the spanwise effect will be studied for this case, since it will give maximum benefits for the trailing aircraft.

Chapter 7 Results for Spanload Optimization Problems in Formation Flight.

Optimum load distributions for minimum induced drag of an arrow formation configuration will be studied as a function of relative distance between aircraft. Induced drag coefficients for each airplane will also be obtained. Arrow formation configurations consisting of one central airplane and two off-centered ones are treated.

7.1 Equal aircraft configuration results

Results for the equal aircraft configuration formation flight study proposed in section 6.1 will be given here. The wing geometry for each aircraft was shown in Table 6-1, and the relative movement between airplanes is stated in Figure 6-1. The effect of relative aircraft distance will be studied in three steps according to the movements of *Aircraft 2* relative to *Aircraft 1*: Streamwise, spanwise and vertical effect.

A code sample output file for this configuration is given in Appendix B.3. It corresponds to the input file from Appendix B.1. The input parameters are repeated in the beginning, followed by the *x*, *y* and *z* location for the vortex control points and the optimum loads (both in terms of lift coefficients and normal force coefficients) at these points. Lift, pitching moment, rolling moment, and induced drag coefficients are given at the end of the file for each aircraft, together with the total configuration induced drag coefficient. The number of vortices used in discretizing each wing was 80. Convergence was actually achieved for a smaller number of vortices (about 40 vortices per wing), but a higher number was used here to obtain smooth load curves.

7.1.1 Streamwise effect

Airplane 2 is moved along the *x* axis from *x/b*=-3 to *x/b*=3 as shown in Figure 6-1. Figure 7-1 shows the change in induced drag coefficient for each aircraft and for the

formation as the streamwise relative distance is changed. Results are shown as the ratio of their induced drag in the formation to their induced drag when flying alone. Induced drag for single flight is the minimum induced drag for an aircraft alone configuration, corresponding to an elliptic lift distribution and a span efficiency factor equal to 1.

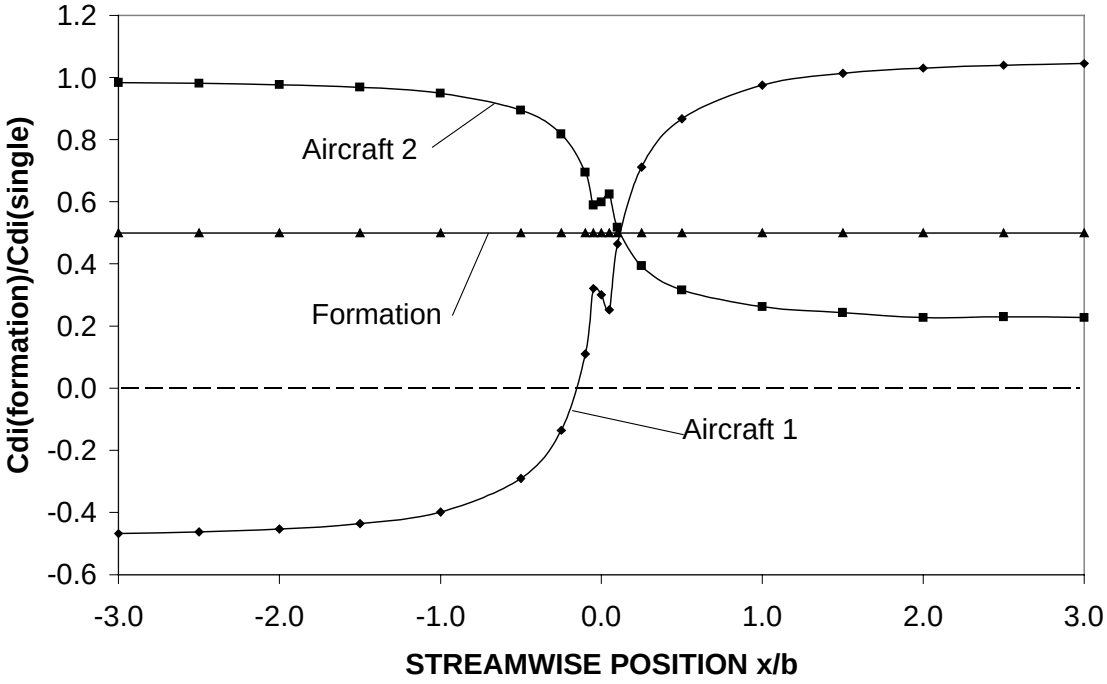

Figure 7-1. Effect of streamwise position, *y/b*=0.89, *z/b*=0.01. Equal aircraft configuration formation flight study.

Note that the induced drag for the formation is independent of the streamwise location of the airplanes, as stated by Munk's theorem[26]. That constant value is the minimum induced drag for the whole configuration. The optimum spanloads corresponding to this minimum drag are shown in Figure 7-2 (only shown half). The load distribution is also independent of streamwise position, so that Figure 7-2 shows the spanload for any *x/b*.

The induced drag coefficients of *Aircraft 1* and *2* are highly dependent on *x* when the aircraft are close in this direction. For a streamwise distance between them greater than three spans, their induced drag reaches a steady value and is no longer dependent on *x* separation.

When *x/b* is negative, the central aircraft is behind the two leading ones, so that it receives the upwash from them. The result is that *Aircraft 1*, under the potential vortex

assumption, achieves a negative induced drag (a thrust forward). The upwash from the leading aircraft is higher than the downwash caused by the central aircraft on itself.

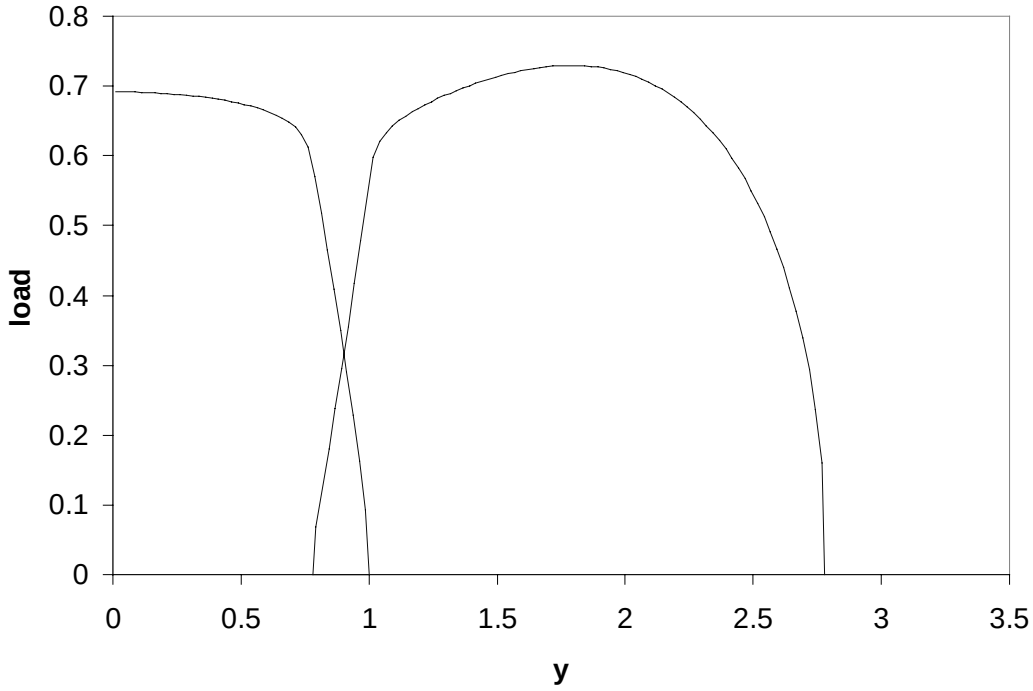

Figure 7-2. Optimum load distribution *z/b*=0.01, *y/b*=0.89. Equal aircraft configuration formation flight study.

For *x/b* positive, the central aircraft is leading the formation, and its upwash influences *Aircraft 2* reducing its induced drag. This time, since it is only the central aircraft influencing two trailing ones, the upwash contribution by *Aircraft 1* on *Aircraft 2* is lower than the downwash caused by *Aircraft 2* on itself.

When *Aircraft 1* leads the formation with a high streamwise separation with respect to *Aircraft 2* (see Figure 7-1 for *x/b*=3), its induced drag ratio is greater than one. The induced drag coefficient when flying alone was established to be the minimum induced drag, corresponding to an elliptical load distribution. Then, the leading aircraft suffers a decrease in performance. This seems contradictory, since almost no downwash should be felt on *Aircraft 1* due to *Aircraft 2* (it is far aft). However, this increase in induced drag coefficient enhances the performance of the trailing airplanes, so that a formation minimum induced drag is obtained. Figure 7-2 shows that the load distribution for the central aircraft is not elliptic. It has higher loads toward the wing tip than an elliptically loaded wing would have. These high loads towards the tip induce greater upwash angles

on the trailing aircraft, reducing their induced drag coefficients. The result is that a decrease in performance in the leading aircraft can help obtaining overall drag reductions for the formation.

The same thing happens for a high negative value of *x/b*. In this case the off-centered airplanes lead the formation and they experience a reduction in performance due to their non-elliptic load distributions. Here, however, the two leading aircraft influence each other so that their induced drag increase is compensated by the upwash they exert on each other.

For *x/b* near zero, the induced drag curves for *Aircraft 1* and *Aircraft 2* have a break (see Figure 7-1). This is caused by the influence of the bound vortex lines on the airplanes. If *Aircraft 1* leads the formation, it feels an upwash from the bound vortex lines of the trailing aircraft, and exerts a downwash on them. When they cross, the upwash and downwash influences are inverted and a break in the induced drag curve appears. The break is a lot smoother if vertical or spanwise distance is increased (for a $y/b = 0.94$ the break no longer appears). Note that a streamwise distance near zero with a vertical distance as small as 0.01 is not really a physically achievable situation.

One further consideration must be pointed out. Figure 7-2 shows the asymmetry in the load distribution of *Aircraft 2*. This asymmetry is a consequence of a V-formation geometry, in which only the central aircraft has a symmetric lift distribution. Despite the asymmetric spanload on *Aircraft 2*, its rolling moment coefficient about its center of gravity is zero (the rolling moment constraint was active). Achieving the desired lift distribution will be the greatest problem, not only because of the asymmetry of the load distribution, but because the spanloads will be dependent on vertical and spanwise distance between airplanes.

7.1.2 Spanwise effect

Aircraft 2 is moved along the *y* direction while *x/b* is fixed at a value of 3.0 and $z/b=0.01$. Figure 7-3 shows the changes in induced drag for each aircraft and the whole formation as the spanwise distance is varied.

The formation induced drag coefficient is very dependent on spanwise position. When *y/b*=1 the right tip of *Aircraft 1* coincides with the left tip of *Aircraft 2* in *y* location. The formation minimum actually occurs for a value of *y/b* less than one, where *Aircraft 2* is in the wake of the leading aircraft. For a spanwise distance of two spans, the drag savings are very small and formation flying is no longer beneficial. Thus it is important to maintain the airplanes in close spanwise position to obtain the largest possible induced drag reduction.

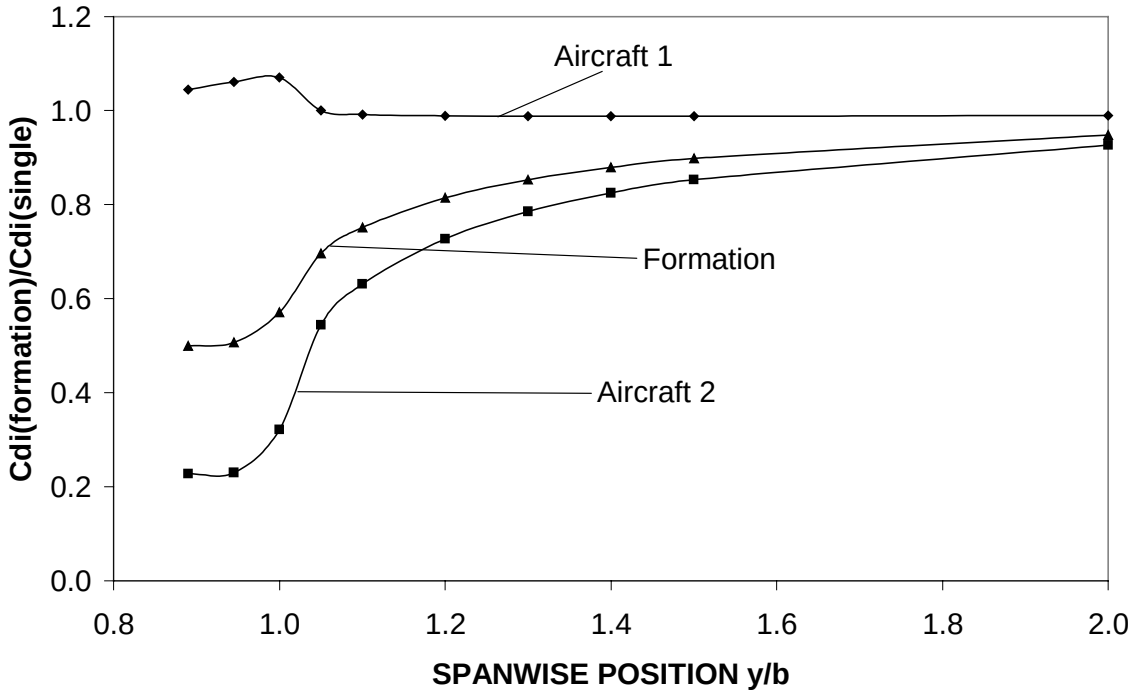

Figure 7-3. Effect of spanwise position, *x/b*=3.0, *z/b*=0.01. Equal aircraft configuration formation flight study

The drag dependence of *Aircraft 2* on spanwise distance is also very strong, with 80% potential induced drag savings for optimum position. *Aircraft 1*, however, has a constant induced drag coefficient equal to its minimum induced drag when flying alone as long as the airplane tips do not get close in the spanwise direction. If the aircraft tips come close or overlap, *Aircraft 1* performance decreases, while the induced drag for *Aircraft 2* and the formation starts decreasing more rapidly.

The previous section showed how a decrease in performance in *Aircraft 1* could produce an induced drag decrease for the trailing airplanes and in turn for the whole formation. But it is necessary to see why this effect only takes place for close spanwise distances. Figure 7-4 shows the optimum load distributions for several spanwise positions.

When the airplane tips start overlapping, their optimum load distributions are very different from the elliptical loading, the main difference being higher loads in the vicinity of the other aircraft's tip. These loads increase drag on *Aircraft 1* but induce a greater upwash on *Aircraft 2*, improving its performance. That is why Figure 7-3 shows a rise in induced drag when tips overlap.

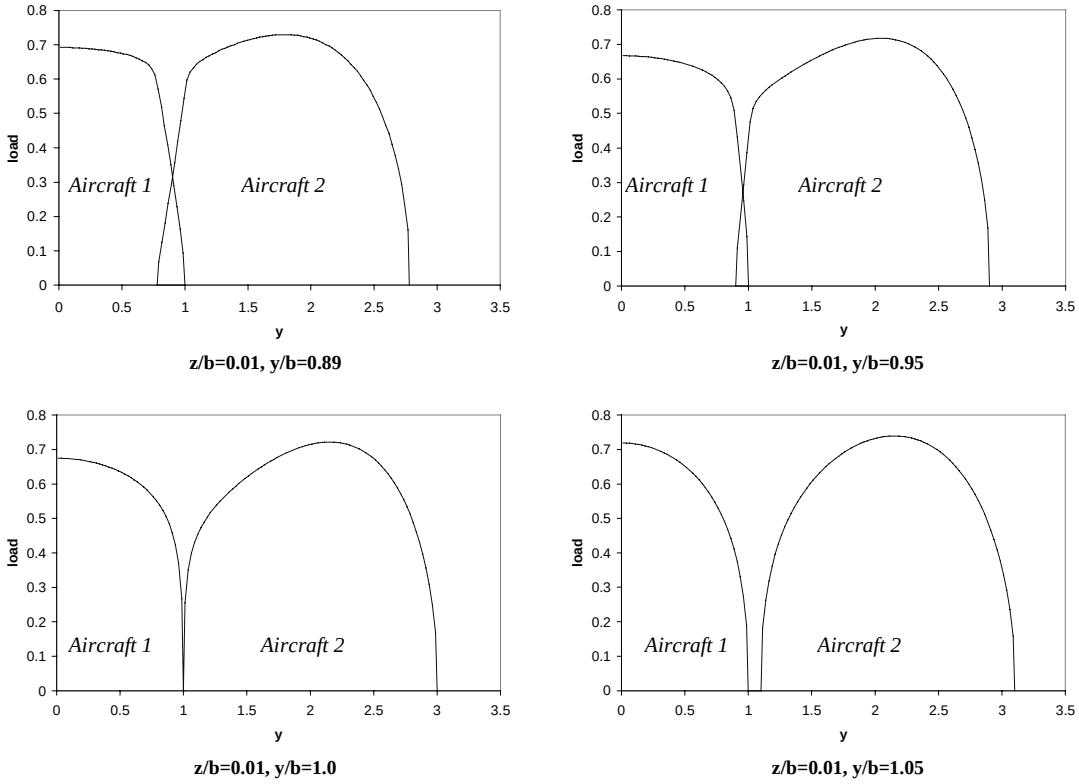

Figure 7-4. Optimum load distributions for different spanwise distances. Equal aircraft configuration formation flight study

For a tip spanwise distance greater than y/b=1, the overlapping does not occur, and the optimum load distributions for both airplanes become nearly elliptic. Their spanloads are now close to the optimum for single flight. In this situation, higher loads towards the

aircraft tip will again decrease leading aircraft performance helping the trailing airplanes. However, the induced upwash on *Aircraft 2* will be much smaller when the aircraft do not overlap (note that induced velocities are inversely proportional to spanwise distance). The result is that the reduction in the trailing aircraft drag will not compensate for the drag increase on the leading aircraft. The formation minimum corresponds to load distributions close to those for solo flight when aircraft tips do not overlap.

The fact that a potential flow vortex model is being used in this analysis should be emphasized here. Overlapping tips means close vortex interactions, where potential flow can fail and viscous effects may need to be included.

7.1.3 Vertical effect

Aircraft 2 is moved in the vertical direction while keeping *y/b*=0.89 and *x/b*=3.0. The induced drag variation is shown in Figure 7-5.

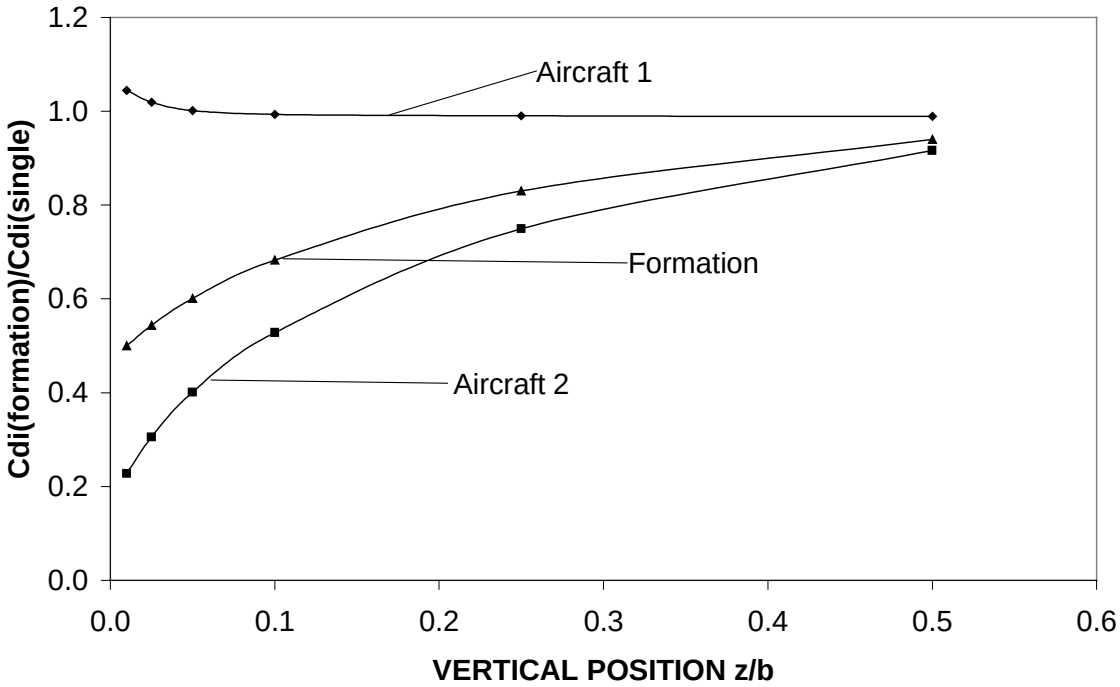

Figure 7-5. Vertical effect, *x/b*=3.0, *y/b*=0.89. Equal aircraft configuration formation flight study.

The strong dependence on *z* location is clear from this figure. Maximum drag reductions for the formation occur at $z=0$ (induced drag variation will be equal for negative values of vertical position). The actual drag reduction values at $z=0$ are not obtained due to numerical problems at these close vertical locations.

When the vertical distance between aircraft is small (less than 0.05), optimum load distributions start deviating from their elliptical shapes, having higher loads near the tip. A decrease in *Aircraft 1* performance that helps formation drag is again observed. The load distribution change with vertical position is similar to that obtained with spanwise distance variation, as seen in Figure 7-6.

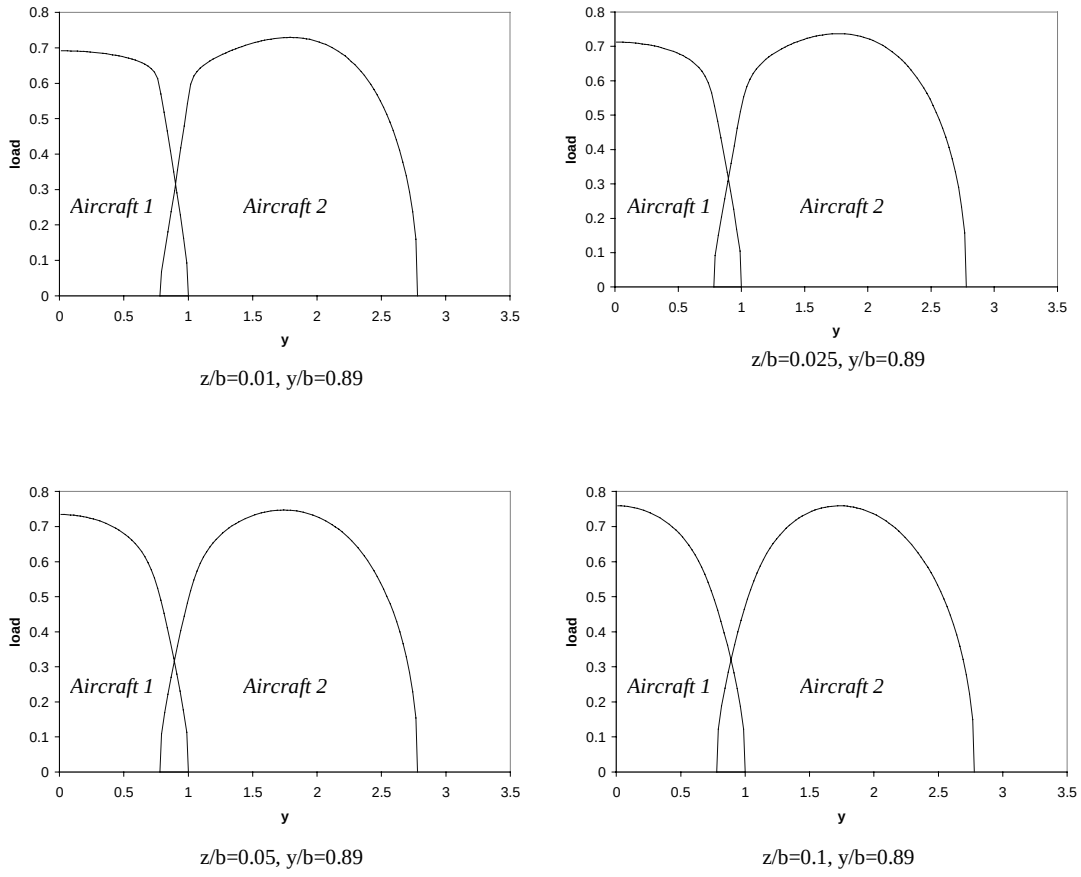

Figure 7-6. Optimum load distributions for different vertical distances. Equal aircraft configuration formation flight study.

7.2 Different aircraft size configuration results

The formation flight configuration composed of a mother aircraft followed by two smaller airplanes, as shown in section 6.2, will be studied here. Figure 6-2 and Table 6-2 give both the planform and relative movement geometry. The effect of relative distance between aircraft will only be studied in the spanwise direction in this case. The purpose of an arrow formation configuration with a big leading airplane is basically the induced drag reduction (and then performance enhancement) of the trailing, smaller aircraft. Figures 7-1 and 7-5 show that the maximum drag reductions for the off-centered airplanes are obtained when they are located trailing the formation with a close vertical spacing with the mother aircraft. That is why, in this study, *x/b* will be fixed to 3.0 and *z/b* to 0.01.

A sample design output file for this configuration is given in Appendix B.4, corresponding to the input file data given in Appendix B.2. Again, the location of the control points and the optimum loads at these points are given, and performance parameters for each aircraft and for the whole formation appear at the end of the file. The number of vortices used in this case was 40 vortices for each wing panel and 20 vortices for each tail panel. This number of vortices was enough to obtain convergence in the spanload and induced drag calculations for the prescribed configuration (see section 5.3).

7.2.1 Spanwise effect

Induced drag variation for each aircraft and the formation as a function of relative spanwise distance is shown in Figure 7-7. Spanwise position is non-dimensionalized by the span of *Aircraft 1*. As in the previous case, when *y/b*=1 the tips of the different aircraft are in the same *y* position.

The induced drag for *Aircraft 2* and the formation is again very dependent of the relative spanwise distance between airplanes. *Aircraft 1* has a constant induced drag coefficient when airplane tips are not very close to each other. When *y/b* approaches 1, *Aircraft 1* experiences a sharp increase in induced drag that benefits the whole system of airplanes

since the drag of *Aircraft 2* is highly decreased. Negative induced drag values (a thrust) are experienced by the trailing aircraft for *y/b* values lower that 1.05.

For this case, higher loads on the tips of the mother aircraft are even more beneficial, since they will cause a high upwash field that can be used by the smaller airplanes. The result is that optimum spanloads for close aircraft positions deviate more from the elliptical loading for this type of configuration.

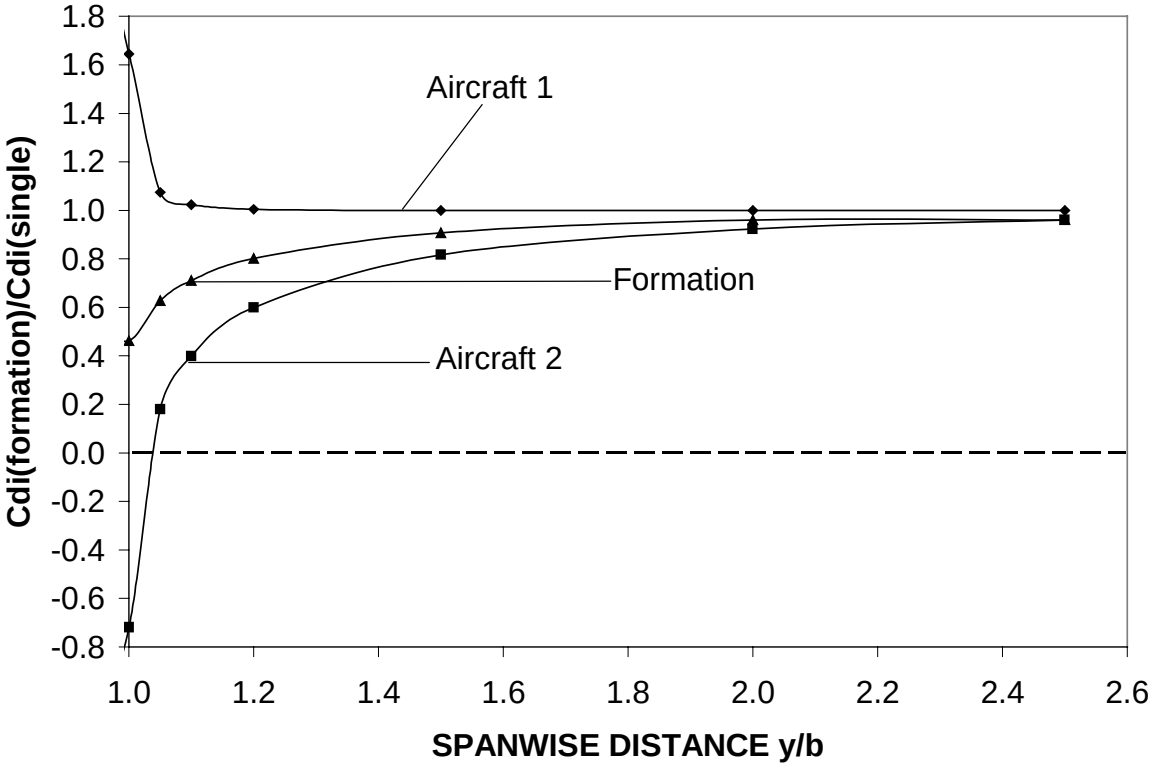

Figure 7-7. Spanwise effect for different aircraft size configuration formation flight study, *x/b*=3.0, *z/b*=0.01

Figure 7-8 shows the optimum load distributions for two cases. For *y/b*=1.0 the spanloads are very different from flying-alone optimums, resulting in an 80% increase in the induced drag of the mother aircraft and a negative induced drag on the smaller ones (see Figure 7-7). For *y/b*=1.05 the optimum spanloads are now nearly elliptic. *Aircraft 1* still has high loads near the tips because of the relative proximity between airplanes. *Aircraft*

1 experiences an increase in induced drag of less than 10% while the trailing aircraft achieve drag reductions greater than 80%.

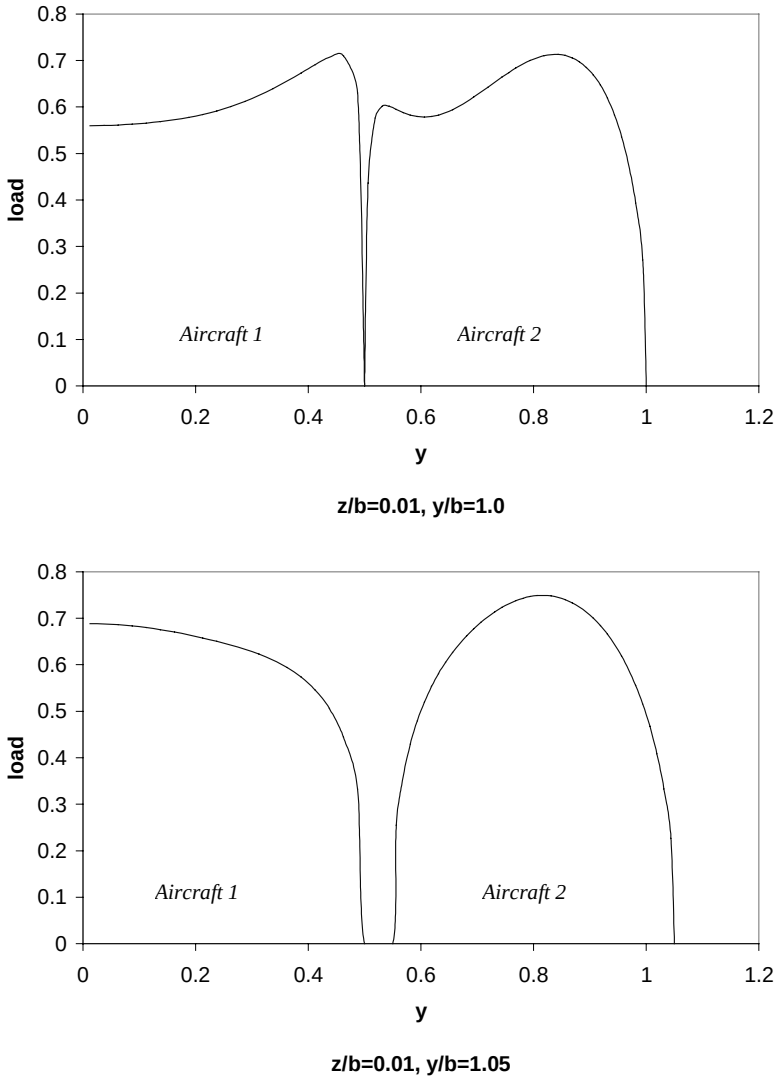

Figure 7-8. Optimum load distributions for different spanwise distances.
Different aircraft size configuration formation flight study

Again, overlapping tips means close vortex interactions where the potential flow vortex model may not be highly accurate.

7.3 Optimum aircraft position

An interesting V-shape configuration will be that in which the induced drag of every airplane will be the same, so that each one of them obtains equal benefits. Figure 7-1 shows that such a configuration requires close spacing between aircraft (x/b=0.1). A more realistic configuration will be that in which aircraft collision can certainly be avoided. When x/b is high both in the negative and positive directions, the danger of collision is not great.

Besides collision avoidance, desired aircraft position must also be limited by the ability of each airplane to maintain its position and optimum load distribution in the configuration.

It was noted above (see Figures 7-4, 7-6 and 7-8) that the optimum load distribution is very dependent on aircraft relative position when airplanes overlap in the spanwise direction and they have a close vertical spacing. The key problem here is how to obtain different load distributions for different aircraft positions.

The approaches of Feifel and Maskew do not encounter that problem since their effective angle of attack at each station is known. Their only problem is finding the aileron deflection required to obtain zero rolling moment about the center of gravity.

In this paper the whole wing is treated as a rolling-control surface. Moreover downwash velocities and optimum spanloads are dependent on aircraft position. A new twist distribution is needed (recall that planform geometry is always constant) for every configuration to achieve these load distributions.

Another problem exists for formation flying. For these cases the rapidly changing conditions when airplane tips are close to each other leads to highly varying rolling moment coefficients that require continuous aileron adjustments. Wolf, Chichka and Speyer[28] developed decentralized controllers and peak-seeking control methods to make these adjustments and maintain the aircraft at their optimum positions. For the peak-seeking control methods, due to the difficulties of measuring drag (or thrust) during flight, airplanes are maintained at a position where the rolling moment coefficient

without aileron deflection to trim is a maximum. It is assumed that the maximum rolling moment coefficient occurs at the minimum induced drag location. This assumption may not always be true, so that real optimum positions are not necessarily obtained. Further work is required in this area before conclusions can be made.

For the case studied here, the changing spanload distributions in the overlap region will be difficult to obtain. However, important drag reductions can be obtained for a *y/b* greater than one (see Figures 7-3 and 7-7). In this region, the optimum load distribution is in fact nearly elliptic, very close to the solo flying optimum.

If the overlapping region is not a feasible solution for a formation configuration due to geometry or control problems, the induced drag benefits will be decreased. In the spanwise study for three equal aircraft, for example, induced drag reductions for *Aircraft 2* will go from 80% to around 40%, and total formation drag savings will decrease from 50% to about 30% (see Figure 7-3).

Chapter 8 Conclusions

Optimum load distributions are possible that can enhance aircraft performance characteristics compared to classical, minimum drag elliptic spanloads. For individual aircraft, the addition of a wing structural constraint in the spanload optimization problem can lead to total aircraft gross weight reductions caused by wing weight savings. A root bending moment constraint was implemented to study possible weight benefits for individual aircraft configurations. For a group of aircraft flying in formation, non-elliptic lift distributions can give large induced drag savings both for the formation and for each airplane, with the consequent performance benefits. Potential drag savings in formation flight configurations have also been studied.

8.1 Spanload optimization with a root bending moment constraint

A method for calculating lift distributions for minimum induced drag with a root bending moment constraint has been developed. These spanloads are related to changes in wing weight, fuel weight and gross weight for transport aircraft configurations. The method can help determine which spanloads bring the maximum benefit to the aircraft under study, so that an optimum lift distribution can be found.

The key insight is that the wing weight decreases nearly linearly with reduced wing root bending moment, while the additional induced drag arising from forcing the wing root bending moment to be less than its minimum drag value results in a parabolic increasing drag. Therefore, the system minimum will always occur for a spanload with a lower wing root bending moment than the aerodynamics alone minimum.

Even for the same airplane fuel weight variations due to different lift distributions change from mission to mission, depending on the range, so that a wing load curve that will produce large benefits when performing a low range mission can result in disadvantages when performing its maximum range mission. It is then necessary to study aircraft

configurations through the whole range of missions they cover to find an optimum spanload that will represent a compromise for these different missions.

A Boeing 777-200IGW class aircraft has been studied with this method. Results show that a reduction of about 1% in maximum take-off gross weight can be obtained. When performing reduced range missions, almost a 2% in take-off weight savings is achieved.

The method described here is applicable to aircraft configurations with cantilever wings. It needs to be extended to treat the case of strut-braced wing concepts, which have recently been shown to be very promising[29,30].

8.2 Spanload optimization in formation flight

Optimum spanload distributions for a group of aircraft flying in V-formation giving minimum induced drag for the whole configuration have been found. The optimization allows the study of induced drag coefficients for separate aircraft and the formation as a function of relative distance between airplanes. Only planform geometry is fixed for each aircraft in the formation, with no twist or camber distribution specified.

When the distance between airplanes is changed, the optimum load distribution giving minimum induced drag also changes. The twist distribution must then be changed as a function of aircraft distance if maximum induced drag savings are expected.

A test case has been studied consisting of three aircraft flying in an arrow formation. It has been shown that the optimum load distribution (and hence the optimum twist distribution) is very dependent on spanwise separation when the aircraft tips are very close to each other or they overlap in this direction. When aircraft tips do not overlap in the spanwise direction the load distribution nearly approaches the optimum spanload when flying alone.

To avoid collisions between aircraft, they should be separated in the streamwise direction. Results show that for a large enough streamwise distance between aircraft

(about three spans), induced drag coefficients for each airplane are no longer dependent on this direction. Induced velocities also become independent of the streamwise direction for these distances. A given twist distribution will provide then the desired optimum lift distribution in this region.

As long as the airplanes are not in a sensitive region with respect to required twist distributions the induced drag reductions can be certainly obtained. For a configuration of three equal aircraft, with the central aircraft leading the formation and the other ones in a non-sensitive region, induced drag reductions for the formation of about 30% are achievable.

A formation with a mother aircraft leading two smaller airplanes half its size in a non-sensitive region can give formation drag reductions of 40%, with induced drag savings in the trailing aircraft greater than 80%.

Unfortunately, regions of maximum drag savings correspond to regions highly sensitive to the required twist distribution. If aircraft were positioned in the aerodynamic optimum, with no regard to required geometries, induced drag reductions of 50% are possible for the equal aircraft formation. For the mother aircraft and its trailing partners, about 60% savings for the formation induced drag can be obtained, and the trailing aircraft would experience a negative induced drag (a thrust forward).

The results obtained here need to be extended to include the design wing shape. With the aircraft position and spanload known, the camber surface required to achieve the design spanload must be found.

References

[1] Prandtl, L., “Uber Tragflugel des Kleinsten Induzierten Widerstandes”, *Zeitshrift fur Flugtechnik und Motorluftschiffahrt* 24 Jg, 1933.

[2] Jones, R. T., “The Spanwise Distribution of Lift for Minimum Induced Drag of Wings Having Given Lift and Root Bending Moment”, NACA TN-2249, 1950.

[3] Jones, R. T. and Lasinski, T., “Effect of Winglets on the Induced Drag of Ideal Wing Shapes”, NASA TM-81230, 1980.

[4] Klein, A. and Viswanathan, S. P, “Approximate Solution for Minimum Induced Drag of Wings with Given Structural Weight”, *Journal of Aircraft*, Vol.12, No.2, 1974.

[5] Klein, A. and Viswanathan, S. P., “Minimum Induced Drag of Wings with Given Lift and Root-Bending Moment,” *Zeitschrift fuer Angewandte Mathematik und Physik*, Vol. 24, Dec. 1973, pp. 886-892.

[6] Kroo, I., “A General Approach to Multiple Lifting Surface Design and Analysis”, AIAA Paper-84-2507, 1984.

[7] McGeer, T., “Wing Design for Minimum Drag with Practical Constraints”, *Journal of Aircraft*, Vol.21, Nov. 1984, p. 879-886.

[8] Craig, A. and McLean, J., “Spanload Optimization for Strength Designed Lifting Surfaces”, AIAA Paper-88-2512, 1988.

[9] Gray,W. and Schenk, K., “A Method for Calculating the Subsonic Steady-State Loading on an Airplane with a Wing of Arbitrary Planform and Stiffness”, NACA TN-3030, 1953.

[10] Haftka, R.T., “Optimization of Flexible Wing Structures Subject to Strength and Induced Drag Constraints”, *AIAA Journal*, Vol. 15, Aug. 1977, p. 1101-1106.

[11] Schlichting, H., “Leistungsersparnis im Verbandsflug. Mitt. Dt. Akad. Luftfahrtforsh.”, H.2 (1942), 97-139.

[12] Hoerner, S. F., *Fluid-Dynamic Drag*, published by Hoerner Fluid Dynamics, 1965. Current address: PO Box 21992, Bakersfield, CA 93390.

[13] Shollenberger, C.A., and Lissaman, P., “Formation Flight of Birds,” *Science*, May 1970, p. 1003-1005.

[14] Jenkinson, L.R., Caves, R.E. and Rhodes, D.P., “A Preliminary Investigation into the Application to Civil Operations”, AIAA Paper-95-3898, 1995.

[15] Feifel, W.M., “Optimization and Design of Three-Dimensional Aerodynamic Configurations of Arbitrary Shape by a Vortex Lattice Method,” NASA SP-405, p.71-88, May 1976

[16] Maskew, B., “Formation Flying Benefits Based On Vortex Lattice Calculations,” NASA CR-151974, April 1977.

[17] Gingras, R.D., “Experimental Investigation of a Multi-Aircraft Formation”, AIAA Paper-99-3143, 1999.

[18] Beukenberg, M., Hummel, D., “Aerodynamics, performance and control of airplanes in formation flight,” Technische Universität Braunschweig, Brunswick, Federal Republic of Germany. ICAS-90-5.9.3, Congress, 17th, Stockholm, Sweden, Sept. 9-14, 1990.

[19] Blackwell.J., “Numerical Method to Calculate the Induced Drag or Optimal Span Loading for Arbitrary Non-planar Aircraft.” NASA SP-405, p.49-70, May 1976.

[20] Lamar, J., “A Vortex Lattice Method for the Mean Camber Shapes of Trimmed Non-Coplanar Planforms with Minimum Vortex Drag.” NASA TN-D-8090, June 1976.

[21] Kuhlman, J., and Ku, T., “Numerical Optimization Techniques for Bound Circulation Distribution for Minimum Induced Drag of Nonplanar Wings: Computer Program Documentation.” NASA CR-3458, 1982.

[22] Grasmeyer, J., “A Discrete Vortex Method for Calculating the Minimum Induced Drag and Optimum Load Distribution for Aircraft Configurations with Noncoplanar Surfaces” VPI-AOE-242, January 1997.

[23] McCullers, L. A., “FLOPS User’s Guide, Release 5.81, text file included with FLOPS code”.

[24] Naghshineh – Pour, A. H., “Preliminary Structural Analysis of a Truss-Braced Wing”, Virginia Tech MS. Thesis, December 1998.

[25] MJ. F. Gundlach IV, A. Naghshineh-Pour, F. Gern, P.-A. Tetrault, A. Ko, J. A. Schetz, W. H. Mason, R. K. Kapania, B. Grossman, R. T. Haftka (University of Florida), "Multidisciplinary Design Optimization and Industry Review of a 2010 Strut-Braced Wing Transonic Transport," MAD Center Report 99-06-03, Virginia Tech, AOE Dept., Blacksburg, VA, June, 1999.

[26] Munk, Max M., “The Minimum Induced Drag of Aerofoils,” NACA Report No. 121, 1921.

[27] Tulinius, J., Clever, W., Nieman, A., Dunn, K., and Gaither, B., “Theoretical Prediction of Airplane Stability Derivatives at Subcritical Speeds”, NASA CR-132681, Jan 1973.

[28] Wolfe, J.D., Chichka, D.F., Speyer, J.L., “Decentralized Controllers for Unmanned Aerial Vehicle Formation Flight,” AIAA Paper-96-3833, 1996.

[29] Grasmeyer, J.M., Naghshineh, A., Tetrault, P.-A., Grossman, B., Haftka, R.T., Kapania, R.K., Mason, W.H., Schetz, J.A., "Multidisciplinary Design Optimization of a Strut-Braced Wing Aircraft with Tip-Mounted Engines," MAD Center Report MAD 98-01-01, January 1998.

[30] F.H. Gern, J.F. Gundlach, A. Ko, A. Naghshineh-Pour, E. Sulaeman, P.-A. Tetrault, B. Grossman, R.K. Kapania, W.H. Mason and J.A. Schetz, "Multidisciplinary Design Optimization of a Transonic Commercial Transport with a Strut-Braced Wing," Paper 1999-01-5621, 1999 World Aviation Conference, October 19-21, 1999, San Francisco, CA.

Appendix A.1

Sample input file for spanload optimization with a root bending moment constraint. Boeing 777-200IGW type aircraft test case, reduced fuel load equal to 185000 lbs.

```
B-777 TYPE AIRCRAFT TEST CASE. REDUCED FUEL LOAD = 185000 LBS.

0.37        eta_break    WING GEOMETRY DEFINITION
109.21      hspan_wing
28.29       sweep_wing_in_1_4_deg
28.29       sweep_wing_out_1_4_deg
6.0         dihedral_wing_deg
52.0        c_wing_center
25.83       c_wing_break
7.35        c_wing_tip
0.111       tc_wing_in
0.10        tc_wing_break
0.08        tc_wing_out
120.0       dx_htail     TAIL GEOMETRY DEFINITION
12.0        dz_htail
36.91       hspan_htail
37.0        sweep_htail_deg
22.61       c_htail_root
7.35        c_htail_tip
0.0         dihedral_htail_deg
588893.0    gw           PERFORMANCE SPECIFICATION
215000.0    wfuel0
8508.0      range
0.85        mach
40000.      altitude
0.29272     sfc_static
0.97        sfc_fact
2           new          ENGINE SPECIFICATION
16278.0     w_engine
0.33        eta_engine_1
0.0         eta_engine_2
35.0        xcg          MISCELLANOUS
-0.000784   cm_fuse
-0.075      cmo_wing
20.33       dia_fuse
0.333       flapr
0.0         fcomp
0.0         faert
0.0         fstrt
3.75        ulf
0.0         cm_design
0.25        cp
0.0         yrbm
0.0         zrbm
80          nvortices_idrag
185000.0    wfuel_new
```

Appendix A.2

Sample output files for spanload optimization with a root bending moment constraint. Boeing 777-200IGW type aircraft, reduced fuel load equal to 185000 lbs.

File *loads.out*:

ETA	MINIMUM_DRAG_LOADS	OPTIMUM_LOADS
0.6967	0.6879	0.7889
2.0901	0.6880	0.7884
3.4834	0.6876	0.7870
4.8768	0.6870	0.7851
6.2702	0.6862	0.7826
7.6635	0.6851	0.7797
9.0569	0.6839	0.7763
10.4503	0.6825	0.7726
11.8436	0.6808	0.7684
13.2370	0.6789	0.7638
14.6304	0.6769	0.7589
16.0237	0.6745	0.7537
17.4171	0.6720	0.7481
18.8105	0.6692	0.7422
20.2038	0.6662	0.7360
21.5972	0.6630	0.7294
22.9906	0.6595	0.7226
24.3840	0.6557	0.7156
25.7773	0.6517	0.7082
27.1707	0.6474	0.7006
28.5641	0.6428	0.6928
29.9574	0.6380	0.6847
31.3508	0.6329	0.6765
32.7442	0.6276	0.6681
34.1375	0.6220	0.6595
35.5309	0.6164	0.6508
36.9243	0.6107	0.6420
38.3176	0.6052	0.6333
39.7110	0.6006	0.6255
41.0822	0.5914	0.6127
42.4313	0.5872	0.6050
43.7804	0.5823	0.5964
45.1294	0.5774	0.5876
46.4785	0.5725	0.5788
47.8276	0.5676	0.5698
49.1766	0.5627	0.5608
50.5257	0.5578	0.5517
51.8748	0.5528	0.5425
53.2238	0.5478	0.5332
54.5729	0.5427	0.5238
55.9219	0.5375	0.5144
57.2710	0.5322	0.5049
58.6201	0.5268	0.4953
59.9691	0.5213	0.4856
61.3182	0.5156	0.4759
62.6673	0.5098	0.4660
64.0163	0.5039	0.4561
65.3654	0.4978	0.4461
66.7145	0.4915	0.4361
68.0635	0.4851	0.4259
69.4126	0.4785	0.4157
70.7617	0.4718	0.4054
72.1107	0.4648	0.3951
73.4598	0.4577	0.3846
74.8089	0.4503	0.3741
76.1579	0.4427	0.3636

77.5070	0.4348	0.3529
78.8560	0.4268	0.3422
80.2051	0.4184	0.3314
81.5542	0.4098	0.3205
82.9032	0.4009	0.3095
84.2523	0.3916	0.2985
85.6014	0.3821	0.2873
86.9504	0.3721	0.2761
88.2995	0.3618	0.2647
89.6486	0.3510	0.2533
90.9976	0.3398	0.2417
92.3467	0.3281	0.2299
93.6958	0.3157	0.2180
95.0448	0.3028	0.2059
96.3939	0.2891	0.1935
97.7429	0.2745	0.1809
99.0920	0.2590	0.1679
100.4411	0.2423	0.1545
101.7901	0.2242	0.1406
103.1392	0.2043	0.1259
104.4883	0.1820	0.1102
105.8373	0.1564	0.0930
107.1864	0.1254	0.0732
108.5355	0.0838	0.0480

File *ww-id.out*:

RBM REDUCT(%)	WING_WEIGHT	INDUCED_DRAG
0.00	83746.35	0.007679
0.50	83311.52	0.007681
1.00	82872.56	0.007685
1.50	82436.89	0.007691
2.00	82005.35	0.007700
2.50	81577.94	0.007712
3.00	81154.60	0.007727
3.50	80735.22	0.007744
4.00	80319.72	0.007763
4.50	79908.00	0.007785
5.00	79500.01	0.007810
5.50	79095.61	0.007838
6.00	78694.74	0.007868
6.50	78297.31	0.007901
7.00	77903.24	0.007936
7.50	77512.46	0.007974
8.00	77124.87	0.008015
8.50	76740.40	0.008058
9.00	76358.97	0.008104
9.50	75980.51	0.008152
10.00	75604.94	0.008203
10.50	75232.19	0.008257
11.00	74862.18	0.008313
11.50	74494.84	0.008372
12.00	74130.10	0.008434
12.50	73767.89	0.008498
13.00	73408.15	0.008565
13.50	73050.80	0.008634
14.00	72695.80	0.008706
14.50	72343.07	0.008781
15.00	71992.56	0.008858
15.50	71644.20	0.008938
16.00	71297.94	0.009021
16.50	70953.73	0.009106
17.00	70611.52	0.009193
17.50	70271.25	0.009284
18.00	69932.88	0.009377
18.50	69596.36	0.009472
19.00	69261.67	0.009571
19.50	68928.76	0.009671
20.00	68597.60	0.009775
20.50	68268.16	0.009881
21.00	67940.42	0.009990
21.50	67614.37	0.010101
22.00	67290.00	0.010215
22.50	66967.29	0.010331
23.00	66646.25	0.010451
23.50	66326.89	0.010572
24.00	66009.22	0.010697
24.50	65693.26	0.010824
25.00	65379.05	0.010954
25.50	65066.62	0.011086
26.00	64756.03	0.011221
26.50	64447.32	0.011358
27.00	64140.55	0.011498
27.50	63835.81	0.011641
28.00	63533.15	0.011787
28.50	63232.68	0.011935
29.00	62934.47	0.012085
29.50	62638.63	0.012238

File *wred-dinc.out*:

```
RBM REDUCT(%) WING_W_REDUCT(%) DRAG_INCREASE(%)
   0.00            0.00000        0.00000
   0.50            0.51923        0.01705
   1.00            1.04338        0.06822
   1.50            1.56360        0.15349
   2.00            2.07890        0.27287
   2.50            2.58926        0.42636
   3.00            3.09477        0.61396
   3.50            3.59554        0.83567
   4.00            4.09168        1.09148
   4.50            4.58330        1.38141
   5.00            5.07048        1.70544
   5.50            5.55337        2.06359
   6.00            6.03204        2.45584
   6.50            6.50660        2.88220
   7.00            6.97715        3.34267
   7.50            7.44378        3.83725
   8.00            7.90659        4.36594
   8.50            8.36568        4.92874
   9.00            8.82113        5.52564
   9.50            9.27305        6.15666
  10.00            9.72151        6.82178
  10.50           10.16661        7.52101
  11.00           10.60843        8.25435
  11.50           11.04707        9.02180
  12.00           11.48259        9.82336
  12.50           11.91510       10.65903
  13.00           12.34466       11.52881
  13.50           12.77136       12.43269
  14.00           13.19526       13.37069
  14.50           13.61645       14.34279
  15.00           14.03499       15.34900
  15.50           14.45096       16.38933
  16.00           14.86442       17.46376
  16.50           15.27543       18.57230
  17.00           15.68407       19.71494
  17.50           16.09038       20.89170
  18.00           16.49442       22.10257
  18.50           16.89624       23.34754
  19.00           17.29590       24.62662
  19.50           17.69342       25.93982
  20.00           18.08885       27.28712
  20.50           18.48223       28.66853
  21.00           18.87357       30.08405
  21.50           19.26290       31.53368
  22.00           19.65023       33.01741
  22.50           20.03558       34.53526
  23.00           20.41892       36.08721
  23.50           20.80027       37.67328
  24.00           21.17959       39.29345
  24.50           21.55687       40.94773
  25.00           21.93206       42.63612
  25.50           22.30512       44.35862
  26.00           22.67600       46.11523
  26.50           23.04463       47.90595
  27.00           23.41093       49.73077
  27.50           23.77482       51.58971
  28.00           24.13621       53.48275
  28.50           24.49500       55.40991
  29.00           24.85109       57.37117
  29.50           25.20435       59.36654
```

File *weights.out*:

RBM_RED	W_WING	W_FUEL	WWING+WFUEL	GW
0.00	83746.4	215000.0	298746.4	588893.0
0.50	83311.5	214797.2	298108.7	588255.3
1.00	82872.6	214616.9	297489.5	587636.1
1.50	82436.9	214462.9	296899.8	587046.4
2.00	82005.3	214335.3	296340.7	586487.3
2.50	81577.9	214234.2	295812.1	585958.8
3.00	81154.6	214159.4	295314.0	585460.6
3.50	80735.2	214110.8	294846.0	584992.7
4.00	80319.7	214088.3	294408.1	584554.7
4.50	79908.0	214091.9	293999.9	584146.6
5.00	79500.0	214121.4	293621.4	583768.1
5.50	79095.6	214176.8	293272.4	583419.0
6.00	78694.7	214257.9	292952.6	583099.3
6.50	78297.3	214364.7	292662.0	582808.7
7.00	77903.2	214497.1	292400.4	582547.0
7.50	77512.5	214655.1	292167.6	582314.2
8.00	77124.9	214838.6	291963.4	582110.1
8.50	76740.4	215047.5	291787.9	581934.5
9.00	76359.0	215281.7	291640.7	581787.3
9.50	75980.5	215541.3	291521.8	581668.5
10.00	75604.9	215826.2	291431.1	581577.8
10.50	75232.2	216136.3	291368.5	581515.2
11.00	74862.2	216471.6	291333.8	581480.5
11.50	74494.8	216832.2	291327.0	581473.6
12.00	74130.1	217217.8	291347.9	581494.6
12.50	73767.9	217628.6	291396.5	581543.2
13.00	73408.2	218064.5	291472.7	581619.3
13.50	73050.8	218525.5	291576.3	581723.0
14.00	72695.8	219011.6	291707.4	581854.1
14.50	72343.1	219522.8	291865.9	582012.6
15.00	71992.6	220059.1	292051.7	582198.3
15.50	71644.2	220620.5	292264.7	582411.4
16.00	71297.9	221207.0	292505.0	582651.6
16.50	70953.7	221818.6	292772.4	582919.0
17.00	70611.5	222455.4	293066.9	583213.5
17.50	70271.2	223117.3	293388.6	583535.2
18.00	69932.9	223804.4	293737.3	583884.0
18.50	69596.4	224516.8	294113.1	584259.8
19.00	69261.7	225254.4	294516.1	584662.7
19.50	68928.8	226017.4	294946.1	585092.8
20.00	68597.6	226805.7	295403.3	585549.9
20.50	68268.2	227619.4	295887.6	586034.2
21.00	67940.4	228458.7	296399.1	586545.7
21.50	67614.4	229323.5	296937.9	587084.5
22.00	67290.0	230213.9	297503.9	587650.6
22.50	66967.3	231130.1	298097.4	588244.1
23.00	66646.2	232072.1	298718.4	588865.0
23.50	66326.9	233040.0	299366.9	589513.6
24.00	66009.2	234034.0	300043.2	590189.9
24.50	65693.3	235054.1	300747.4	590894.0
25.00	65379.1	236100.5	301479.6	591626.2
25.50	65066.6	237173.3	302239.9	592386.6
26.00	64756.0	238272.7	303028.7	593175.3
26.50	64447.3	239398.7	303846.1	593992.7
27.00	64140.6	240551.7	304692.3	594838.9
27.50	63835.8	241731.7	305567.5	595714.2
28.00	63533.2	242939.0	306472.1	596618.8
28.50	63232.7	244173.7	307406.3	597553.0
29.00	62934.5	245436.0	308370.5	598517.1
29.50	62638.6	246726.2	309364.8	599511.5

File *weight-variation.out*:

```
WEIGHT INCREASE FOR DIFFERENT COMPONENETS IN %
 RBM_RED      WWING     WFUEL    WWING+WFU    GW
  0.00       0.0000    0.0000    0.0000    0.0000
  0.50      -0.5192   -0.0943   -0.2134   -0.1083
  1.00      -1.0434   -0.1782   -0.4207   -0.2134
  1.50      -1.5636   -0.2498   -0.6181   -0.3136
  2.00      -2.0789   -0.3092   -0.8053   -0.4085
  2.50      -2.5893   -0.3562   -0.9822   -0.4983
  3.00      -3.0948   -0.3910   -1.1489   -0.5829
  3.50      -3.5955   -0.4136   -1.3056   -0.6623
  4.00      -4.0917   -0.4240   -1.4522   -0.7367
  4.50      -4.5833   -0.4224   -1.5888   -0.8060
  5.00      -5.0705   -0.4086   -1.7155   -0.8703
  5.50      -5.5534   -0.3829   -1.8323   -0.9295
  6.00      -6.0320   -0.3452   -1.9393   -0.9838
  6.50      -6.5066   -0.2955   -2.0366   -1.0332
  7.00      -6.9771   -0.2339   -2.1242   -1.0776
  7.50      -7.4438   -0.1604   -2.2021   -1.1171
  8.00      -7.9066   -0.0751   -2.2705   -1.1518
  8.50      -8.3657    0.0221   -2.3292   -1.1816
  9.00      -8.8211    0.1310   -2.3785   -1.2066
  9.50      -9.2730    0.2518   -2.4183   -1.2268
 10.00      -9.7215    0.3843   -2.4486   -1.2422
 10.50     -10.1666    0.5285   -2.4696   -1.2528
 11.00     -10.6084    0.6845   -2.4812   -1.2587
 11.50     -11.0471    0.8522   -2.4835   -1.2599
 12.00     -11.4826    1.0315   -2.4765   -1.2563
 12.50     -11.9151    1.2226   -2.4602   -1.2481
 13.00     -12.3447    1.4254   -2.4347   -1.2351
 13.50     -12.7714    1.6398   -2.4000   -1.2175
 14.00     -13.1953    1.8659   -2.3561   -1.1953
 14.50     -13.6164    2.1036   -2.3031   -1.1684
 15.00     -14.0350    2.3531   -2.2409   -1.1368
 15.50     -14.4510    2.6142   -2.1696   -1.1006
 16.00     -14.8644    2.8870   -2.0892   -1.0599
 16.50     -15.2754    3.1715   -1.9997   -1.0144
 17.00     -15.6841    3.4676   -1.9011   -0.9644
 17.50     -16.0904    3.7755   -1.7934   -0.9098
 18.00     -16.4944    4.0951   -1.6767   -0.8506
 18.50     -16.8962    4.4264   -1.5509   -0.7868
 19.00     -17.2959    4.7695   -1.4160   -0.7183
 19.50     -17.6934    5.1244   -1.2721   -0.6453
 20.00     -18.0889    5.4910   -1.1190   -0.5677
 20.50     -18.4822    5.8695   -0.9569   -0.4854
 21.00     -18.8736    6.2598   -0.7857   -0.3986
 21.50     -19.2629    6.6621   -0.6054   -0.3071
 22.00     -19.6502    7.0762   -0.4159   -0.2110
 22.50     -20.0356    7.5024   -0.2172   -0.1102
 23.00     -20.4189    7.9405   -0.0094   -0.0048
 23.50     -20.8003    8.3907    0.2077    0.1054
 24.00     -21.1796    8.8530    0.4341    0.2202
 24.50     -21.5569    9.3275    0.6698    0.3398
 25.00     -21.9321    9.8142    0.9149    0.4641
 25.50     -22.3051   10.3132    1.1694    0.5932
 26.00     -22.6760   10.8245    1.4334    0.7272
 26.50     -23.0446   11.3483    1.7070    0.8660
 27.00     -23.4109   11.8845    1.9903    1.0097
 27.50     -23.7748   12.4334    2.2833    1.1583
 28.00     -24.1362   12.9949    2.5861    1.3119
 28.50     -24.4950   13.5691    2.8988    1.4706
 29.00     -24.8511   14.1563    3.2215    1.6343
 29.50     -25.2044   14.7564    3.5543    1.8031
```

Appendix B.1

Sample design input file. Spanload optimization in formation flight. Equal aircraft configuration.

```
idrag input file
equal formation design
0               input mode
1               write flag
2               number of aircraft
0               cm_flag
0.25            center of pressure for airfoil sections
0.6             cl_design / Design parameters for aircraft 1
0               cm_design
0.0             yrbm
0.0             zrbm
0.03            x cg position
0.5             reference area
0.25            reference chord
0.0             x movement of aircraft 1
0.0             y movement of aircraft 1
0.0             z movement of aircraft 1
0.6             cl_design / Design parameters for aircraft 2
0               cm_design
1.0             yrbm
0.0             zrbm
0.03            x cg position
0.5             reference area
0.25            reference chord
6.0             x movement of aircraft 2
0.78             y movement of aircraft 2
0.02             z movement of aircraft 2
3               number of panels
0   0   0       x,y,z for 4 corners of panel 1
0.125   1   0
0.25    1   0
0.375   0   0
40              number of vortices for panel 1
0               vortex spacing for panel 1
1               aircraft number to which panel 1 corresponds
1               rolling flag for panel 1
0.125 0.0 0.0   x,y,z for 4 corners of panel 2
0.0   1.0 0.0
0.375 1.0 0.0
0.25  0.0 0.0
40              number of vortices for panel 2
0               vortex spacing for panel 2
2               aircraft number to which panel 2 corresponds
1               rolling flag for panel 2
0.0   1.0 0.0   x,y,z for 4 corners of panel 3
0.125 2.0 0.0
0.25  2.0 0.0
0.375 1.0 0.0
40              number of vortices for panel 3
0               vortex spacing for panel 3
2               aircraft number to which panel 3 corresponds
1               rolling flag for panel 3
```

Appendix B.2

Sample design input file. Spanload optimization in formation flight. Different aircraft size configuration.

```
idrag input file
diff. formation design
0               input mode
1               write flag
2               number of aircraft
1               cm_flag
0.25            center of pressure for airfoil sections
0.6             cl_design / Design parameters for aircraft 1
0               cm_design
0.0             yrbm
0.0             zrbm
0.03            x cg position
0.2             reference area
0.2             reference chord
0.0             x movement of aircraft 1
0.0             y movement of aircraft 1
0.0             z movement of aircraft 1
0.6             cl_design / Design parameters for aircraft 2
0               cm_design
0.25             yrbm
0.0              zrbm
0.015            x cg position
0.05             reference area
0.1             reference chord
3.0              x movement of aircraft 2
0.55             y movement of aircraft 2
0.01             z movement of aircraft 2
4               number of panels
0   0   0       x,y,z for 4 corners of panel 1
0   0.5   0
0.2 0.5   0
0.2 0   0
20              number of vortices for panel 1
0               vortex spacing for panel 1
1               aircraft number to which panel 1 corresponds
1               rolling flag for panel 1
1    0.0 0.1   x,y,z for 4 corners of panel 2
1    0.2 0.1
1.1  0.2 0.1
1.1  0.0 0.1
10              number of vortices for panel 2
0               vortex spacing for panel 2
1               aircraft number to which panel 2 corresponds
0               rolling flag for panel 2
0.0 0.0 0.0     x,y,z for 4 corners of panel 3
0.0 0.5 0.0
0.1 0.5 0.0
0.1 0.0 0.0
40              number of vortices for panel 3
0               vortex spacing for panel 3
2               aircraft number to which panel 3 corresponds
1               rolling flag for panel 3
0.5  0.15 0.1     x,y,z for 4 corners of panel 4
0.5  0.35 0.1
0.55 0.35 0.1
0.55 0.15 0.1
20              number of vortices for panel 4
0               vortex spacing for panel 4
2               aircraft number to which panel 4 corresponds
0               rolling flag for panel 4
```

Appendix B.3

Sample design output file. Spanload optimization for formation flight. Equal aircraft configuration.

```
idrag output file
equal formation design
    0    = input mode
    1    = write flag
    2    = number of aircraft
    0    = moment coefficient flag
    0.25 = center of pressure for airfoil sections

 Design parameters for aircraft 1
    0.60 = design lift coefficient
    0.00 = design moment coefficient
    0.00 = reference y location for root bending moment
    0.00 = reference z location for root bending moment
    0.03 = x cg position
    0.50 = reference area
    0.25 = reference chord

 Design parameters for aircraft 2
    0.60 = design lift coefficient
    0.00 = design moment coefficient
    1.78 = reference y location for root bending moment
    0.02 = reference z location for root bending moment
    6.03 = x cg position
    0.50 = reference area
    0.25 = reference chord

    3    = number of panels

    x        y        z    for panel 1
    0.00     0.00     0.00
    0.13     1.00     0.00
    0.25     1.00     0.00
    0.38     0.00     0.00
   40    = number of vortices
    0    = vortex spacing flag
    1    = aircraft to which it corresponds
    1    = rolling moment flag for panel

    x        y        z    for panel 2
    6.13     0.78     0.02
    6.00     1.78     0.02
    6.38     1.78     0.02
    6.25     0.78     0.02
   40    = number of vortices
    0    = vortex spacing flag
    2    = aircraft to which it corresponds
    1    = rolling moment flag for panel

    x        y        z    for panel 3
    6.00     1.78     0.02
    6.13     2.78     0.02
    6.25     2.78     0.02
    6.38     1.78     0.02
   40    = number of vortices
    0    = vortex spacing flag
    2    = aircraft to which it corresponds
    1    = rolling moment flag for panel

    i   x        y        z        load     cn
    1   0.0945   0.0125   0.0000   0.6919   0.4651
    2   0.0961   0.0375   0.0000   0.6918   0.4730
    3   0.0977   0.0625   0.0000   0.6917   0.4812
    4   0.0992   0.0875   0.0000   0.6914   0.4895
```

5	0.1008	0.1125	0.0000	0.6911	0.4981
6	0.1023	0.1375	0.0000	0.6907	0.5070
7	0.1039	0.1625	0.0000	0.6903	0.5161
8	0.1055	0.1875	0.0000	0.6897	0.5255
9	0.1070	0.2125	0.0000	0.6891	0.5352
10	0.1086	0.2375	0.0000	0.6884	0.5453
11	0.1102	0.2625	0.0000	0.6876	0.5556
12	0.1117	0.2875	0.0000	0.6867	0.5663
13	0.1133	0.3125	0.0000	0.6857	0.5774
14	0.1148	0.3375	0.0000	0.6846	0.5889
15	0.1164	0.3625	0.0000	0.6834	0.6008
16	0.1180	0.3875	0.0000	0.6821	0.6131
17	0.1195	0.4125	0.0000	0.6806	0.6258
18	0.1211	0.4375	0.0000	0.6790	0.6391
19	0.1227	0.4625	0.0000	0.6773	0.6528
20	0.1242	0.4875	0.0000	0.6753	0.6670
21	0.1258	0.5125	0.0000	0.6732	0.6817
22	0.1273	0.5375	0.0000	0.6709	0.6970
23	0.1289	0.5625	0.0000	0.6683	0.7128
24	0.1305	0.5875	0.0000	0.6654	0.7292
25	0.1320	0.6125	0.0000	0.6621	0.7460
26	0.1336	0.6375	0.0000	0.6583	0.7632
27	0.1352	0.6625	0.0000	0.6538	0.7807
28	0.1367	0.6875	0.0000	0.6483	0.7980
29	0.1383	0.7125	0.0000	0.6413	0.8143
30	0.1398	0.7375	0.0000	0.6311	0.8276
31	0.1414	0.7625	0.0000	0.6128	0.8309
32	0.1430	0.7875	0.0000	0.5703	0.8004
33	0.1445	0.8125	0.0000	0.5187	0.7545
34	0.1461	0.8375	0.0000	0.4648	0.7016
35	0.1477	0.8625	0.0000	0.4087	0.6411
36	0.1492	0.8875	0.0000	0.3505	0.5723
37	0.1508	0.9125	0.0000	0.2903	0.4941
38	0.1523	0.9375	0.0000	0.2277	0.4049
39	0.1539	0.9625	0.0000	0.1625	0.3023
40	0.1555	0.9875	0.0000	0.0927	0.1809
41	6.1555	0.7925	0.0200	0.0685	0.1337
42	6.1539	0.8175	0.0200	0.1245	0.2316
43	6.1523	0.8425	0.0200	0.1804	0.3208
44	6.1508	0.8675	0.0200	0.2375	0.4043
45	6.1492	0.8925	0.0200	0.2960	0.4832
46	6.1477	0.9175	0.0200	0.3558	0.5581
47	6.1461	0.9425	0.0200	0.4169	0.6293
48	6.1445	0.9675	0.0200	0.4793	0.6972
49	6.1430	0.9925	0.0200	0.5426	0.7615
50	6.1414	1.0175	0.0200	0.5972	0.8098
51	6.1398	1.0425	0.0200	0.6204	0.8137
52	6.1383	1.0675	0.0200	0.6335	0.8044
53	6.1367	1.0925	0.0200	0.6428	0.7911
54	6.1352	1.1175	0.0200	0.6503	0.7765
55	6.1336	1.1425	0.0200	0.6568	0.7615
56	6.1320	1.1675	0.0200	0.6626	0.7466
57	6.1305	1.1925	0.0200	0.6679	0.7319
58	6.1289	1.2175	0.0200	0.6728	0.7177
59	6.1273	1.2425	0.0200	0.6774	0.7038
60	6.1258	1.2675	0.0200	0.6818	0.6904
61	6.1242	1.2925	0.0200	0.6859	0.6775
62	6.1227	1.3175	0.0200	0.6899	0.6650
63	6.1211	1.3425	0.0200	0.6936	0.6528
64	6.1195	1.3675	0.0200	0.6972	0.6411
65	6.1180	1.3925	0.0200	0.7006	0.6298
66	6.1164	1.4175	0.0200	0.7039	0.6188
67	6.1148	1.4425	0.0200	0.7069	0.6081
68	6.1133	1.4675	0.0200	0.7098	0.5977
69	6.1117	1.4925	0.0200	0.7125	0.5876
70	6.1102	1.5175	0.0200	0.7151	0.5778
71	6.1086	1.5425	0.0200	0.7174	0.5682
72	6.1070	1.5675	0.0200	0.7196	0.5589
73	6.1055	1.5925	0.0200	0.7215	0.5497
74	6.1039	1.6175	0.0200	0.7233	0.5408
75	6.1023	1.6425	0.0200	0.7249	0.5320

76	6.1008	1.6675	0.0200	0.7262	0.5234
77	6.0992	1.6925	0.0200	0.7273	0.5149
78	6.0977	1.7175	0.0200	0.7282	0.5066
79	6.0961	1.7425	0.0200	0.7289	0.4984
80	6.0945	1.7675	0.0200	0.7292	0.4902
81	6.0945	1.7925	0.0200	0.7294	0.4903
82	6.0961	1.8175	0.0200	0.7292	0.4986
83	6.0977	1.8425	0.0200	0.7288	0.5070
84	6.0992	1.8675	0.0200	0.7280	0.5154
85	6.1008	1.8925	0.0200	0.7270	0.5239
86	6.1023	1.9175	0.0200	0.7256	0.5325
87	6.1039	1.9425	0.0200	0.7239	0.5412
88	6.1055	1.9675	0.0200	0.7218	0.5499
89	6.1070	1.9925	0.0200	0.7193	0.5587
90	6.1086	2.0175	0.0200	0.7165	0.5675
91	6.1102	2.0425	0.0200	0.7132	0.5763
92	6.1117	2.0675	0.0200	0.7095	0.5852
93	6.1133	2.0925	0.0200	0.7054	0.5940
94	6.1148	2.1175	0.0200	0.7008	0.6028
95	6.1164	2.1425	0.0200	0.6957	0.6116
96	6.1180	2.1675	0.0200	0.6900	0.6203
97	6.1195	2.1925	0.0200	0.6838	0.6288
98	6.1211	2.2175	0.0200	0.6771	0.6372
99	6.1227	2.2425	0.0200	0.6697	0.6455
100	6.1242	2.2675	0.0200	0.6616	0.6534
101	6.1258	2.2925	0.0200	0.6529	0.6611
102	6.1273	2.3175	0.0200	0.6434	0.6684
103	6.1289	2.3425	0.0200	0.6331	0.6753
104	6.1305	2.3675	0.0200	0.6219	0.6815
105	6.1320	2.3925	0.0200	0.6098	0.6871
106	6.1336	2.4175	0.0200	0.5967	0.6918
107	6.1352	2.4425	0.0200	0.5825	0.6955
108	6.1367	2.4675	0.0200	0.5671	0.6980
109	6.1383	2.4925	0.0200	0.5504	0.6989
110	6.1398	2.5175	0.0200	0.5322	0.6979
111	6.1414	2.5425	0.0200	0.5123	0.6947
112	6.1430	2.5675	0.0200	0.4906	0.6886
113	6.1445	2.5925	0.0200	0.4667	0.6788
114	6.1461	2.6175	0.0200	0.4402	0.6645
115	6.1477	2.6425	0.0200	0.4107	0.6442
116	6.1492	2.6675	0.0200	0.3773	0.6160
117	6.1508	2.6925	0.0200	0.3389	0.5768
118	6.1523	2.7175	0.0200	0.2935	0.5218
119	6.1539	2.7425	0.0200	0.2372	0.4414
120	6.1555	2.7675	0.0200	0.1598	0.3118

```
Calculated parameters for aircraft          1
   0.60000 = actual lift coefficient
   -.21946 = actual moment coefficient
   0.00000 = rolling moment coefficient
   0.01478 = induced drag coefficient
   0.96893 = span efficiency factor

Calculated parameters for aircraft          2
   0.60000 = actual lift coefficient
   -.21789 = actual moment coefficient
   0.00000 = rolling moment coefficient
   0.00322 = induced drag coefficient
   4.45273 = span efficiency factor

   0.00707 = formation induced drag coefficient
```

Appendix B.4

Sample design output file. Spanload optimization for formation flight. Different aircraft size configuration.

```
idrag output file
diff. formation design
    0    = input mode
    1    = write flag
    2    = number of aircraft
    1    = moment coefficient flag
    0.25 = center of pressure for airfoil sections

 Design parameters for aircraft 1
    0.60 = design lift coefficient
    0.00 = design moment coefficient
    0.00 = reference y location for root bending moment
    0.00 = reference z location for root bending moment
    0.03 = x cg position
    0.20 = reference area
    0.20 = reference chord

 Design parameters for aircraft 2
    0.60 = design lift coefficient
    0.00 = design moment coefficient
    0.80 = reference y location for root bending moment
    0.01 = reference z location for root bending moment
    3.02 = x cg position
    0.05 = reference area
    0.10 = reference chord

    4    = number of panels

    x        y        z    for panel 1
    0.00     0.00     0.00
    0.00     0.50     0.00
    0.20     0.50     0.00
    0.20     0.00     0.00
   20    = number of vortices
    0    = vortex spacing flag
    1    = aircraft to which it corresponds
    1    = rolling moment flag for panel

    x        y        z    for panel 2
    1.00     0.00     0.10
    1.00     0.20     0.10
    1.10     0.20     0.10
    1.10     0.00     0.10
   10    = number of vortices
    0    = vortex spacing flag
    1    = aircraft to which it corresponds
    0    = rolling moment flag for panel

    x        y        z    for panel 3
    3.00     0.55     0.01
    3.00     1.05     0.01
    3.10     1.05     0.01
    3.10     0.55     0.01
   40    = number of vortices
    0    = vortex spacing flag
    2    = aircraft to which it corresponds
    1    = rolling moment flag for panel

    x        y        z    for panel 4
    3.50     0.70     0.11
    3.50     0.90     0.11
    3.55     0.90     0.11
    3.55     0.70     0.11
```

```
20    = number of vortices
 0    = vortex spacing flag
 2    = aircraft to which it corresponds
 0    = rolling moment flag for panel

 i   x        y        z        load     cn
 1   0.0500   0.0125   0.0000   0.6886   0.6886
 2   0.0500   0.0375   0.0000   0.6877   0.6877
 3   0.0500   0.0625   0.0000   0.6860   0.6860
 4   0.0500   0.0875   0.0000   0.6833   0.6833
 5   0.0500   0.1125   0.0000   0.6798   0.6798
 6   0.0500   0.1375   0.0000   0.6754   0.6754
 7   0.0500   0.1625   0.0000   0.6702   0.6702
 8   0.0500   0.1875   0.0000   0.6642   0.6642
 9   0.0500   0.2125   0.0000   0.6576   0.6576
10   0.0500   0.2375   0.0000   0.6504   0.6504
11   0.0500   0.2625   0.0000   0.6424   0.6424
12   0.0500   0.2875   0.0000   0.6333   0.6333
13   0.0500   0.3125   0.0000   0.6227   0.6227
14   0.0500   0.3375   0.0000   0.6098   0.6098
15   0.0500   0.3625   0.0000   0.5938   0.5938
16   0.0500   0.3875   0.0000   0.5731   0.5731
17   0.0500   0.4125   0.0000   0.5453   0.5453
18   0.0500   0.4375   0.0000   0.5057   0.5057
19   0.0500   0.4625   0.0000   0.4442   0.4442
20   0.0500   0.4875   0.0000   0.3325   0.3325
21   1.0250   0.0100   0.1000  -0.0400  -0.0800
22   1.0250   0.0300   0.1000  -0.0395  -0.0790
23   1.0250   0.0500   0.1000  -0.0385  -0.0769
24   1.0250   0.0700   0.1000  -0.0369  -0.0738
25   1.0250   0.0900   0.1000  -0.0348  -0.0695
26   1.0250   0.1100   0.1000  -0.0321  -0.0641
27   1.0250   0.1300   0.1000  -0.0287  -0.0575
28   1.0250   0.1500   0.1000  -0.0247  -0.0494
29   1.0250   0.1700   0.1000  -0.0196  -0.0393
30   1.0250   0.1900   0.1000  -0.0129  -0.0259
31   3.0250   0.5563   0.0100   0.2545   0.2545
32   3.0250   0.5688   0.0100   0.3607   0.3607
33   3.0250   0.5813   0.0100   0.4294   0.4294
34   3.0250   0.5938   0.0100   0.4801   0.4801
35   3.0250   0.6062   0.0100   0.5201   0.5201
36   3.0250   0.6187   0.0100   0.5530   0.5530
37   3.0250   0.6313   0.0100   0.5809   0.5809
38   3.0250   0.6438   0.0100   0.6051   0.6051
39   3.0250   0.6563   0.0100   0.6264   0.6264
40   3.0250   0.6687   0.0100   0.6452   0.6452
41   3.0250   0.6812   0.0100   0.6621   0.6621
42   3.0250   0.6937   0.0100   0.6773   0.6773
43   3.0250   0.7063   0.0100   0.6909   0.6909
44   3.0250   0.7188   0.0100   0.7030   0.7030
45   3.0250   0.7312   0.0100   0.7138   0.7138
46   3.0250   0.7437   0.0100   0.7232   0.7232
47   3.0250   0.7562   0.0100   0.7312   0.7312
48   3.0250   0.7688   0.0100   0.7378   0.7378
49   3.0250   0.7813   0.0100   0.7429   0.7429
50   3.0250   0.7937   0.0100   0.7466   0.7466
51   3.0250   0.8062   0.0100   0.7487   0.7487
52   3.0250   0.8187   0.0100   0.7491   0.7491
53   3.0250   0.8312   0.0100   0.7478   0.7478
54   3.0250   0.8437   0.0100   0.7448   0.7448
55   3.0250   0.8562   0.0100   0.7399   0.7399
56   3.0250   0.8687   0.0100   0.7330   0.7330
57   3.0250   0.8812   0.0100   0.7242   0.7242
58   3.0250   0.8937   0.0100   0.7131   0.7131
59   3.0250   0.9062   0.0100   0.6998   0.6998
60   3.0250   0.9187   0.0100   0.6839   0.6839
61   3.0250   0.9312   0.0100   0.6654   0.6654
62   3.0250   0.9437   0.0100   0.6438   0.6438
63   3.0250   0.9562   0.0100   0.6187   0.6187
64   3.0250   0.9687   0.0100   0.5895   0.5895
65   3.0250   0.9812   0.0100   0.5554   0.5554
```

```
  66   3.0250   0.9937   0.0100   0.5152   0.5152
  67   3.0250   1.0063   0.0100   0.4673   0.4673
  68   3.0250   1.0187   0.0100   0.4086   0.4086
  69   3.0250   1.0313   0.0100   0.3334   0.3334
  70   3.0250   1.0437   0.0100   0.2267   0.2267
  71   3.5125   0.7050   0.1100  -0.0073  -0.0146
  72   3.5125   0.7150   0.1100  -0.0123  -0.0246
  73   3.5125   0.7250   0.1100  -0.0168  -0.0336
  74   3.5125   0.7350   0.1100  -0.0210  -0.0420
  75   3.5125   0.7450   0.1100  -0.0249  -0.0499
  76   3.5125   0.7550   0.1100  -0.0286  -0.0572
  77   3.5125   0.7650   0.1100  -0.0319  -0.0637
  78   3.5125   0.7750   0.1100  -0.0348  -0.0696
  79   3.5125   0.7850   0.1100  -0.0373  -0.0746
  80   3.5125   0.7950   0.1100  -0.0393  -0.0787
  81   3.5125   0.8050   0.1100  -0.0409  -0.0818
  82   3.5125   0.8150   0.1100  -0.0419  -0.0837
  83   3.5125   0.8250   0.1100  -0.0423  -0.0845
  84   3.5125   0.8350   0.1100  -0.0420  -0.0840
  85   3.5125   0.8450   0.1100  -0.0410  -0.0820
  86   3.5125   0.8550   0.1100  -0.0392  -0.0784
  87   3.5125   0.8650   0.1100  -0.0364  -0.0728
  88   3.5125   0.8750   0.1100  -0.0324  -0.0648
  89   3.5125   0.8850   0.1100  -0.0268  -0.0536
  90   3.5125   0.8950   0.1100  -0.0183  -0.0367


Calculated parameters for aircraft           1
   0.60000 = actual lift coefficient
   0.00000 = actual moment coefficient
   0.00000 = rolling moment coefficient
   0.02421 = induced drag coefficient
   0.94682 = span efficiency factor

Calculated parameters for aircraft           2
   0.60000 = actual lift coefficient
   0.00000 = actual moment coefficient
   0.00000 = rolling moment coefficient
   0.00405 = induced drag coefficient
   5.65475 = span efficiency factor

   0.01413 = formation induced drag coefficient
```

Vita

Sergio Iglesias was born on August 6, 1977 in Toledo, Spain. He graduated from high school in Madrid in 1995. Due to his interest in the aerospace industry he decided to pursue his education in this field. He then entered Parks College, at Saint Louis University, because of the greater emphasis on industry related, closer to real life studies that exist in American Universities. After four years of study in this university, he graduated as a Bachelor of Science in Aerospace Engineering in May 1999. Later, he decided to continue his efforts in the post graduate level, so he joined the Aerospace and Ocean Engineering Department at Virginia Polytechnic Institute and State University in August 1999, and graduated with the Master of Science degree in Aerospace Engineering in November 2000. He now hopes to perform an industry-related work that matches his studies. He will come back to Europe, where he expects to find a position in the aerospace industry.